A Search For The Rare Decay of a Charged B Meson into a Charged K Meson, a Neutrino and an Anti-Neutrino

Joachim Harnois-Déraps

Master of Physics

Physics Department

McGill University

Montreal,Quebec

December 22, 2006

A thesis submitted to the Faculty of Graduate Studies and Research in partial fulfillment of the requirements for the degree of Master of Science *pour mon père, ma mère, KaS et Jonathan*

ACKNOWLEDGEMENTS

We are grateful to the great luminosity and detetector quality provided by the PEP-II and *BABAR* engineers and physicists that allowed the high-quality data aquisition; to Paul Mercure and Juan Callego for their efforts put in the computing system in the McGill Physics Departement; to Miika Klemetti and Sheila Mclachlin for their help in writing root and C++ macros; to FCAR and McGill University for their financial assistance; to Steven H. Robertson for the high quality of his supervision throughout the analysis process and the writing of this document.

ABSTRACT

The document describes a search for the rare decay $B^- \to K^- \nu\overline{\nu}$ in a data set of about 230 millions of $B\overline{B}$ pairs recorded by the *BABAR* detector at the PEP-II B Factory, via the process $e^+e^- \to \Upsilon(4S) \to B\overline{B}$. The method used selects events in which the B^+ meson is fully reconstructed, and looks for a K^- in the rest of the event. This is accomplished by applying kinematical and topological restrictions that select $B^- \to K^- \nu\overline{\nu}$ events with the largest possible efficiency, while rejecting a maximum amount of background events. The number of background events is estimated from data and from simulated events, while the value of the selection efficiency relies solely on the simulation of $B^- \to K^- \nu\overline{\nu}$ decays in the *BABAR* detector. These two numbers are required in order to set an upper limit on the branching ratio. We analyze a subset of the data sample and provide an interpretation of the result.

ABRÉGÉ

Ce document décrit une recherche de la désintégration rare $B^- \to K^-\nu\overline{\nu}$ parmi un échantillon de données d'environ 230 millions de paires $B\overline{B}$, récoltées par le détecteur *BABAR* au complexe PEP-II grâce au processus $e^+e^- \to \Upsilon(4S) \to B\overline{B}$. La méthode utilisée consiste à sélectionner des événements pour lesquels il est possible de reconstituer entièrement le méson B^+, puis de chercher un méson K^- parmi les particules restantes. Pour ce faire, diverses restrictions topologiques et cinématiques sont appliquées sur les données et tentent de sélectionner le plus de processus $B^- \to K^-\nu\overline{\nu}$ possible, tout en rejetant un nombre maximal d'événements indésirables. Certains, parmi ceux-ci, se retrouvent tout de même dans notre sélection finale. À l'aide des données et de simulations, nous en estimons la quantité, ainsi que l'efficacité avec laquelle le processus $B^- \to K^-\nu\overline{\nu}$ est sélectionné, et ces deux quantités nous permettent de poser une limite supérieure sur le taux de branchement. Nous analysons un échantillon des données et fournissons une interprétation du résultat.

TABLE OF CONTENTS

LIST OF TABLES

LIST OF FIGURES

CHAPTER 1
Introduction

The present document describes a data analysis that attempts to set an upper limit on the branching fraction of a rare process, predicted by the Standard Model of particle physics (SM) but not yet observed : $B^{\pm} \rightarrow K^{\pm}\nu\overline{\nu}$ ($\nu\overline{\nu} = \nu_e\overline{\nu}_e$, $\nu_\mu\overline{\nu}_\mu$ or $\nu_\tau\overline{\nu}_\tau$). The last experimental upper limits measured by the *BABAR* ($\mathcal{B}(B^- \rightarrow K^-\nu\overline{\nu})$ $< 5.2 \times 10^{-5}$[1]) and BELLE ($\mathcal{B}(B^- \rightarrow K^-\nu\overline{\nu}) < 3.6 \times 10^{-5}$[2]) collaborations are about an order of magnitude above the prediction of the SM ($\mathcal{B}(B^- \rightarrow K^-\nu\overline{\nu}) =$ $(3.8^{+1.2}_{-0.6}) \times 10^{-6}$[3]).

This analysis uses a data set of about 230 million $B\overline{B}$ pairs produced by the PEP-II B Factory at the Stanford Linear Accelerator Center (SLAC), and recorded by the *BABAR* detector between February 2000 and July 2004. The strategy is to select events in which the B^+ meson is fully reconstructed, and to search in the rest of the event for a K^-, presumably coming from a $B^- \rightarrow K^-\nu\overline{\nu}$ decay [1] . Based on an estimation of the selection efficency, on the number of background events expected, and on the number of data events observed after all the selections criteria are applied, we attempt to set a new upper limit on the branching ratio. However, we observe significant discrepancies in MC-data comparisons, which prevent the limit from being

[1] We also reconstruct the mode $B^+ \rightarrow K^+\nu\overline{\nu}$, but for the sake of clarity, charge congugate processes are implied throughout this paper.

extracted in this work, so instead, we discuss possible sources for these discrepancies and provide suggestions for a future analysis strategy.

The document is organized in five chapters. Chapter 2 covers the theoretical background of particle physics that is required to understand the analysis. The design and performance of the accelerator and of the *BABAR* detector are described in Chapter 3. Chapter 4 is a detailed description of the analysis, and the final results are presented in Chapter 5.

CHAPTER 2
The Standard Model

The study of particle physics led to the construction of a coherent model, named the Standard Model (SM), which describes very accurately many processes, and predicts the output of various experiments. The main ingredients are the electromagnetic (EM) force, the weak nuclear force, the strong force, and its particle content[1] . The different properties of elementary particles, like their masses or their electric charges, are measured experimentally and become parameters in the SM. The latter incorporates them into a system that models the physics of various interactions, predicting cross-sections of collisions, life-time of unstable particles, etc. The SM is a specific case of Quantum Field Theory (QFT), a general framework which describes how "force carrier" particles (*gauge bosons*) interact between themselves or with "matter" particles (*fermions*) [4].

2.1 Particle Content

Bosons and fermions are defined according to their spin : bosons have integer spin and fermions have half-integer spin. For each elementary particle corresponds an anti-particle of equal mass, but some quantum numbers take a different value

[1] Gravity force is not included in the SM

(e.g. the opposite electric charge). By convention, if p represents a particle, its anti-particle is labelled $\bar{p}$.

2.1.1 Bosons and Fermions

Each force has its own set of gauge bosons that can operate on particles with the appropriate "charge", respecting the gauge symmetries of the SM. The EM force is carried by the photon, γ, and can operate on particles with an electric charge Q. The weak force is carried by the $W^{\pm}$ and the Z^0*gauge* bosons, and these interact together and with all fermions. These two forces unify into the electro-weak force, whose charge is called the *hypercharge*, and is $SU(2) \times SU(1)$ symmetric.

The strong force, $SU(3)$ symmetric, is carried by gluons, which interact with particles having a "colour" charge : b, r and g (for *blue*, *red* and *green*). In analogy with the optical light, a uniform mix of blue, red and green colour produces white colour charge. In this picture, mixing a colour with its anti-colour also produces white. Finally, the SM needs the Higgs particle to allow, via the mechanism of spontaneous symmetry breaking [5], the $W^{\pm}$ and the Z^0 bosons to become massive; it also couples with the fermions, which explains at the same time how these acquire their mass. The Higgs particle is a spin-0 boson, but not a gauge boson, hence it does not carry any force. To simplify the text, from now on the word "charge" refers to the electric charge, unless specified.

Matter particles are organized in two groups of six members each : *leptons*, which do not have a colour charge, and *quarks*, which do. Generally speaking, heavier particles decay very rapidly into lighter particles, and that process occurs via one of the three forces. There are two types of members in the lepton group : electron-type

(e^-, μ^-, τ^-) with $Q = -1$ and a neutrino-type (ν_e, ν_μ, ν_τ) with $Q = 0$. Quarks come in 6 flavors, also separated in two types : "up-type" quarks (u, c, t) with $Q = +2/3$, and "down-type" (d, s, b) with $Q = -1/3$. All flavors can carry any of the three colour charge. Quarks and leptons are grouped in hypercharge doublets $(\binom{u}{d}, \binom{c}{s} \ldots)$ that define three "generations" of matter. A summary of the particle content of the SM is presented in Table 2–1.

Table 2–1: Elementary particles in the SM, with their electric charge Q. The Higgs boson has not been observed yet [6].

	fermions			Q	bosons
quarks	u	c	t	+2/3	γ
	d	s	b	-1/3	*gluon*
leptons	ν_e	ν_μ	ν_τ	0	Z^0
	e^-	μ^-	τ^-	-1	$W^\pm$
generation	1	2	3		*Higgs*

2.1.2 Hadrons and Quark Mixing

The dynamics of the quarks are modeled by the quantum chromo-dynamics (QCD) [4], which explains why they are tightly confined into bound-states, or *hadrons*, with a white colour charge. Although many combinations are possible, only two are experimentally observed : *mesons* with one quark and one anti-quark, *baryons* with three quarks. Examples of hadrons are presented in Table 2–2. Many excited states with higher internal angular momentum exist for each hadron, yielding higher masses. For example a $b\bar{b}$ quark pair can form $\Upsilon(1S)$, $\Upsilon(2S)$, $\Upsilon(3S)$, $\Upsilon(4S)$ ...

In particle physics experiments, we can measure the mass of various mesons and baryons, but because quarks are confined into hadrons, their individual mass can only be infered using various quark models [7] [8] [9]. These models describe the dynamics

Table 2–2: Examples of hadrons with their quark content [6].

quark content	lightest state	excited state
$u\ d\ d$	neutron	N, Δ^0
$s\ \overline{d}$, $s\ \overline{u}$	K_S^0 or K_L^0, K^-	K^{*0}, K^{*-}
$b\ \overline{d}$, $b\ \overline{u}$	$\overline{B}^0$, B^-	$\overline{B}^{*0}$, B^{*-}
$u\ \overline{d}$	π^+	ρ^+
mixture of $u\overline{u}$ and $d\overline{d}$	π^0	ρ^0, η^0

of the bound states using *form factors* that can be measured experimentally. The objective is to find the binding energy between the quarks and to extract their mass.

The special feature with quarks is that the weak interaction does not operate on their mass eigenstates (d, s ...) but on their weak eigenstates (d', s' ...). For example, there are probabilities that a fermion with the mass of a d quark interacts weakly as a d, a s or a b quark. The transformation between these eigenstates can be represented by a 3×3 rotation matrix, called the Cabibbo-Kobayashi-Maskawa matrix (V_{CKM}) [10] [11], and the calculation of any process with weakly interacting quarks involves matrix elements V_{ij}. One of the parametrization of V_{CKM} is presented below, where the imaginary phase δ_{13} has a value of about 60^o.

$$\begin{pmatrix} d' \\ s' \\ b' \end{pmatrix} = \begin{pmatrix} V_{ud} & V_{us} & V_{ub} \\ V_{cd} & V_{cs} & V_{cb} \\ V_{td} & V_{ts} & V_{tb} \end{pmatrix} \begin{pmatrix} d \\ s \\ b \end{pmatrix} = \begin{pmatrix} 0.97 & 0.22 & 0.003e^{-i\delta_{13}} \\ 0.22e^{i\delta_{13}} & 0.97e^{i\delta_{13}} & 0.04 \\ 0.007e^{i\delta_{13}} & 0.04e^{i\delta_{13}} & 1.00 \end{pmatrix} \begin{pmatrix} d \\ s \\ b \end{pmatrix} \tag{2.1}$$

2.2 Beyond SM

Some phenomena can not be explained by the current state of the SM, like the neutrino oscillation [12] or the existence of dark matter particles in most galaxies [13]. Particle physicists are now trying to sample physics beyond the SM, by searching for exotic particles and interactions that would only exist in high energy environments. They have created new models that could lead to measurable discrepancies with the SM expectations, for example by adding compact extra dimensions [14], a 4th generation of leptons or quarks with special interactions [15] [16] [17], dark matter scalars [18] or various super-symmetric particles [19]. As it will be shown later, the measurement presented in this document is possibly sensitive to exotic physics.

2.2.1 *CP* Violation

For any interaction involving particles and anti-particles, we can imagine a corresponding process in which the particles and the anti-particles exchange their roles, or a process in which the (x, y, z) coordinates are reversed. If these processes actually exist in nature, they are symmetric under charge conjugation (C) or parity transformation (P) respectively. As opposed to all strong and EM decays, which are symmetric under both C and P, weak decays violate these transformations separately. However, only a few rare decays violate both at the same time, and these processes are explained in the SM by the existence of the δ_{13} phase [23].

CP violation was discovered in the neutral K system [24], but is now also observed in the neutral B meson decays [23]. This measurement is a major goal in particle physics as the amount of asymmetry is closely related to the imaginary phase and to the value of V_{CKM} matrix elements. That relation is very clean when the decay states are accessible to both B^0 and $\overline{B}^0$ mesons, because it is then possible to measure the amount of *CP* violation that occurs in the interference between their decays with and without $B^0\overline{B}^0 \rightarrow \overline{B}^0 B^0$ mixing [23]. This is a time-dependent situation that involves the measurement of the difference between the decay-times of the two $B^0\overline{B}^0$ mesons, and achieving the required precision is challenging: with a life-time of about 1.67×10^{-12} seconds, a B meson would travel about 0.5 mm before decaying if it was moving at the speed of light. Thanks to special relativity, that measurement becomes available if the B mesons are Lorentz boosted in the laboratory. The best option is to generate, in an asymmetric collision of electrons and positrons beams, Lorentz boosted $\Upsilon(4S)$ mesons, which then decay exclusively into B^+B^- or $B^0\overline{B}^0$ mesons [25]. We can then measure the distances between the $\Upsilon(4S)$ decay vertex and those of the B mesons to extract their life-time. Principal cross-sections for e^+- e^- collisions are listed in Table 2–3, computed at a CM energy of 10.58 GeV/c^2.

Table 2–3: Cross-sections used in this analysis, calculated at a CM energy of 10.58 GeV/c^2 [23].

type	σ (nb)
$e^+e^- \rightarrow b\overline{b}$	1.05
$e^+e^- \rightarrow c\overline{c}$	1.30
$e^+e^- \rightarrow s\overline{s}$	0.35
$e^+e^- \rightarrow u\overline{u}$	1.39
$e^+e^- \rightarrow d\overline{d}$	0.35
$e^+e^- \rightarrow \tau^+\tau^-$	0.94
$e^+e^- \rightarrow e^+e^-$	~ 40

2.2.2 Flavor Changing Neutral Currents

Other important measurements can be done in these facilities, also called B Factories [26]. Some b quark decays could be sensitive to exotic physics scenarios, especially those involving flavour-changing neutral currents (FCNC) like $b \rightarrow (s/d)\gamma$, $b \rightarrow (s/d)\ell^+\ell^-$ or $b \rightarrow (s/d)\nu\overline{\nu}$. The name refers to processes in which the original and the final quarks have the same electric charge, and the dilepton systems ($\ell^+\ell^-$

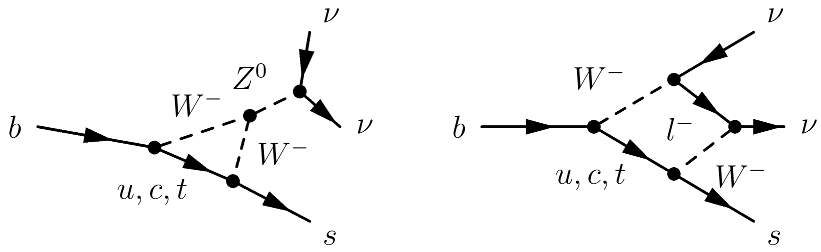

Figure 2–1: Examples of Feynman diagrams for the FCNC process $b \to s\nu\overline{\nu}$, a decay allowed in the SM [3].

or $\nu\overline{\nu}$) can be of any generation. FCNC processes are allowed in the SM in decays that contain at least one "loop", within which could appear exotic particles and interactions. The contribution from new physics could enhance significantly the relative rate, or the branching ratio $\mathcal{B}$, of these decays. The Feynman diagrams for the $b \to s\nu\overline{\nu}$ is shown in Figure 2–1.

In FCNC processes, the calculation of the decay rate has no analytical solution. However, it can be approximated using the method of effective Hamiltonian, which replaces the exact loop contribution by an expansion of operators, a process called Operator Product Expansion (OPE) [27]. The SM operators Q are weighted by Wilson coefficients C in the expansion of $b \to s\nu\overline{\nu}(\ell^+\ell^-)$:

$$H_{eff} = \frac{-G_f}{\sqrt{2}} V_{ts}^* V_{tb} (\sum_{i=1}^{10} C_i Q_i + C_L^{\nu} Q_L^{\nu}) + h.c. \tag{2.2}$$

While the OPE of $b \to s\ell^+\ell^-$ decays has three non-vanishing terms, the $b \to s\nu\overline{\nu}$ has only one, C_L^{ν}. This reduces significantly the theoretical uncertainty of the process, hence makes it more interesting to compare with experiment.

The branching ratios are predicted to be $\mathcal{B}(b \to d\nu\overline{\nu}) = 3.5 \times 10^{-5}$ and $\mathcal{B}(b \to s\nu\overline{\nu}) = (4.1^{+0.8}_{-1.0}) \times 10^{-5}$ [3] in the SM. There is currently no experimental upper limit on the former process, but an upper limit of $\mathcal{B}(b \to s\nu\overline{\nu}) < 6.4 \times 10^{-4}$ is set by the ALEPH collaboration [28]. New physics scenarios contain new operators in the Hamiltonian and affect the SM branching ratios by $\mathcal{O}(1)$ corrections [3].

2.3 The $B^- \to K^-\nu\overline{\nu}$ Process at *BABAR*

Because of quark confinement, the decay of the b occurs within a B hadron, and the final (s, d) can bind in various ways with the other quarks. In a B meson Factory like PEP-II, it is hard to search for all possible $b \to (s/d)\nu\overline{\nu}$ processes because of the two neutrinos that do not interact with the *BABAR* detector. The observed decays look like $B \to X_{d,s}+$ *missing energy*, where $X_{d,s}$ is any hadronic state containing an s or a d quark. Although it can be faked by other decays in which a particle falls outside the acceptance of the detector and is lost, some channels are easier to identify. In particular, the process $B^- \to K^-\nu\overline{\nu}$, predicted to compose about 9% of all $b \to s\nu\overline{\nu}$ decays [3], is well designated, as $K^\pm$ are well detected and identified by the *BABAR* detector.

As a three-body decay, the momentum of the $\nu\overline{\nu}$ system, q_μ, is kinematically constrained in the range $4m_\nu^2 \leq q^2 \leq (m_B - m_K)^2$, where m_B is the B meson mass of 5.28 GeV/c^2, m_K the $K^\pm$ mass of 494 MeV/c^2, and $m_\nu \sim 0$. In the SM, the decay rate is given by [3]

$$\frac{d\Gamma}{ds}(B^- \to K^-\nu\overline{\nu}) = \frac{G_f^2\alpha^2 m_B^5}{256\pi^5}|V_{ts}V_{tb}|^2\lambda_K^{3/2}(s)f_+^2(s)|C_L^\nu|^2 \qquad (2.3)$$

where s is $\frac{q^2}{m_B^2}$, G_f the Fermi constant, α the fine structure constant and $\lambda_K(s) = 1 + (\frac{m_K}{m_B})^4 + s^2 - 2s - 2(1+s)(\frac{m_K}{m_B})^2$. $|C_L^\nu|$ is the Wilson coefficient, which takes the value of -6.6 in the SM [27]. The form factor $f_+(s)$ is parametrized as

$$f_+(s) = \frac{f_+(0)}{1 - \sigma_1 s + \sigma_2 s^2}, \qquad (f_+(0), \sigma_1, \sigma_2) = (0.33, 0.0519, 0.00065) \tag{2.4}$$

in the "Godfrey Isgur" quark model [29]. As both $f_+^2(s)$ and $\lambda_K^{3/2}(s)$ are decreasing functions of s in the allowed range, $\frac{d\Gamma}{ds}(B^- \to K^- \nu\overline{\nu})$ predicts more low-q^2 decays, or, equivalently, more events in which the K^- has a high momentum.

The branching ratio is predicted to be $\mathcal{B}(B^- \to K^- \nu\overline{\nu}) = (3.8^{+1.2}_{-0.6}) \times 10^{-6}$ in the SM, but could go up to $\mathcal{O}(10^{-5})$ in new physics scenarios [3]. The theoretical uncertainty is an order of magnitude smaller than that of the $b \to s\nu\overline{\nu}$ process and comes from the form factors, the Wilson coefficient the V_{CKM} matrix elements and the mass of the t quark.

CHAPTER 3
The PEP-II B Factory

The main components of the *BABAR* project, based at the Stanford Linear Accelerator Center (SLAC), are the asymmetric PEP-II B Factory, which consists of a linear accelerator, two storage rings plus an interaction region (IR), and the *BABAR* detector, surrounding the IR (Figures 3–1 and 3–2). They are briefly described here, and more details can be found in the technical design reports [30] [31].

3.1 PEP-II

Electrons are injected in a linear accelerator and enter one of the PEP-II storage rings at 9.0 GeV. The accelerator also extracts a fraction of high-energy electrons to generate positrons, which are also accelerated and injected in the second storage ring with a beam energy of 3.1 GeV. e^+e^- beams collide head-on at a center-of-mass (CM) energy of 10.58 GeV, corresponding to the mass of the $\Upsilon(4S)$. The CM frame has a Lorentz boost of $\beta\gamma = 0.56$ with respect to the laboratory, as prescribed for measuring time-dependent CP violation parameters (see section 2.2.1).

In order to collide the two beams in the IR, dipolar (B1) and quadrupolar (Q1) bending magnets must be placed a only a few cm away from the interaction point (see Fig. 3–2). This limits the angular acceptance of the detector and causes beam backgrounds. For example, in the case of a radiative Bhabha event ($e^+e^- \rightarrow e^+e^-\gamma$), one of the lepton can interact with a B1 magnet, generating many particles via a cascade of Bremsstrahlung radiation ($e^{\pm} + atom \rightarrow e^{\pm} + atom + \gamma$) and $e^{+}e^{-}$ pair-production (EM shower). These shower debris can finally make their way back into the detector and interact with its components.

As of August 2006, a luminosity of 380 fb^{-1} of data were recorded since February 2000 by the *BABAR* detector at the $\Upsilon(4S)$ resonnance, corresponding to almost 400 million $B\overline{B}$ events. Another data sample of 34 fb^{-1} were recorded at a CM energy about 40 MeV below the $\Upsilon(4S)$ mass in order to study background events. These two data samples are refered to as *onpeak* and *offpeak* data respectively. However, the current analysis is based on the data recorded as of July 2004, corresponding to 208.73 fb^{-1} and 21.49 fb^{-1} of onpeak and offpeak data respectively.

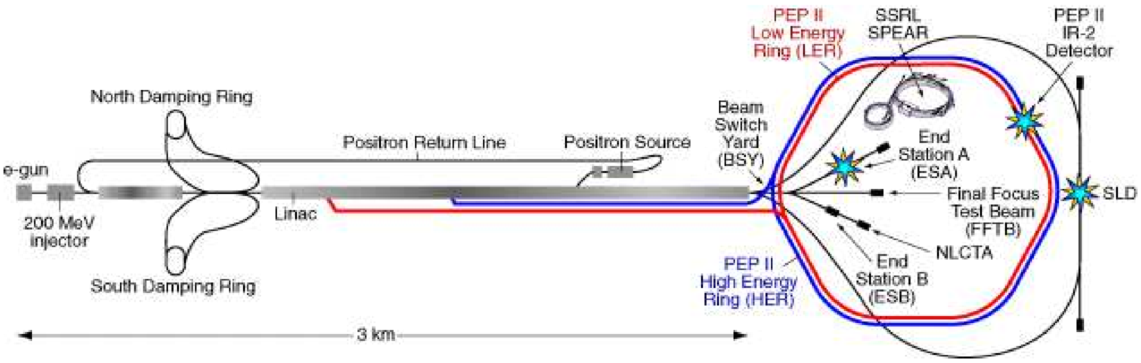

Figure 3–1: PEP-II B Factory [33].

3.2 The *BABAR* Detector

One of the main goals of the *BABAR* detector is to reconstruct and measure the decay channels of the B meson. For that purpose, it must have a large angular acceptance ; a good vertex resolution ; a high reconstruction efficiency and resolution for charged particles with momentum between 60 MeV/c and 9 GeV/c, and photons with energy between 20 MeV and 4 GeV; and an accurate method to identify $K^{\pm}$, $\pi^{\pm}$, $e^{\pm}$, $\mu^{\pm}$ and protons at the 4σ level.

The five main components of the detector are the silicon vertex tracker (SVT), the drift chamber (DCH), the detector of internally reflected Cherenkov light (DIRC), the electromagnetic calorimeter (EMC) and the instrumented flux return (IFR) [32].

BABAR has also a 2-level trigger system that filters many beam background events produced by PEP-II. The first trigger level (L1) rejects events which do not satisfy basic requirements on the tracks present in the DCH and on the clusters in the EMC. The information about the surviving events is then passed to the next trigger level (L3), which makes a more refined trim based on the full detector output. Selected events are finally recorded in the "event store", waiting to be analyzed.

Except for the IFR, all the *BABAR* components mentioned above are surrounded by a 1.5 T magnetic field that points in the direction of the e^- beam (forward direction), generated by a super-conducting solenoid. The trajectory of charged particles curves in the magnetic field, revealing information about their charge and momentum. Because the beam energies are unequal, the detector is also asymmetric in shape. Figure 3–2 shows the different parts of the *BABAR* detector.

3.2.1 The Silicon Vertex Tracker

The SVT consists of 5 layers of double-sided silicon strips that interact with charged particles (left part of Fig. 3–3). It measures the z and ϕ coordinates of each charged particle passing through a layer, as well as the energy loss ($\frac{dE}{dx}$) in that *hit*, and has a polar coverage extending from 30° forward to 20° backward. Sensor strips are organized in modules that are disposed around the beam pipe such that there

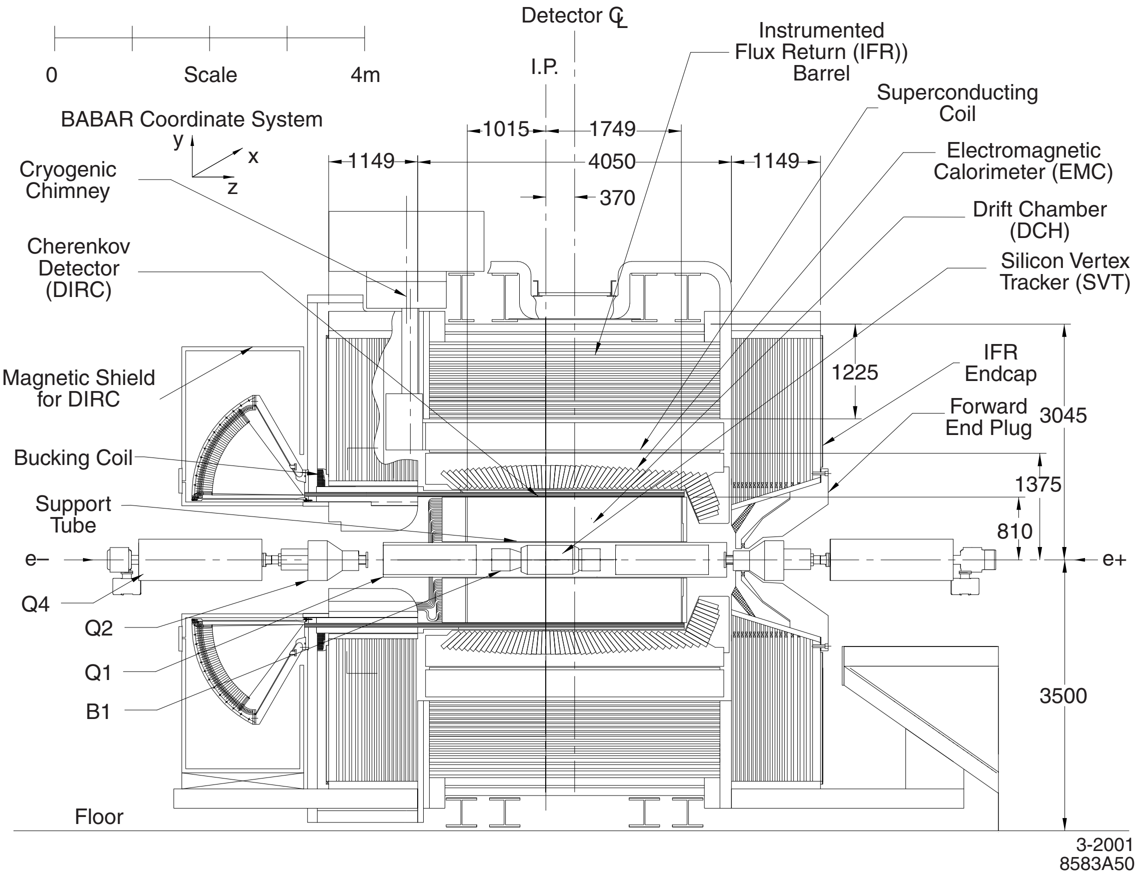

Figure 3–2: Longitudinal view of the *BABAR* detector, with PEP-II bending magnets near the interaction point (IP) [31].

is an overlap at each interstice, hence it prevents the loss of particles between two modules (right part of Fig. 3–3).

The outer two layers are well suited to measure the trajectories of low-momentum charged particles, with a spatial resolution of about 40 μm. The three inner layers have a spatial resolution of 10-15 μm and the position of the B meson decay vertex can be known to better than 80 μm.

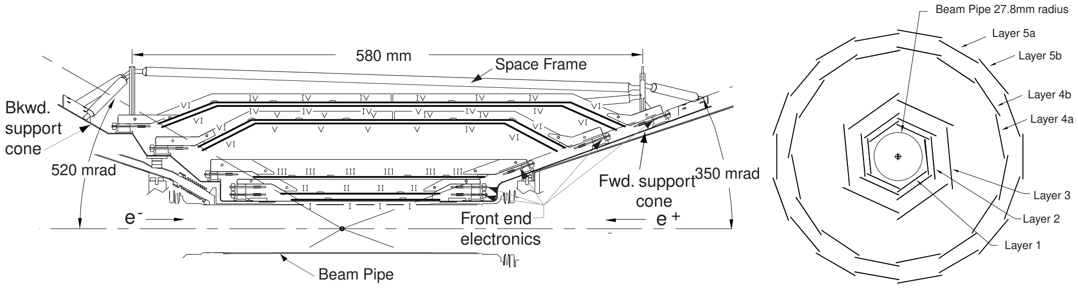

Figure 3–3: Longitudinal (left) and sectional (right) views of the SVT [31].

The energy deposition in a silicon wafer depends on the momentum and on the nature of the particle, and that information is contained in the central value of each signal pulse. This is called a $\frac{dE}{dx}$ measurement, it can be sampled up to ten times per particle, and can be compared with the measured distribution for different types (see left part of Fig. 3–4) in order to identify the particle .

3.2.2 The Drift Chamber

The DCH is a 5.2 m^3 cylinder surrounding the SVT, filled with a gas mixture of helium and isobutene and 28768 electric wires organized in 7104 hexagonal cells, grouped in 40 layers. The wires in 24 of the layers are placed at a small angle to create a stereo effect and permit a z position measurement. A typical cell has 6 wires kept at ground potential, surrounding one "sense" wire kept at 1960 V : this regular arrangement results in a stable electric field pointing towards the central wire (see right part of Fig. 3–4).

A charged particle passing in the DCH can ionize the gas in a few cells, and the free electrons thus created rapidly drift towards the sense wires. The charges are detected, and we can measure the ϕ and z coordinates with a resolution of

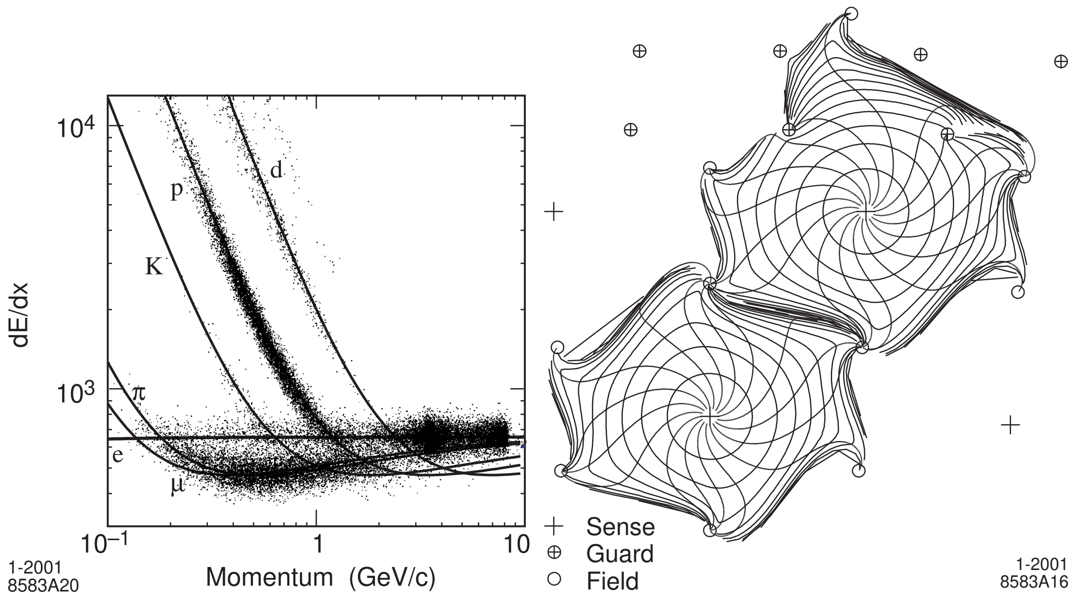

Figure 3–4: Left : $\frac{dE}{dx}$ measurement in the DCH for beam background events, compared with theoretical prediction by Bethe-Bloch (solid curve) [34] [31]. Right : Electric field configuration of two adjacent drift cells in layers 3 and 4 of the DCH [31].

about 1 mm. The total charge deposited by ionized electrons results in another $\frac{dE}{dx}$ measurement, which is sampled generally 20-40 times per particle.

A *track* is what the *BABAR* detector reconstructs using the information from both the SVT and the DCH. The tracking system reconstructs the full trajectories and measures the momentum of all tracks, with an efficiency between 93 % and 98 % for tracks with momentum p above 200 MeV/c, depending on θ_{trk}, the angle between the tracks and the beam pipe. The efficiency goes to 98.8%, and the resolution varies between 0.5 % and 1.0 % for tracks with $1 < p < 4\,\mathrm{GeV}/c$.

3.2.3 The Detector of Internally Reflected Cherenkov Light

The DIRC is completely dedicated to the particle identification, and takes advantage of the Cherenkov radiation that is emitted by particles whenever their speed is higher than the speed of light in a material. The angle at which the photons are emitted is a function of the speed (v) of the particle. By combining the result with the momentum (p) measured by the tracking system for the same particle, we can extract the mass m using the relation $p = mv$, and hence determine the particle type.

The DIRC material is a set of 144 bars made of fused synthetic silica, grouped in 12 bar boxes of 12 bars each. Photons emitted inside the bar propagate towards the end, via multiple total internal reflections from the bar faces, then they pass through a water tank whose wall is filled with photo-multiplier tubes (PMTs) that detect them (see Figures 3–5 and 3–6).

The number of Cherenkov photons emitted for a single track varies between 20 and 60, depending on θ_{trk}, and these produce a partial ring that is identify by a pattern recognition algorithm. The two Cherenkov angles θ_c and ϕ_c, the time of detection and the number of photons are used to estimate the likelihood of $K^{\pm}$, $\pi^{\pm}$, $e^{\pm}$, $\mu^{\pm}$ and proton hypothesis. For tracks with momentum over 700 MeV/c, it provides a $K^{\pm}$ selection efficiency of 96.2 $\pm$ 0.2 % with only 2.1 % of $\pi^{\pm}$ misidentification, and a $K^{\pm}$-$\pi^{\pm}$ separation of 4.2σ. The angular coverage extends to 25.5° in the forward direction and 38.6° in the backward direction.

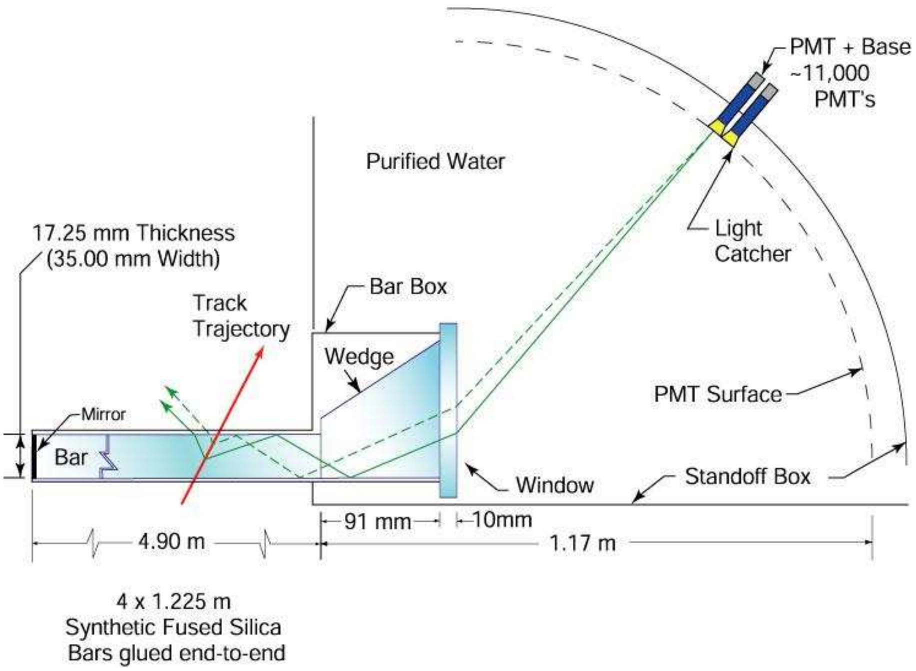

Figure 3–5: Longitudinal view of the path of a Cherenkov photon in the DIRC [35].

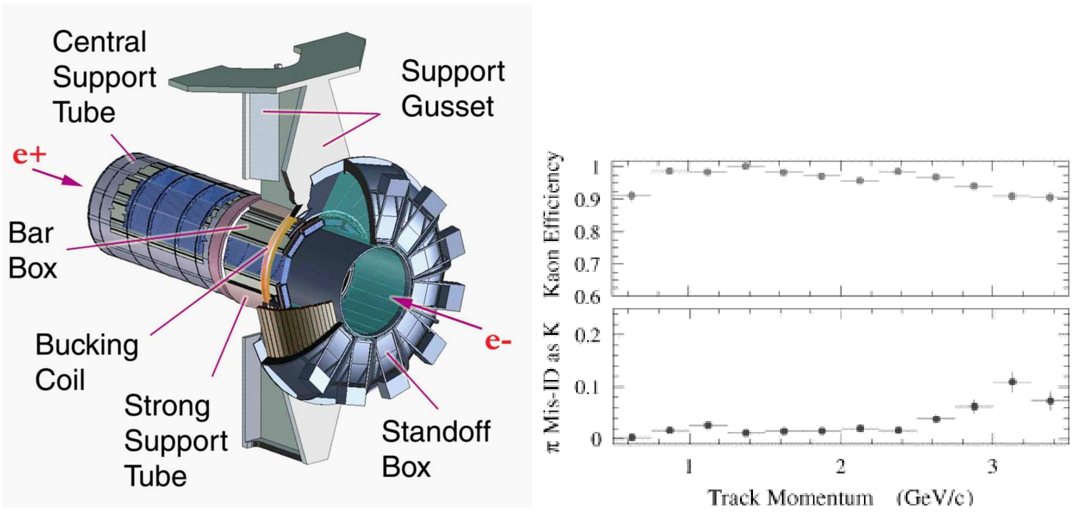

Figure 3–6: Left : The DIRC geometry [36]. Right : The $K^{\pm}$-$\pi^{\pm}$ separation efficiency and the rate at which $\pi^{\pm}$ are mis-identified as $K^{\pm}$ in a sample of $D^0 \to K^-\pi^+$, as a function of the track momentum [31].

3.2.4 The Electromagnetic Calorimeter

The EMC is made of thallium-doped cesium iodide crystals (CsI(Tl)), designed to provoke EM showers from photon and electron interactions, and measure the energy and shape of these showers. It has a barrel section containing 5760 crystals, and an end-cap section made of 820 crystals, for a total angular coverage of $15.8°$ and $38.2°$ in the forward and backward directions respectively (see Fig. 3–7).

An EM shower typically extends over a few adjacent crystals, forming a *cluster*. The spatial energy distribution of a cluster can have two local maxima, or bumps, which are assumed to come from individual particles. A bump is identified as a charged particle if the trajectory of a track points toward its centroid. Otherwise, it is considered as coming from a neutral particle. The EMC is designed to detect clusters with energy between 20 MeV to 9 GeV with a resolution of $\frac{\sigma_E}{E} = \frac{2.32\%}{\sqrt[4]{E}} \oplus 1.85\%$.

The energy and momentum (E and p) of a track can be combined to measure (E/p), a variable that identifies electrons with an efficiency of 94.8 % with only 0.3 % of $\pi^{\pm}$ misidentification in the range $0.5 < p < 2.0\,\mathrm{GeV}/c$.

3.2.5 The Instrumented Flux Return

The IFR is designed to detect neutrons, K_L^0 and $\mu^{\pm}$. It is compartmented in a barrel and two end caps, and is made with 18 steel plates between which are installed resistive plate chambers (RPC). These consist in small pockets of gas mixture (Argon, Freon and isobutane) enclosed between two graphite sheets, which are kept at potential difference of 8 kV. Sensor strips placed just behind the graphite and measure the x and y coordinates.

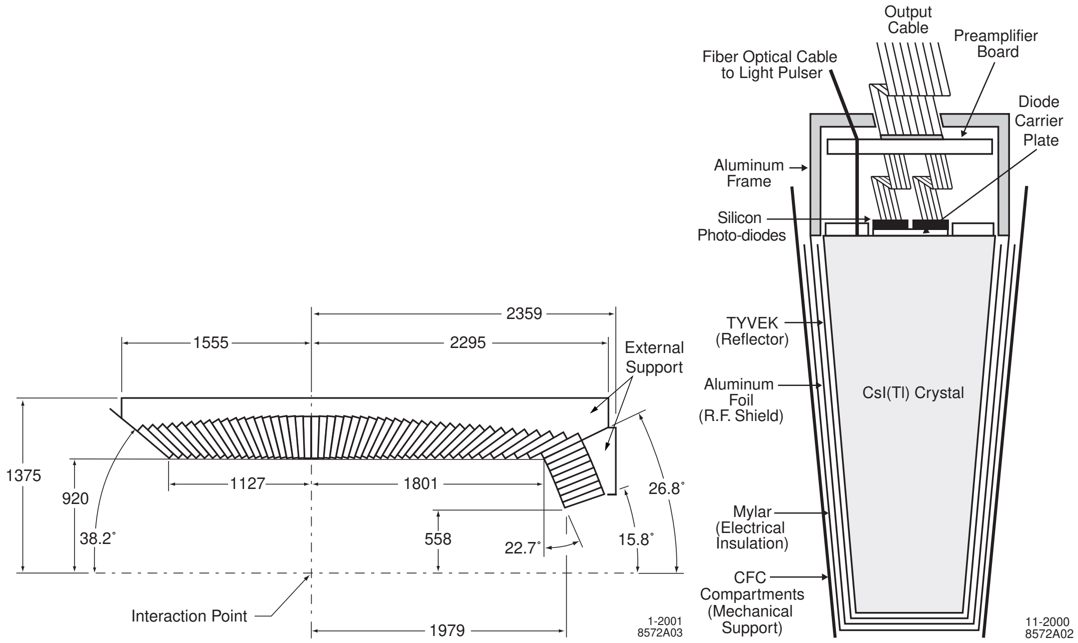

Figure 3–7: Left : Longitudinal half-section of the EMC [31]. The dimensions are in mm. Right : Individual CsI(Tl) crystal [31].

A $\mu^{\pm}$ passing through a chamber ionizes the gas, the ions are attracted by the electric field and thus drift towards the strips. Neutral hadrons produce hadronic showers in the steel, and the charged debris are detected by the strips. IFR clusters that are associated with tracks from the tracking system are identified as a $\mu^{\pm}$, else they are considered as neutral hadrons. Almost 53000 different channels are available to identify the location of the interaction.

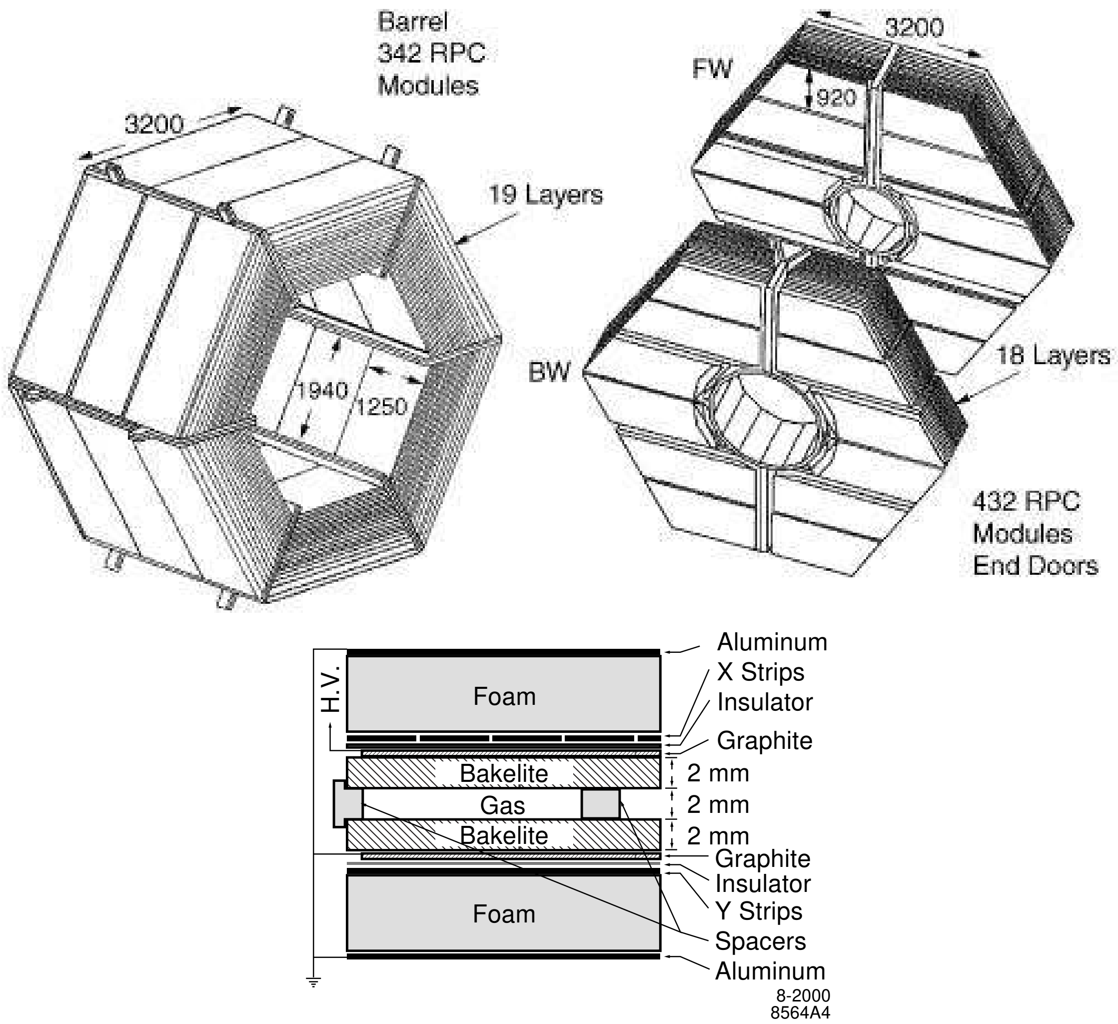

Figure 3–8: Barrel and end caps of the IFR, with a schematic view of a RPC [31]. Only one graphite sheet is kept at a high voltage (H.V.). Dimensions are in mm.

CHAPTER 4
Analysis

We search for the process $B^- \to K^-\nu\overline{\nu}$ in about 230 million of $\Upsilon(4S) \to B\overline{B}$ data events recorded by the *BABAR* detector, and attempt to set an upper limit on its branching ratio. As presented in Table 2–3, the main event types produced by PEP-II are $c\overline{c}$, $s\overline{s}$, $d\overline{d}$, $u\overline{u}$, $\tau^+\tau^-$, $\mu^+\mu^-$, e^+e^- and $b\overline{b}$, whose $\Upsilon(4S)$ component decays exclusively into B^+B^- and $B^0\overline{B}^0$ in equal proportion [6]. The specific behavior of these different event types is studied within a *BABAR* detector simulation based on `GEANT4` [38]. We also generate samples of $B^- \to K^-\nu\overline{\nu}$ "signal" events and observe how such processes would look in the detector.

The objective is to apply a series of selection requirements on data events in order to accept $B^- \to K^-\nu\overline{\nu}$ events with the largest efficiency, while rejecting a maximum amount of the other non-signal, or "background" events. Our strategy is to select events in which we can reconstruct a B^+ meson from clean decays of the type $B^+ \to D^{(*)0}X^+$, where X^+ is a set of hadrons ($K^\pm$, K^0_S, $\pi^\pm$ or π^0), and to look in the rest of the event for a single high momentum K^-, produced by the decay $B^- \to K^-\nu\overline{\nu}$. We recall that the charge conjugate modes are implied through this document. The first set of requirements thus concerns the reconstructed B^+, and a second set puts constraints on the rest of the event, a procedure called the recoil analysis method [37].

In a perfect environment, the signal K^- would be the only particle not used in the reconstruction of the B^+. In practice however, the K^- is not alone :

- Low energy tracks, mainly $\pi^\pm$ or $e^\pm$, are coming from a mis-reconstruction of the B^+ or from the pair-production of a background photon,
- Low energy clusters are mostly coming from hadronic "split-off" in the EMC. This happens because hadronic showers often produce a main cluster plus a few isolated bumps, which are consequently reconstructed as photons.

Since background events typically have higher particle multiplicity, we get rid of many unwanted events by rejecting events in which the combined energy from these low energy tracks and clusters exceeds the level that is expected in typical signal events. We finally reject events that contains photon pairs that are consistent with π^0 candidates and that were not incorporated in the reconstruction of the B^+.

The calculation of the branching ratio involves four quantities :

1. ε_{tot}, the efficiency at reconstructing a $B^- \to K^-\nu\overline{\nu}$ event
2. $N_{B^+B^-}$, the total number of B^+B^- pairs in the data sample
3. N_{obs}, the number of data events observed at the end
4. N_{bg}, an estimate on the number of background events

The branching ratio is :

$$\mathcal{B}(B^- \to K^-\nu\overline{\nu}) = \frac{N_{obs} - N_{bg}}{2 \times N_{B^+B^-} \times \varepsilon_{\text{tot}}} \tag{4.1}$$

and the best results are obtained when ε_{tot} is maximized and N_{bg} minimized. Since we use samples of simulated events in our estimation of these two numbers, we must make sure that the simulation agrees with the data. Observed discrepancies are either accounted for by applying corrections to the MC samples or by including them in systematic uncertainties.

After applying consecutively a few selection criteria, the statistics of the data start to go low, and the signal could potentially become dominant in specific regions of some plots. It would thus be easy to boost N_{obs} by playing with some selection requirements on a event-by-event basis, and the final result would thus be "arranged". In order to avoid this sort of concious or unconcious bias, we explicitely avoid plotting any onpeak datum unless there is at least 10 times as many background events as potential signal in any bin of any histogram during the optimization phase of the analysis. This is done by comparing the background distribution with an amplified version of the signal, assuming a branching ratio equal to 10 times the last upper limit from the previous *BABAR* analysis. This amplified signal distribution is only visible in some histograms, and the regions to be blinded are found when it becomes more important than the background. Once the selection procedure is finalized, the analysis is manually "un-blinded" to reveal the presence or absence of a signal within the sensitive region of these histograms. The blinding strategy does not apply to the sample of 80.03 fb^{-1} that has been analyzed in the previous measurement of $\mathcal{B}(B^- \to K^-\nu\overline{\nu})$ by the *BABAR* collaboration [1]. In the current analysis, this sample reveals a discrepancy between the simulation and the data samples, and we believe that this behavior is present in the full sample. Consequently, we do not attempt to extract a limit from the rest of the data sample in this analysis.

In this chapter, we explain how we estimate $\varepsilon_{\mathrm{tot}}$ and N_{bg}, starting with a description of the different data types used (section 4.1), and then explaining the method that allows the reconstruction of $B^+ \to D^{(*)0}X^+$ vs $B^- \to K^-\nu\overline{\nu}$ events (sections 4.3 and 4.4). The statistical and systematic uncertainties on various quantities are shown in their context through the chapter, but the full error analysis related to the measurement of the branching ratio is presented in section 4.6. Section 4.7 describes how we deal with the observed discrepancy, why we cannot set a new limit on the branching ratio, and we give recommendations for the next analysis.

4.1 Data and Monte Carlo Samples

This analysis is based on onpeak and offpeak data recorded by the *BABAR* detector, and on 10 samples of simulated events produced by the *BABAR* Simulation Development Group [39]. Since $\mu^+\mu^-$ and e^+e^- are well filtered by the detector triggers, their contributions are neglected in this analysis. B^+B^-, $B^0\overline{B}^0$, $c\overline{c}$, $s\overline{s}$, $d\overline{d}$, $u\overline{u}$ and $\tau^+\tau^-$ events are generated at the interaction point and are allowed to decay via all known channels. Such samples, whose decay process are unconstrained, are labeled "generic" samples. ($s\overline{s}$, $d\overline{d}$, $u\overline{u}$) events are simulated together as "uds", in proportions corresponding to their relative cross-sections, and the L1 and L3 trigger requirements are applied explicitely on all generated events, so that the MC-data samples are compatible.

The probability of each decay channel is weighted by the observed branching ratio, and for individual events, the generator "rolls the dice" following the probability distribution. In the case of decays not yet observed, the branching ratio is chosen following a theoretical prediction. This Monte Carlo (MC) method is also applied to the dynamics of the decays : the momentum spectrum of each decay product corresponds to an experimental or theoretical distribution. As for data events, the virtual response of the detector to these MC events is recorded in the event store.

In signal MC events, the B^- meson is restricted to decay into the signal channel $B^- \to K^- \nu\overline{\nu}$. The B^+ meson is either allowed to decay to anything ("generic" signal MC) or restricted to decay via specific hadronic channels ("cocktail" signal MC): $B^+ \to \overline{D}^{(*)0}\pi^+$ or $B^+ \to \overline{D}^{(*)0}(\rho/a_1)^+$. We use samples of generic $B^- \to K^{*-}\nu\overline{\nu}$ and $B^- \to \pi^-\nu\overline{\nu}$ in order to cross-check the B^+ reconstruction algorithm. The size of the data and MC samples used in this analysis is listed in Table 4–1.

Table 4–1: Data and Monte Carlo samples used in this analysis [40]. The equivalent luminosities of generic and cocktail signal events depend on the assumed branching ratios.

Event Type	Number of Events	Equivalent Luminosity
OnPeak data Runs 1-4	3 008 071 549	208.73 fb^{-1}
OffPeak data Runs 1-4	284 113 757	21.49 fb^{-1}
$B^+B^- \to$ anything	584 026 000	1 112.43 (fb^{-1})
$B^0\overline{B}^0 \to$ anything	540 742 000	1 029.98 (fb^{-1})
$c\overline{c} \to$ anything	425 792 000	327.53 (fb^{-1})
$uds \to$ anything	677 217 000	324.03 (fb^{-1})
$\tau^+\tau^- \to$ anything	346 636 000	368.76 (fb^{-1})
$B^- \to K^-\nu\overline{\nu}$ vs $B^+ \to$ anything	285 000	-
$B^- \to K^-\nu\overline{\nu}$ vs $B^+ \to \overline{D}^{(*)0}\pi^+$	127 000	-
$B^- \to K^-\nu\overline{\nu}$ vs $B^+ \to \overline{D}^{(*)0}(\rho/a_1)^+$	123 000	-
$B^- \to K^{*-}\nu\overline{\nu}$ vs $B^+ \to$ anything	235 000	-
$B^- \to \pi^-\nu\overline{\nu}$ vs $B^+ \to$ anything	57 000	-

4.2 Particle Reconstruction

In this section, we describe how we reconstruct the different particle types produced by various decays. We use a bottom-up approach, starting with the final state particles detected ($e^{\pm}$, $K^{\pm}$, $\pi^{\pm}$, γ, ...), then combining them into intermediate states (K_S^0, D^0, $D^{\pm}$...), and finally reconstructing the B meson.

Since we do not observe particles directly but only traces of their passage in the detector, we can only infer their true nature. As a consequence, tracks and clusters are considered as *candidates* for charged and neutral particles respectively, and their identity is known only to a certain level of confidence.

4.2.1 Reconstructing the Decay Products

By default, tracks are considered as $\pi^{\pm}$ candidates, since these particles compose about 90 % of all tracks produced at PEP-II. K_S^0 candidates are reconstructed whenever the combined 4-momentum of a $\pi^+\pi^-$ pair has an invariant mass in the range $0.47 < m_{\pi^+\pi^-} < 0.52$ GeV/c^2. A track is identified as a $K^{\pm}$ using information from the $\frac{dE}{dx}$ measurements in the SVT and DCH, as well as the Cherenkov angles in the DIRC. Clusters are required to have a total energy above 20 MeV in order to be considered as photon candidates, and two clusters are combined to form a π^0 candidate if their combined mass is in the interval 0.115 - 0.150 GeV/c^2. We recall from Chapter 3 that an EMC cluster with a track pointing to it is considered as a "charged candidate", otherwise the cluster is considered as a "neutral candidate".

D^0 candidates are reconstructed via the channels $D^0 \to K^-\pi^+$, $D^0 \to K^-\pi^+\pi^0$, $D^0 \to K^-\pi^+\pi^+\pi^-$ or $D^0 \to K_S^0\pi^+\pi^-$, and can be combined with a γ or a π^0 to produce a D^{*0} candidate. Similarly, D^- candidates are reconstructed via the channels $D^- \to (K\pi\pi)^-$, $D^- \to (K\pi\pi)^-\pi^0$, $D^- \to K_S^0\pi^-$, $D^- \to K_S^0\pi^-\pi^0$ or $D^- \to K_S^0(\pi\pi\pi)^-$, and they can be combined with a π^0 to form a D^{*-}.

4.2.2 Reconstructing the B Mesons

As explained in section 2.3 and at the beginning of Chapter 4, the $B^- \to K^-\nu\overline{\nu}$ decay cannot be fully reconstructed due to the undetected $\nu\overline{\nu}$ system, but by reconstructing the B^+ companion, the signal process can leave an observable signature : a single high-momentum K^- (see Figure 4–1).

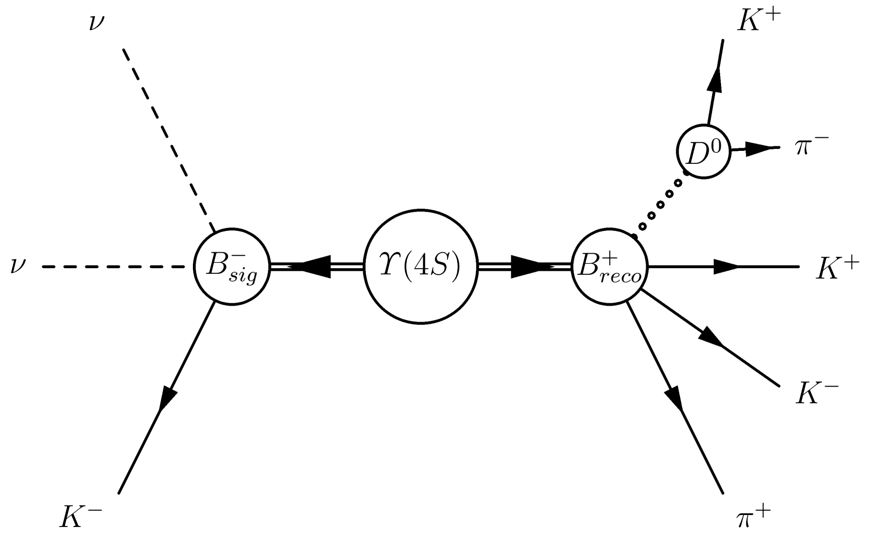

Figure 4–1: Schematic representation of a signal $B^- \to K^-\nu\overline{\nu}$ event, in which the B_{reco} decays in a K^+, a K^-, a π^+ and a $\overline{D}^0$, which in turn decays in a K^+ and a π^-.

To ensure that this signature is clean enough, the reconstructed B^+, or B_{reco}, is required to decay into one of a few high-purity and high-efficiency channels. Namely, B_{reco} candidates are reconstructed exclusively via the processes $B^+ \to D^{(*)0}X^+$, where X^+ is a combination of up to 5 ($\pi^\pm + K^\pm$), up to 2 π^0 and 1 K^0_S. Similarly, B^0 candidates are reconstructed via the decays $B^0 \to D^{(*)-}X^+$. Cocktail signal events are specially designed to be easily reconstructed by this method.

In the reconstruction of the B_{reco}, all the allowed X^+ systems are considered as hypotheses. For each event, there is thus different B^+ and/or B^0 candidates, among which the "best" B_{reco} is selected based on two criteria. The first is that in the CM frame, the energy of the candidate E^*_B must be within 200 MeV of the beam energy E^*_{beam}. The second is that the invariant mass of the B_{reco} candidate must be close to the nominal mass $m_B = 5.28\,\text{GeV}/c^2$. For that calculation, E^*_B is replaced by E^*_{beam} in order to improve the resolution, and we demand that this "Energy-Subsituted mass" satisfies $5.220 < m_{\text{ES}} < 5.230\,\text{GeV}/c^2$, where $m_{\text{ES}} = \sqrt{{E^*_{\text{beam}}}^2 - p^*_B}$ and p^*_B is the momentum of the candidate B meson in the CM frame. If more than one B candidates are reconstructed, the one with the smallest $|E^*_B - E^*_{\text{beam}}|$ is chosen. This procedure is called the semi-exclusive reconstruction of B mesons [41]

Table 4–2 summarizes the decay channels used in the reconstruction of various candidates. Even though there is no net geometrical separation, particles used in the reconstruction of the B^+ meson are said to be on the *reco side*, while those left over are on the *signal side* of the event and they are used to reconstructed the $B^- \to K^-\nu\overline{\nu}$ process.

Table 4–2: Mass constraints used in reconstruction of intermediate states; allowed channels and selection criteria for the best B_{reco}

Decay Channels	Mass Constraints
$\pi^0 \to \gamma\gamma$	$0.115 < m_{\pi^0} < 0.150\ \mathrm{GeV}/c^2$
$K^0_S \to \pi^+\pi^-$	$0.473 < m_{K^0_S} < 0.523\ \mathrm{GeV}/c^2$
$D^0 \to K^-(\pi^+, \pi^+\pi^+\pi^-)$	$1.850 < m_{D^0} < 1.880\ \mathrm{GeV}/c^2$
$D^0 \to K^-\pi^+\pi^0$	$1.840 < m_{D^0} < 1.890\ \mathrm{GeV}/c^2$
$D^0 \to K^0_S\pi^+\pi^-$	$1.845 < m_{D^0} < 1.885\ \mathrm{GeV}/c^2$
$D^{*0} \to D^0(\pi^0, \gamma)$	$0.140 < m_{D^{*0}} - m_{D^0} < 0.144\ \mathrm{GeV}/c^2$
$D^- \to (K\pi\pi)^-$	$1.849 < m_{D^-} < 1.889\ \mathrm{GeV}/c^2$
$D^- \to K^0_S\pi^-$	$1.849 < m_{D^-} < 1.889\ \mathrm{GeV}/c^2$
$D^- \to K^0_S(\pi\pi\pi, \pi^-\pi^0)$	$1.839 < m_{D^-} < 1.899\ \mathrm{GeV}/c^2$
$D^- \to (K\pi\pi)^-\pi^0$	$1.839 < m_{D^-} < 1.899\ \mathrm{GeV}/c^2$
$D^{*-} \to D^-\pi^0$	$0.137 < m_{D^{*-}} - m_{D^-} < 0.147\ \mathrm{GeV}/c^2$
$B^+ \to D^{(*)0}X^+$	
$B^0 \to D^{(*)-}X^+$	
$X^+ = a(K^+ + \pi^+) + b\pi^0 + cK^0_S$ with a, b and $c \leq 5$, 2 and 2 respectively	

Best B_{reco} selection criteria
$\lvert E^*_B - E^*_{\mathrm{beam}}\rvert < 0.2\ \mathrm{GeV}$
$5.220 < m_{\mathrm{ES}} < 5.230\,\mathrm{GeV}/c^2$

4.2.3 Types of Background Events

In a perfect detector environment and with a perfect B_{reco} reconstruction, the m_{ES} (energy-subsituted mass) distribution for a $B\overline{B}$ events would be a sharp peak centered at m_B. However, there is an uncertainty of 2.6 MeV on E^*_{beam}, and, even more important, the B_{reco} reconstruction algorithm can select events that are just random combinations of tracks and clusters, thus reducing the value of m_{ES}. The unphysical B_{reco} types relevant for this analysis are classified in three categories [23]:

1. *Continuum background* (i) : No $\Upsilon(4S)$ is produced, the collision is a $e^+e^- \rightarrow \tau^+\tau^-$ event, but the hadrons coming from the decays of the $\tau^+\tau^-$ leptons are randomly combined by the algorithm into a B_{reco} candidate.
2. *Continuum background* (ii) : No $\Upsilon(4S)$ is produced, the collision is a $e^+e^- \rightarrow (u\overline{u}, d\overline{d}, s\overline{s}, c\overline{c})$ event, but these quarks hadronize and produce $K^{\pm}$, $\pi^{\pm}$, etc, that are randomly combined to fake a $B^+ \rightarrow D^{(*)0}X^+$ channel. Note that $D^{(*)0}$ can be real in the $c\overline{c}$ MC sample.
3. *Combinatorial background* : $\Upsilon(4S)$ is produced and decays into B^+B^- or $B^0\overline{B}^0$, however the best B_{reco} candidate selected by the reconstruction algorithm is not the real B meson, but a random combination of tracks and clusters that happens to fake a $B^+ \rightarrow D^{(*)0}X^+$ decay.

The m_{ES} distribution of B_{reco} samples is thus populated by continuum and combinatorial backgrounds, on top of which lies a "peaking component" from correctly reconstructed $B\overline{B}$ events, as shown in Figure 4–2. In the histograms contained in this chapter, onpeak and offpeak data are represented by full and hollow circles respectively, while generic MC samples are shown as grey regions. The signal MC sample is shown in white, above the background distributions, always with the same x-axis range and units. All generic MC samples are stacked on each other, and we finally superimpose on these histograms the data distribution. The luminosities of offpeak data and generic MC events are scaled to the onpeak luminosity of $208.73\,\mathrm{fb}^{-1}$, and the CM energy of the offpeak data is scaled to that of the onpeak. Unless otherwise specified, the signal events are also scaled to $208.73\,\mathrm{fb}^{-1}$ assuming a branching ratio of $< 5.2 \times 10^{-5}$, corresponding to the last experimental upper limit obtained at *BABAR* [1].

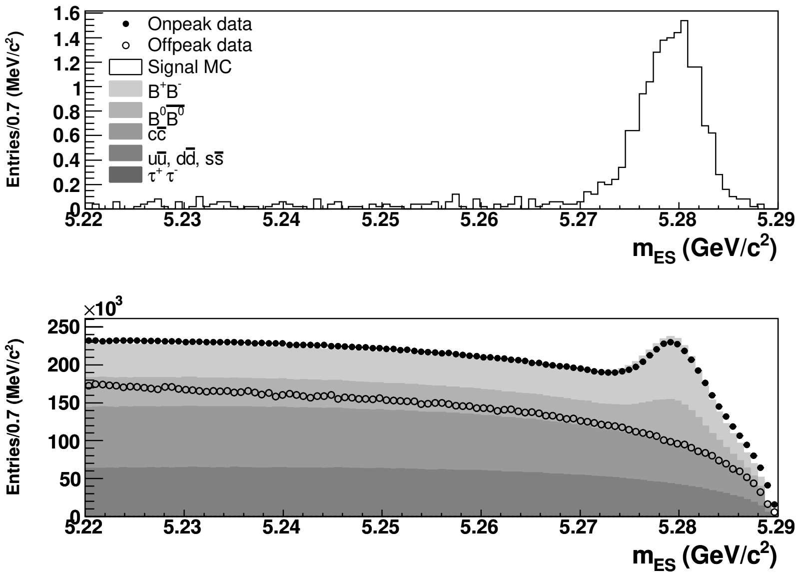

Figure 4–2: m_{ES} distribution for skimmed events. Both B^+B^- and $B^0\overline{B}^0$ contain a peaking component near the nominal mass of the B meson of 5.28 GeV/c^2. Such a small number of $\tau^+\tau^-$ events survive the skim that they are nearly impossible to observe on most plots. The skim is explained in section 4.3.1. To avoid surcharging the figures, from now on the title of the x-axis (i.e. m_{ES} (GeV/c^2)) will appear only once, under the bottom part of the figure.

4.3 Reconstructed Side Selection

This section describes the skim selection and the restrictions we apply on the B_{reco} in order to reject most of the non-peaking events selected by the algorithm. Candidates selected by these requirements are labeled B_{tag}.

4.3.1 Skim Selection

We first skim all events in order to suppress the $e^+e^- \to \tau^+\tau^-$ events. Most of these interactions produce a low number of charged tracks in the detector, and have a particular jet-like shape. They can be filtered out by requiring that there is at least three tracks in the detector, and that R2, the ratio of the zeroth to the second Fox-Wolfram moments [42], calculated with both tracks and clusters, is smaller than 0.5. Less than 0.002% of these $\tau^+\tau^-$ events survive the skim.

4.3.2 B_{tag} Selection

As mentioned in section 4.2.2, the best B_{reco} candidate can be either neutral or charged. Following our strategy, we are looking for a reconstructed B^+ against which we search for a $B^- \to K^-\nu\overline{\nu}$ event, hence the first step is to require the B_{reco} to have a charge Q_{tag} of ±1. The Q_{tag} distribution is plotted in Figure 4–3 for skimmed events, and we observe that this first criteria rejects roughly a third of the background events.

The goal of the second step is to suppress the continuum background. It uses the fact that the initial quarks in these events carry a lot of kinetic energy, hence their decay products tend to be confined in two back-to-back jets. The distribution of θ_T, the angle between the thrust axis of the selected B_{reco} and the thrust axis of all the signal side particles, has a strong peak at $\pm180^o$ for uds, $c\overline{c}$ and $\tau^+\tau^-$ events. On

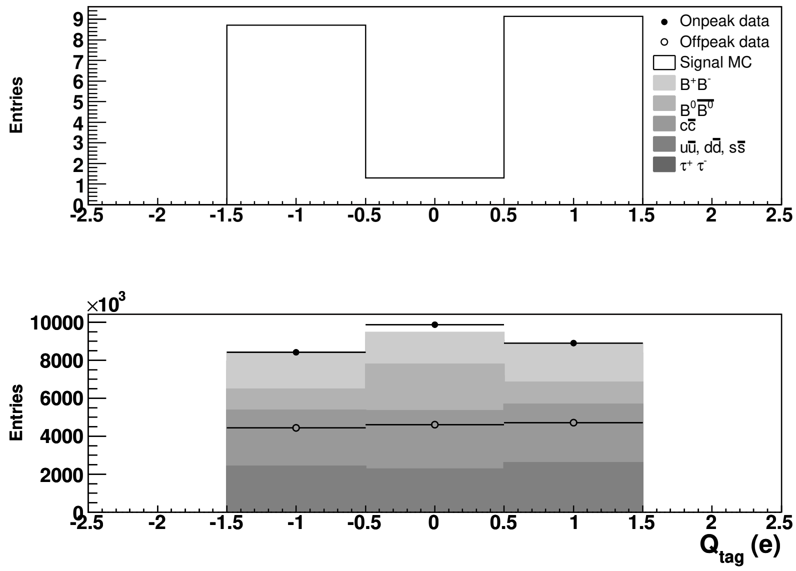

Figure 4–3: Q_{tag} distribution for skimmed events. The B^+B^- and signal CM events with $Q_{\text{tag}} = 0$ are purely combinatorial background. We require $Q_{\text{tag}} = \pm 1$.

the contrary, since $m_B \simeq m_{\Upsilon(4S)}/2$, the two B mesons in a $B\overline{B}$ event are produced with very little kinetic energy in the CM frame, hence the spatial distribution of their decay is more isotropic. Figure 4–4 presents the $|\cos\theta_T|$ distribution for skimmed events with $Q_{\text{tag}} = \pm 1$. By selecting events with $|\cos\theta_T| < 0.85$, we suppress about 65 % of the continuum background, for only ∼15 % of $B\overline{B}$ events.

The objective of the last step is to select mostly the peaking component in the m_{ES} distribution, which is shown in Figure 4–5 for skimmed events that satisfy the two previous selection requirements. There is a good agreement between generic MC samples and onpeak data away from the peak, which suggests that the data are well modeled by the continuum and combinatoric backgrounds simulation. The offpeak data are also in good agreement with simulated continuum background under

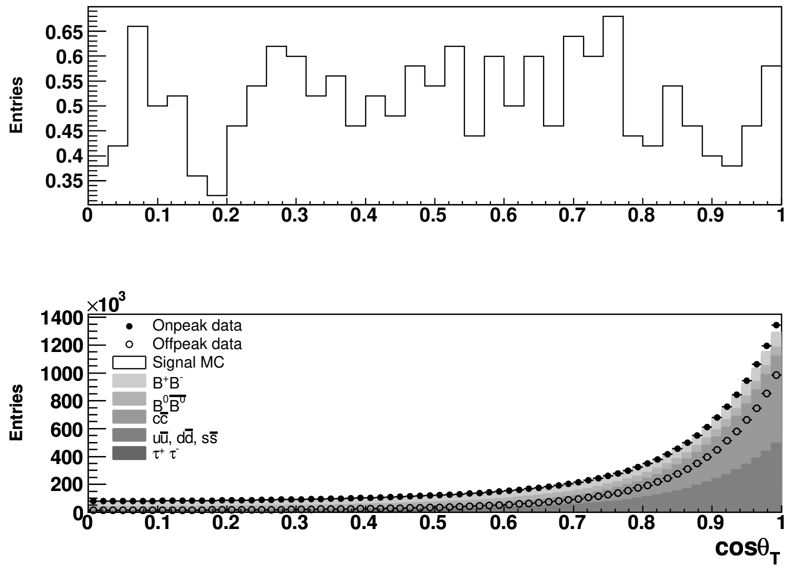

Figure 4–4: $|\cos\theta_T|$ distribution for skimmed events with $Q_{\text{tag}} = \pm 1$. $B\overline{B}$ events have a flat distribution, while continuum background events are concentrated in the right hand side of the bottom distribution. We require $|\cos\theta_T| < 0.85$.

the peak, but do not match with the MC distribution for lower m_{ES} values. This suggests that in the B_{reco} reconstruction algorithm, there is a problem with the m_{ES} calculation for CM energy much lower than m_B.

An important feature of this distribution is the excess of MC events in the peaking region, an effect that has a direct impact on the analysis and must be studied carefully. Since combinatorial and continuum events seem well modeled, our hypothesis is that the discrepancy comes from the B^+B^- MC sample. We can investigate this by studying the distribution of event shape variables in which different event types behave differently, for events in the peaking region. For example, by looking at the distributions of R2 for all tracks and clusters (Figure 4–6) and of $\cos\theta_B$, the

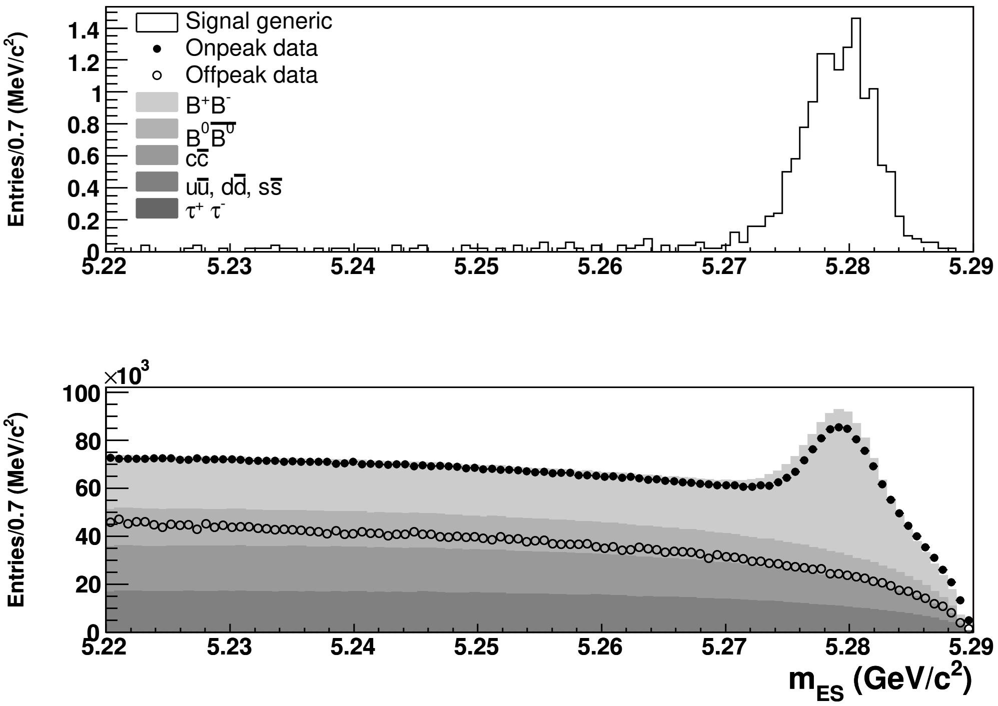

Figure 4–5: $m_{\rm ES}$ distribution for events with $Q_{\rm tag} = \pm 1$ and $|\cos\theta_T| < 0.85$. MC samples agree well with onpeak data in the region below 5.27 GeV/c^2, but there is an excess of B^+B^- in the peaking region. Offpeak data is well modeled by continuum only in the signal box. We require $5.270 < m_{\rm ES} < 5.288\,{\rm GeV}/c^2$.

angle between the momentum of the B candidate and the beam pipe (Figure 4–7), we observe in both cases a good agreement between offpeak data and continuum background, and a clear excess of generic B^+B^- MC events. Since these events are well modeled at lower $m_{\rm ES}$ values, we conclude that their combinatorial component is correct, but their peaking component is over-estimated. This could be due to the uncertainties on the branching ratios of some B decays and on the efficiency of the reconstruction algorithm. This results in an excess of B_{tag} candidates coming from the $B^{+}B^{-}$ MC samples, a number that we will quantify and correct in section 4.3.3.

Finally, we observe a slight shift in the m_{ES} peak central position, but if we select a large enough portion of the peak, the remaining "edge effect" can be neglected in the analysis. For that purpose, we fit with a Gaussian function the m_{ES} distribution for signal MC events with $Q_{\mathrm{tag}} = \pm 1$ (see Figure 4–8), and we select events which are in a 3σ "signal box" around the mean.

To summarize the requirements applied at this stage, we first skimmed all events by demanding that:

- there is at least three tracks in the event
- R2 < 0.5

then we defined B_{tag} candidates by selecting events with:

- $Q_{\mathrm{tag}} = \pm 1$
- $5.270 < m_{\mathrm{ES}} < 5.288\,\mathrm{GeV}/c^2$
- $|\cos\theta_T| < 0.85$

We apply these requirements consecutively on generic MC samples and on data, and the numbers of events selected at each steps are presented in Tables 4–3 and 4–4. As expected, the total number of MC events surviving the full selection exceeds the data.

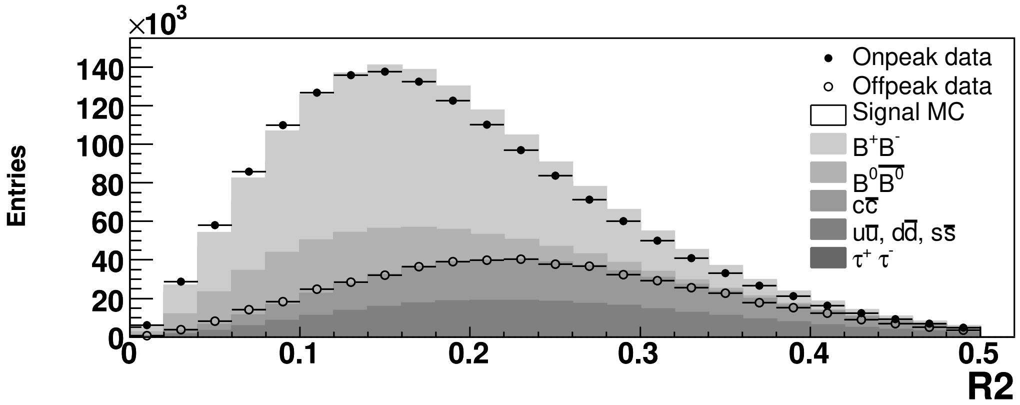

Figure 4–6: R2 of tracks and clusters, for events with $Q_{\text{tag}} = \pm 1$, inside the m_{ES} signal box, and with $|\cos\theta_T| < 0.85$. There is a good agreement between offpeak data and continuum background, but there is an excess of $B^{+}B^{-}$ events.

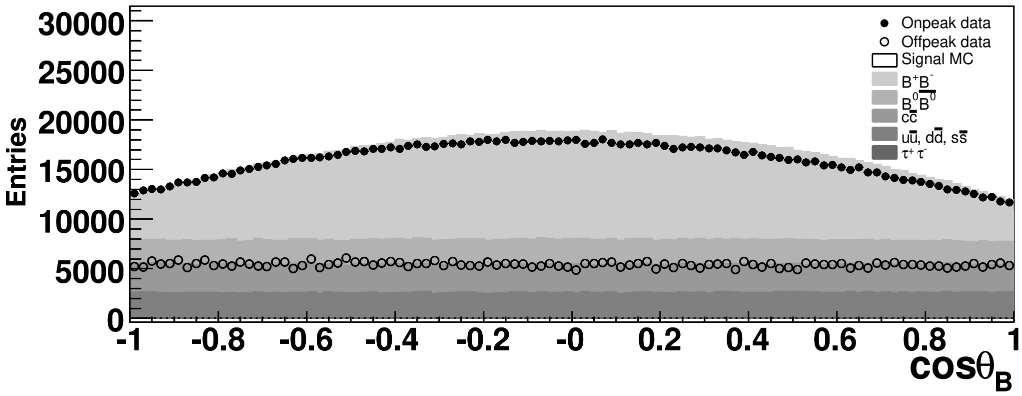

Figure 4–7: $\cos\theta_B$ distribution for events with $Q_{\text{tag}} = \pm 1$, inside the m_{ES} signal box, and with $|\cos\theta_T| < 0.85$. There is a good agreement between offpeak data and continuum background, but there is an excess of $B^{+}B^{-}$ events.

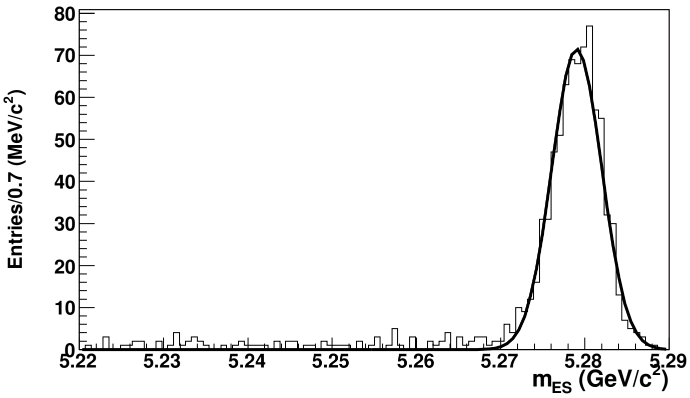

Figure 4–8: Gaussian fit of the $m_{\rm ES}$ distribution for generic signal events with $Q_{\rm tag} = \pm 1$. Fitted parameters : mean $\mu = 5.2790 \pm 0.0001\,\mathrm{GeV}/c^2$, width $\sigma = 0.00295 \pm 0.00009$.

Table 4–3: Cumulative effect of the skim and of the B_{tag} selection requirements on the number of generic MC events. MC samples have been scaled to the onpeak data luminosity of 208.73 fb^{-1}. The peaking B^+B^- yield has not been corrected yet.

	B^+B^-	$B^0\overline{B}^0$	$c\overline{c}$	uds	$\tau^+\tau^-$
Produced	1.0958×10^8	1.0958×10^8	2.7135×10^8	4.3625×10^8	1.9821×10^8
Skimmed	8.7820×10^6	7.5276×10^6	1.5707×10^7	1.3228×10^7	3 225
Q_{tag}	4.0069×10^6	2.3386×10^6	6.1833×10^6	5.0518×10^6	650.9
m_{ES}	1.0796×10^6	3.3001×10^5	8.6669×10^5	7.2417×10^5	105.3
$\cos\theta_T$	8.6388×10^5	2.5003×10^5	2.9364×10^5	2.6204×10^5	38.5
$\pm$ (stat)	$\pm\ 4.0 \times 10^2$	$\pm\ 2.3 \times 10^2$	$\pm\ 4.3 \times 10^2$	$\pm\ 4.1 \times 10^2$	$\pm$ 4.5

Table 4–4: Cumulative effect of the skim and of the B_{tag} selection requirements on the number of generic MC and data events. MC and Offpeak data have been scaled to the onpeak data luminosity of 208.73 fb^{-1}. We observe that a higher number of generic MC events survive the "reco" selection.

	Onpeak	All MC	Offpeak	Continuum MC
Recorded	3.0081×10^9		2.7601×10^9	
Produced		1.1250×10^9		9.0581×10^8
Skimmed	4.6416×10^7	4.5248×10^7	2.6258×10^7	2.8939×10^7
Q_{tag} cut	1.7324×10^7	1.7581×10^7	9.1364×10^6	1.1241×10^6
m_{ES} cut	2.9342×10^6	3.0005×10^6	1.6269×10^6	1.5910×10^6
$\cos\theta_T$ cut	1.5876×10^6	1.6696×10^6	5.4164×10^5	5.5573×10^5
$\pm$ (stat)	$\pm\ 1.3 \times 10^3$	7.5×10^2	$\pm\ 7.4 \times 10^2$	6.0×10^2

4.3.3 Tagging Yield Correction

In this section, we describe how we measure and correct the impact of the over-estimated peaking component observed in the B^+B^- MC sample. We first parametrize the m_{ES} distribution as a background function on top of which lies a peak, we then substract that background function from the distribution and count directly the number of peaking events remaining. Since there is a good agreement between MC and data samples for m_{ES} values below 5.27 GeV/c^2, we conclude that the same background function should be used for both samples. By comparing the peaking yields obtained from MC and data, we can extract the scale factor that best corrects the over-estimation. This method avoids the systematic uncertainty related to the parametrization of the peaking distribution, and prescribes that any quantity obtained from counting peaking events in simulated B^+B^- samples should be scaled down by the correction factor.

The best parametrization of background events is provided by the Argus function, which contains a normalization N and two shape parameters (α, β) [43] :

$$Argus(x) = N \cdot x \cdot (1 - (\frac{x}{5.29})^2)^{\alpha} \cdot e^{\beta(1-(\frac{x}{5.29})^2)} \tag{4.2}$$

A feature of $Argus(x)$ is that variations of (α, β) modify significantly the behavior of the function in the peaking region. Since the "real" shape of the background function is not known, the best we can do is to compute different correction factors using different values for the shape parameters, and to assign a systematic uncertainty on the result.

We obtain five different sets of shape parameters by fitting an Argus function on the m_{ES} distribution of offpeak data, $c\bar{c}$, uds, continuum and $B^0\overline{B}^0$, and three other sets by fitting $B\overline{B}$, onpeak and (onpeak - offpeak) with Argus + Gaussian. Here, the Gaussian serves as a dummy function, since we only extract the Argus shape parameters. Following our recipe, for each of these eight combinations of (α, β), we count the number of peaking events and compute the ratio between the two yields. The results are presented in Table 4–5, and we observe that although the absolute peaking yields vary by about 200 events/ fb^{-1} ($\sim 10\%$), the relative yields between onpeak data and generic MC samples are stable.

We present a detailed example of this method, in which the shape parameters are obtained by fitting the m_{ES} distribution of the $B^0\overline{B}^0$ MC sample alone ($\alpha = 0.489, \beta = -17.7$). Figure 4–9 shows the m_{ES} distributions of the MC samples and of the onpeak data, fitted with Argus + Gaussian, while Figure 4–10 shows a comparison of their peaking components after the Argus substraction. In this isolated example, the correction factor is of 91.4%.

We combine the eight different results and obtain on average 2599.9 events in data and 2841.0 in generic MC events, resulting in a scaling factor of :

$$\boxed{\text{Scale factor} = (91.5 \pm 5.0 \text{ (syst) })\%}$$

We then apply that correction to the B^+B^- sample, and, as seen in Figure 4–11, the m_{ES} distribution shows an improved agreement. The systematic uncertainties on the scaling factor and on the peak shape, which still does not match the data perfectly, will be discussed in section 4.6.

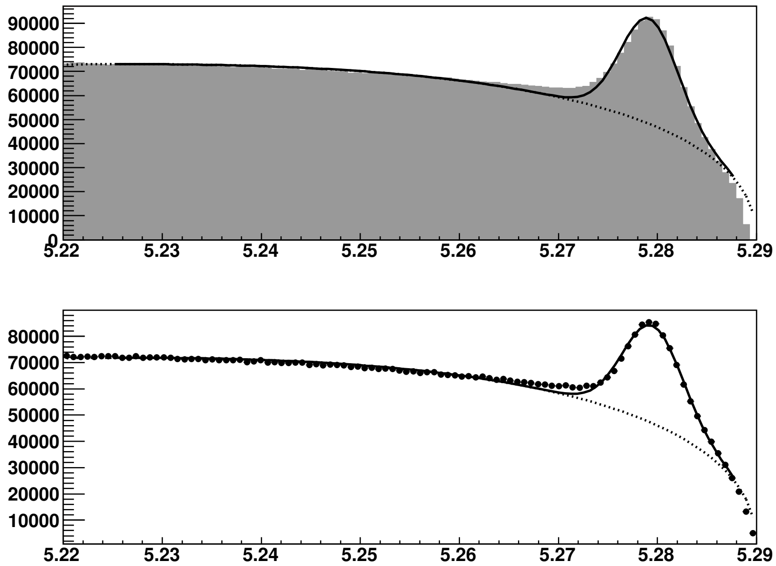

Figure 4–9: Fit of the m_{ES} distributions for events with $Q_{\mathrm{tag}} = \pm 1$ and $|\cos\theta_T| < 0.85$. Thick points are onpeak data and dark grey is generic MC sample. In these plots, the Argus shape parameters were found by fitting tagged $B^0\overline{B}^0$ events. The thick line is an Argus + Gaussian fit, and the dotted line is the fitted Argus function alone. We observe that in both data and MC samples, the fit is not perfect near the edges of the peak. This effect is present for all eight Argus shapes, and could have been avoided if we used another function to model the peak. However, the exact shape of the peak is not important in the calculation of the correction factor, only the total yield matters.

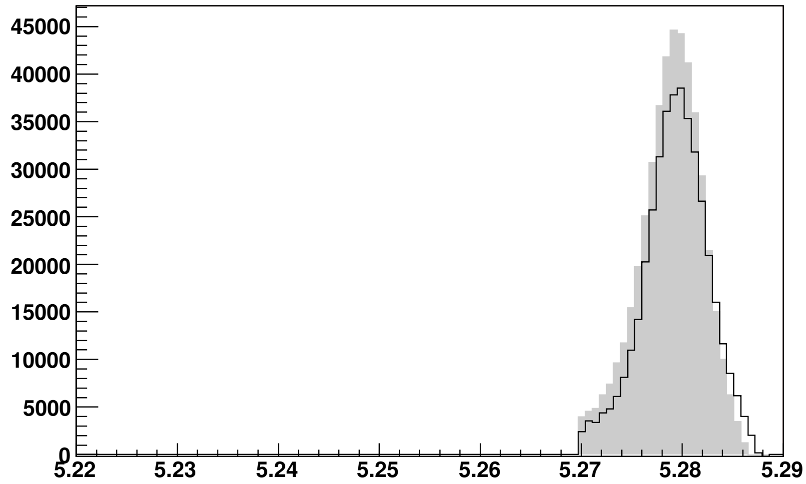

Figure 4–10: Peaking background in onpeak data (line) and generic MC sample (grey), after substracting the Argus function in Figure 4–9. We find 2562.6 (2802.3) peaking events per fb^{-1} in data (MC) samples, resulting in a ratio of 91.4 %. Values obtained with the other Argus shapes are listed in Table 4–5.

Table 4–5: Peaking yields for onpeak data and generic MC samples, after substracting Argus shapes obtained from different fits. Generic MC samples have been scaled to the onpeak data luminosity. The $\frac{data}{MC}$ ratio is very stable under variations of the Argus shape parameters α and β (less than 0.2 % variation.) We obtain on average 2599.9 events in data and 2841.0 in generic MC events, resulting in a scaling factor of $(91.5 \pm 5.0\ (\mathrm{syst})\ )\%$.

	uds	$c\bar{c}$	continuum	$B^0\overline{B}^0$	$B\overline{B}$	Offpeak	On-Off	Onpeak
α	0.559	0.570	0.565	0.489	0.501	0.524	0.378	0.437
β	-25.7	-26.4	-26.1	-17.7	-26.8	-15.5	-25.9	-18.9
data	2 643.0	2 648.0	2 653.5	2 562.6	2 580.8	2 687.1	2 478.1	2 546.4
MC yield	2 874.4	2 880.2	2 884.3	2 802.3	2 822.7	2 932.8	2 733.6	2 797.7
Ratio	91.9%	91.9%	92.0%	91.4%	91.4%	91.6%	90.7%	91.0%

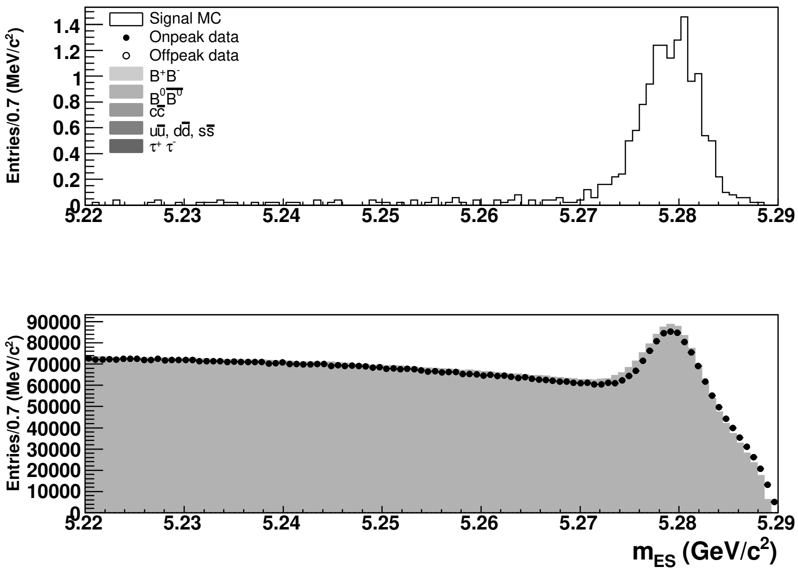

Figure 4–11: m_{ES} distribution for events with $Q_{\text{tag}} = \pm 1$ and $|\cos\theta_T| < 0.85$, after the correction on the peaking yield has been applied on generic B^+B^- events. The agreement is improved when compared to Figure 4–5.

4.3.4 The Tagging Yield Efficiency

We explained at the beginning of this chapter how the calculation of $\mathcal{B}(B^- \rightarrow K^-\nu\overline{\nu})$ involves the quantity $\varepsilon_{\rm tot}$, the efficiency at which we would reconstruct a signal process if it was to occur. In this analysis, we break this number in two multiplicative pieces: $\varepsilon_{\rm tag}$, the efficiency at which we can reconstruct a B_{tag} given a signal event, and $\varepsilon_{\rm sig}$, the efficiency at which we can select a $B^- \rightarrow K^-\nu\overline{\nu}$ event given a B_{tag}. In this section we concentrate our attention on $\varepsilon_{\rm tag}$, and we leave the discussion on $\varepsilon_{\rm sig}$ for section 4.4.4.

The tagging efficiency $\varepsilon_{\rm tag}$ is the ratio between the number of B_{tag} and the number of events produced for signal MC. In order to increase the statistical accuracy and precision on $\varepsilon_{\rm tag}$, we use three samples of signal MC events : $B^- \rightarrow K^-\nu\overline{\nu}$, $B^- \rightarrow K^{*-}\nu\overline{\nu}$ and $B^- \rightarrow \pi^-\nu\overline{\nu}$. These have a similar topology, hence the reconstruction algorithm is expected to have equal efficiencies. As a matter of fact, when we reconstruct the event, the signal side tracks can be incorporated in a combinatorial B_{reco}, hence the efficiency is affected by the number of charged particle in the signal process. As presented in Table 4–6, we apply consecutively the $Q_{\rm tag}$, $m_{\rm ES}$ and $\cos\theta_T$ requirements on each sample look at the number of events selected at each steps. We observe that for the three samples, $\varepsilon_{\rm tag}$ agrees within error, confirming that it is common for events with this topology. The three samples are thus combined to improve the statistical error and we obtain a value of $\varepsilon_{\rm tag} = (0.244 \pm 0.007 \text{ (stat) })\%$. This step is important because the small size of our MC signal sample, combined with a low reconstruction efficiency, results in a very low statistical resolution.

Since these three MC signal samples are generated with the same simulator and reconstructed with the same algorithm as the generic B^+B^- sample, and since $B^- \rightarrow K^{(*)-}\nu\overline{\nu}$ and $B^- \rightarrow \pi^-\nu\overline{\nu}$ events form part of the peaking component, we believe that their reconstruction efficiencies are similarly over-estimated compared with data. Our method then prescribes that $\varepsilon_{\rm tag}$ should be scaled down by the correction factor, and:

$$\varepsilon_{\rm tag} = (0.244 \pm 0.007 \text{ (stat) })\% \times (91.5 \pm 5.0 \text{ (syst) })\%$$

$$\boxed{\varepsilon_{\rm tag} = (0.224 \pm 0.009 \text{ (stat) } \pm 0.012 \text{ (syst) }) \ \%}$$

Table 4–6: Cumulative effect of the skim and of the B_{tag} selection requirements on the number of signal MC events. In order to present the real statistical precision, these samples have not been scaled here.

	$B^- \rightarrow K^-\nu\overline{\nu}$	$B^- \rightarrow K^{*-}\nu\overline{\nu}$	$B^- \rightarrow \pi^-\nu\overline{\nu}$	Combined
Produced	285 000	235 000	57 000	320 500
Skimmed	1 266	1 445	249	2 960
$Q_{\rm tag} = \pm 1$	893	879	194	1 966
$m_{\rm ES}$ signal box	774	660	170	1 604
$\lvert\cos\theta_T\rvert < 0.85$	685	573	152	1 410
$\varepsilon_{\rm tag}$	0.240%	0.244%	0.267%	0.244 %
$\pm$ (stat)	0.009%	0.010%	0.022%	0.007 %

4.4 Signal Side Selection

Since momentum is conserved in a $\Upsilon(4S) \to B\overline{B}$ event, the momenta of the two B mesons produced must point in opposite directions when calculated in the CM frame. This enables us to compute the momentum of the recoiling B^-, or "B_{sig}", based on the information we have on the B_{tag} candidate, and to boost any quantity "X" in the B_{sig} rest frame (denoted X^B). Typical events produce $B\overline{B}$ events with about 320 MeV/c of momentum.

In this section, we first analyze the signal side tracks. We then describe our K^- selection and put restrictions on the rest of the signal side particles, such that we can finally obtain our signal efficiency $\varepsilon_{\rm sig}$ and total efficiency $\varepsilon_{\rm tot}$. In most of the figures presented, the MC-data distributions do not agree at an acceptable level in the full range of the distributions, and we must investigate the real impact of the observed discrepancies on our final measurement. Our signal side selection is thus a compromise between maximizing $\varepsilon_{\rm sig}$, minimizing the number of background events selected and avoiding regions of distributions where the agreement is poor enough to induce systematic uncertainties. In all the plots that are presented, the correction on the yield of the peaking component has not been applied.

4.4.1 Requirements on Tracks and on the K^-

The number of signal side tracks per event, $N_{\rm trk}$, is plotted in Figure 4–12 for events with a B_{tag}, and we observe that generic MC events have on average fewer tracks per event than data (7.25 in MC compared to 7.58 in data). Without compromizing $\varepsilon_{\rm sig}$, we initially reject events with $N_{\rm trk} > 7$. The momentum spectrum

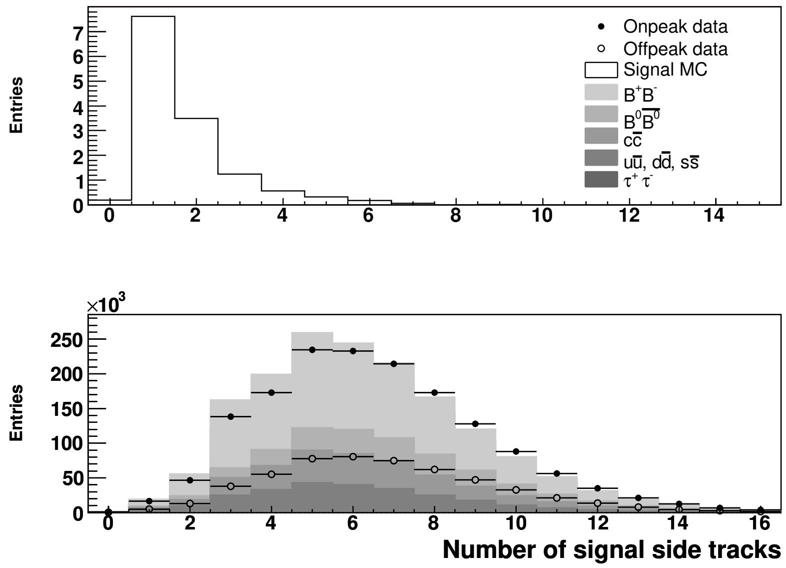

Figure 4–12: $N_{\rm trk}$ distribution for tagged events. In the region $N_{\rm trk} < 7$, there is an over-estimate of MC events, between all generic MC and onpeak data, and between continuum MC and offpeak data.

of the tracks, $p^B_{\rm trk}$, shows a good agreement above 1 GeV/c, as shown in Figure 4–13, but data contain more tracks with momentum between 0.15 and 0.85 GeV/c. When we compare this figure with the $p^B_{\rm trk}$ distribution for the track with the highest momentum only (Figure 4–14), we observe that in the latter, generic MC and data events are both shifted towards higher momenta, while the signal MC sample loses the pile up of low momentum tracks. There is a good MC-data agreement in the region above 1.1 GeV/c, but we see again an over-estimate of MC events in the region 0.4-12 GeV/c.

According to the SM predictions, presented in section 2.3, most of the K^- produced by a $B^- \to K^-\nu\overline{\nu}$ event have high momenta $p^B_{\rm K}$. We thus loop over all

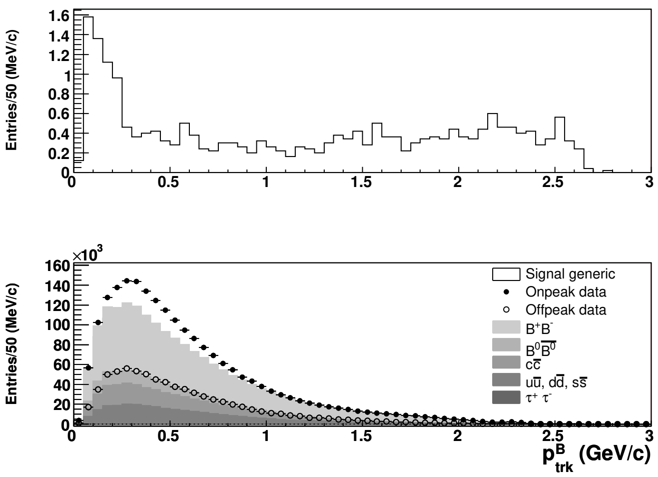

Figure 4–13: p^B_{trk} distribution for tagged events with $N_{\mathrm{trk}} < 7$. There is a good agreement in the region $p^B_{\mathrm{trk}} > 0.8\,\mathrm{GeV}/c^2$.

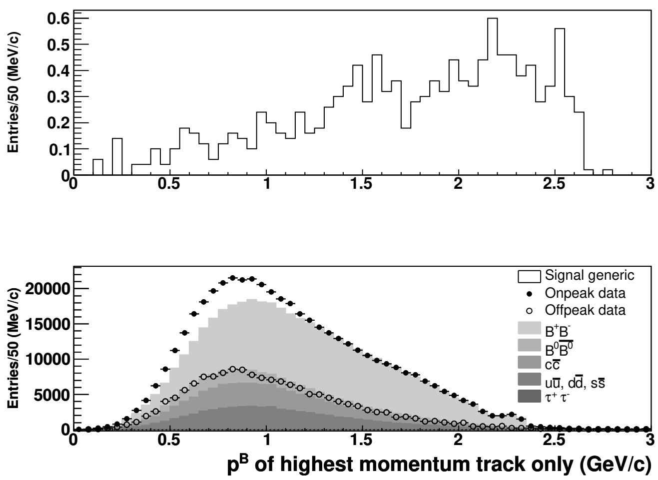

Figure 4–14: p^B_{trk} distribution of the track with the highest momentum, for tagged events with $N_{\mathrm{trk}} < 7$. There is a shift of about 100 MeV/c in the central peak position.

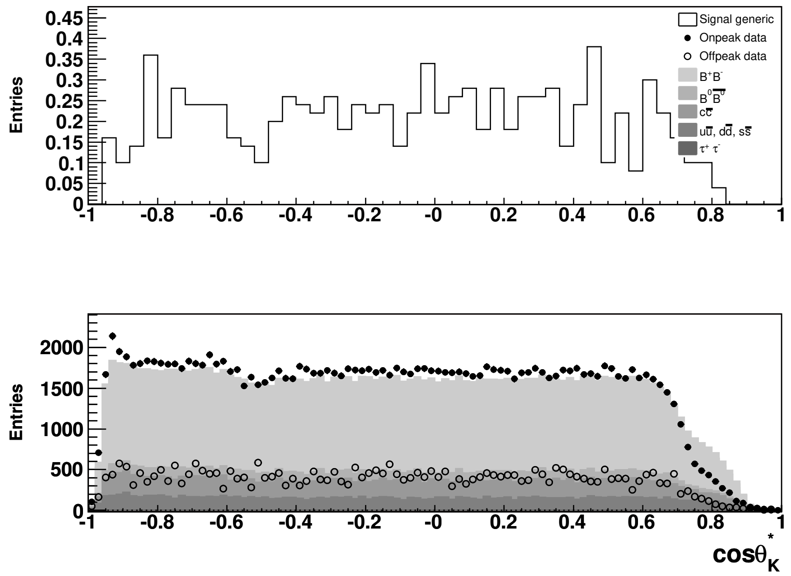

Figure 4–15: $\cos\theta^*_K$ distribution of $K^\pm$ candidate for tagged events with $N_{\rm trk}$ <7. There is bump in MC samples near $\cos\theta^*_K$ = 0.8, probably caused by unmodeled material in the IR that would otherwise absorb the $K^\pm$. There is also a peak in the onpeak data near $\cos\theta^*_K$ = -0.95, probably due to unmodeled bhabha events. We require $|\cos\theta^*_K| < 0.85$.

signal side tracks and search for the K^- with the highest $p^B_{\rm K}$. We require that its charge is opposite to $Q_{\rm tag}$ and that it falls within the angular acceptance of the DIRC, defined as $|\cos\theta^*_K| < 0.85$. The $\cos\theta^*_K$ distribution is presented in Figure 4–15, and we observe near $\cos\theta^*_K = 1$ an unmodeled "bump" in B^+B^- MC samples, probably caused by the presence of material in the forward region of the detector that is not included in the simulation. Its impact will be discussed in the section on systematic uncertainty.

We mentioned in the beginning of this chapter that even in a $B^- \to K^-\nu\overline{\nu}$ event, the signal K^- candidate is not always the only signal side track. The *extra*

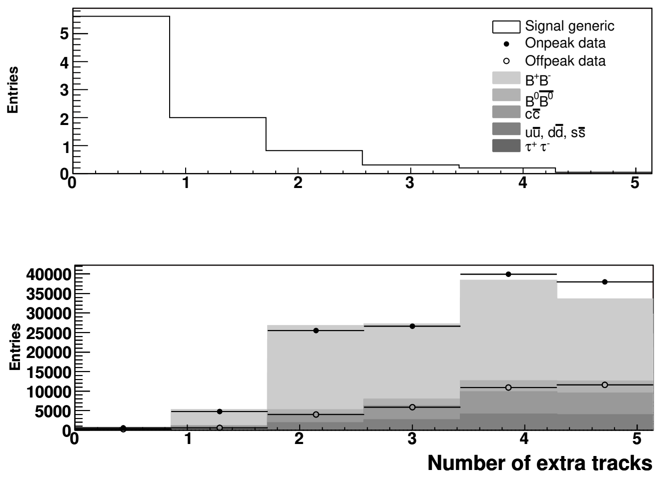

Figure 4–16: N_{extra} distribution for tagged events with a $K^{\pm}$ candidate. We require $N_{\text{extra}} < 3$, and this rejects the portion of the distribution that has a poor agreement.

tracks either come from misreconstructing the B_{tag} or from a background photon that pair-produces charged particles, which propagate inside the detector. In both cases, the extra tracks do not come from the decay of the B_{sig}. Figure 4–16 presents N_{extra}, the number of extra tracks per event, for events with a B_{tag} and a K^{-} candidate. We observe that generic MC samples under-estimates the data in the region $N_{\text{extra}} > 3$, a behavior that is correlated with the discussed disagreements in Figures 4–13 and 4–14. Hence we only accept events with $N_{\text{extra}} < 3$, and expect a better MC-data agreement. Physically, this requirement rejects signal events in which more than one background photon pair-produces, or in which the B_{tag} is highly combinatorial.

The sum over the energy of the extra tracks defines the total energy from extra tracks, and its distribution is shown in Figure 4–17 for events with a $K^{\pm}$ candidate and $N_{\text{extra}} < 3$. There is a small discrepancy in the region below 0.8 GeV. Figure 4–18 plots p^{B}_{K} for events satisfying the requirement on N_{extra}. We show this distribution

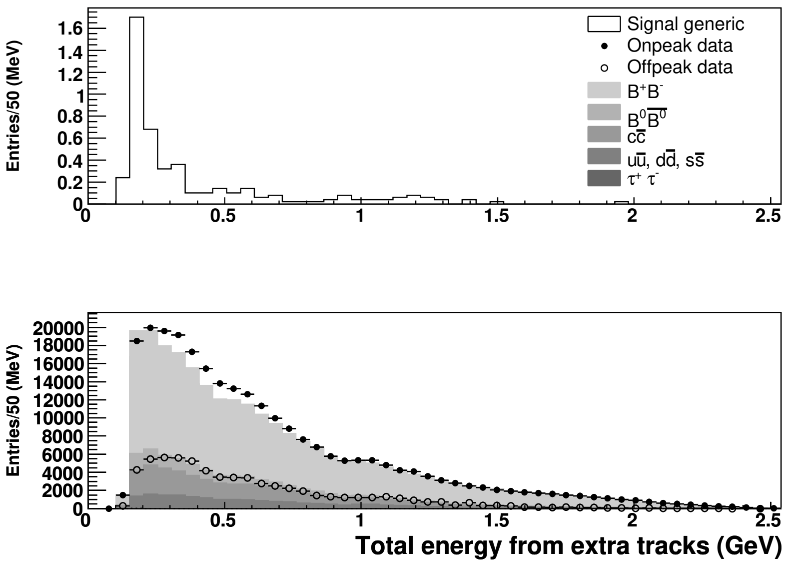

Figure 4–17: Total energy of extra tracks, for tagged events with a $K^{\pm}$ candidate and $N_{\mathrm{extra}} < 3$. The MC samples do not model well the data below 700 MeV.

for both generic and cocktail signal samples in order to increase the statistics and have a second point of view on this spectrum. There is an excess of generic Monte Carlo in the region 0.7-2.0 GeV/c, but this effect becomes negligible after the peaking yield correction is applied. Signal $K^{\pm}$ are required to satisfy $p_{\mathrm{K}}^{B} > 1.1\,\mathrm{GeV}/c$.

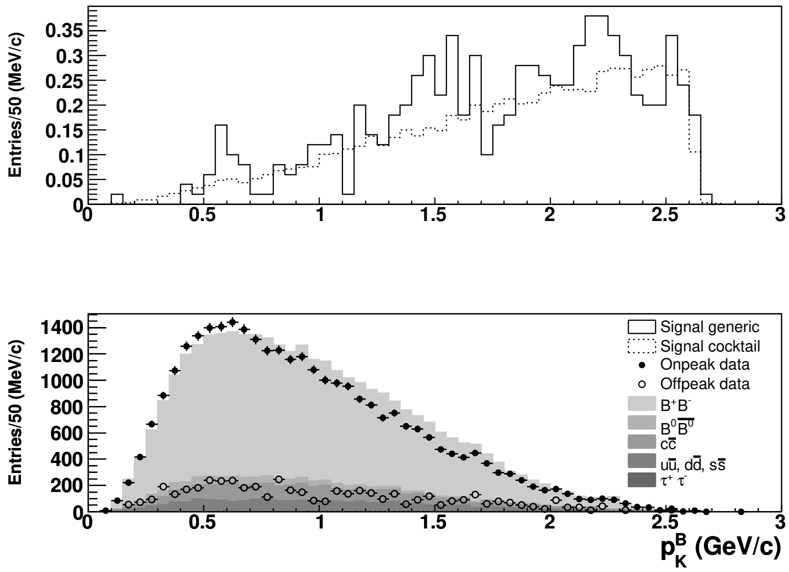

Figure 4–18: p_{K}^{B} distribution for tagged events with $N_{\mathrm{extra}} < 3$. There is a discrepancy in the shape, but after correcting for the peaking yield of the $B^{+}B^{-}$, the MC-data mostly agree within statistical uncertainty in the selected region ($p_{\mathrm{K}}^{B} > 1.1\,\mathrm{GeV}/c$).

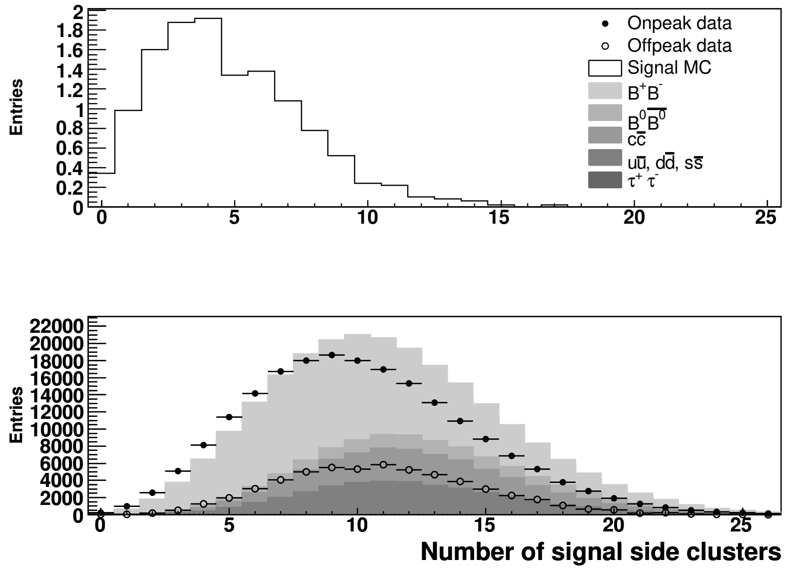

Figure 4–19: N_{clus} distribution for tagged events with $N_{\text{trk}} < 4$. There is a shift of about 1 cluster in the central position of the peak.

4.4.2 Requirements on Clusters and on π^0

The number of clusters for tagged events and $N_{\text{trk}} < 4$ (no K^- requirement) is shown in Figure 4–19, and it appears from the shift in the peak summit that data events have on average less reconstructed clusters per events, (11.2 in data versus 12.7 in generic MC samples). We initially require events to have less than 10 clusters and get rid of about half the background events. It is enlightening to look at the energy spectrum of these clusters, presented in Figure 4–20, as it demonstrates that the multiplicity excess in MC samples is mainly due to photons with energy below 50 MeV. This is a known feature of the *BABAR* simulation production, observed in all MC events, and we thus expect this excess to be similarly present in signal MC samples.

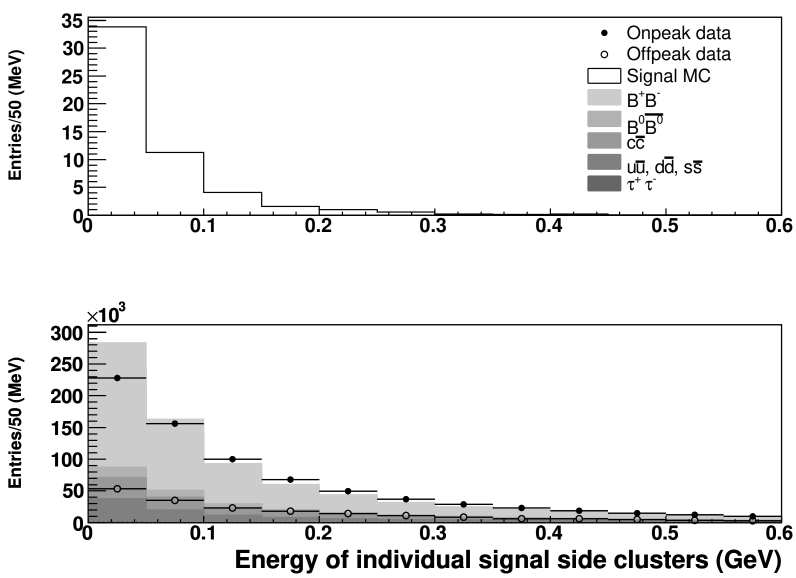

Figure 4–20: Energy distribution of individual signal side clusters for tagged events with $N_{\mathrm{trk}} < 4$. The number of clusters with less than 50 MeV are over-estimated in MC samples.

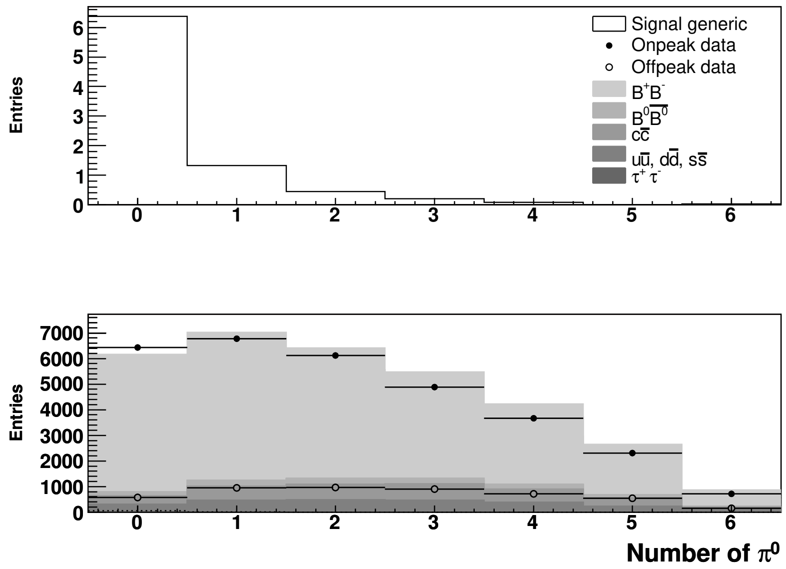

Figure 4–21: Number of π^0 candidates for tagged events with a $K^{\pm}$ candidate and $N_{\mathrm{extra}} < 3$. We require events to have no π^0.

The number of signal side π^0 candidates falling in the mass range $0.121 < m_{\pi^0} < 0.145\ \mathrm{GeV}/c^2$ is shown in Figure 4–21 for events with a $K^{\pm}$ candidate and $N_{\mathrm{extra}} < 3$. Generic MC and data samples contain a lot of reconstructed π^0 candidates, either physical or of combinatorial nature, while the π^0 candidates that populate signal MC events are purely combinatorial, obtained by combining randomly clusters from bremsstrahlung or hadronic split-offs, or clusters that should have been incorporated in the B_{tag} reconstruction but were not. We apply a veto on events with such π^0 candidates.

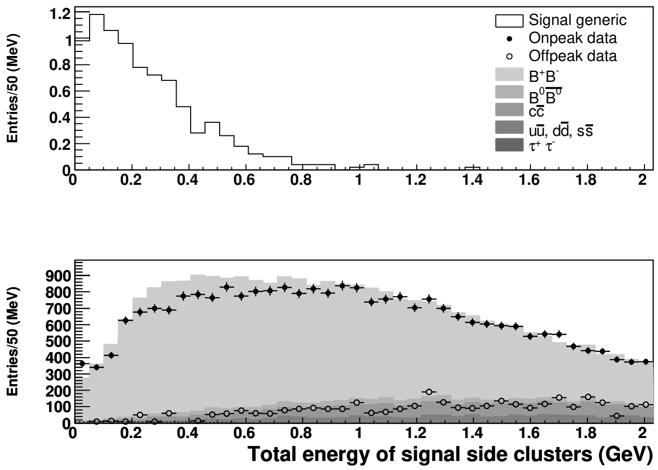

Figure 4–22: Total energy of signal side clusters for tagged events with a $K^{\pm}$ candidate and $N_{\text{extra}} < 3$. The importance of the discrepancy in the region below 1 GeV should be lowered after applying the peaking yield correction factor.

4.4.3 Requirements on the Extra Energy and on the Missing Momentum

We mentioned earlier that the $B^- \to K^-\nu\overline{\nu}$ signature is an isolated K^- with no other particles present, so we need to limit the rest of the signal side energy. The motivation of the last requirements are presented here. We have shown in previous figures that in background events, the number of clusters peaks at $\sim$ 10 and, at the same time, their energy spreads well above 1 GeV. Since, in that respect, signal MC events behave differently, we start by looking at the sum over the energy of all signal side clusters, or the "total neutral signal side energy". Figure 4–22 shows that distribution for events with a K^- candidate and $N_{\text{extra}} < 3$. There is an excess of B^+B^- for energies between 0.1 and 1.2 GeV, coming from the over-estimation of low energy clusters discussed in the last section.

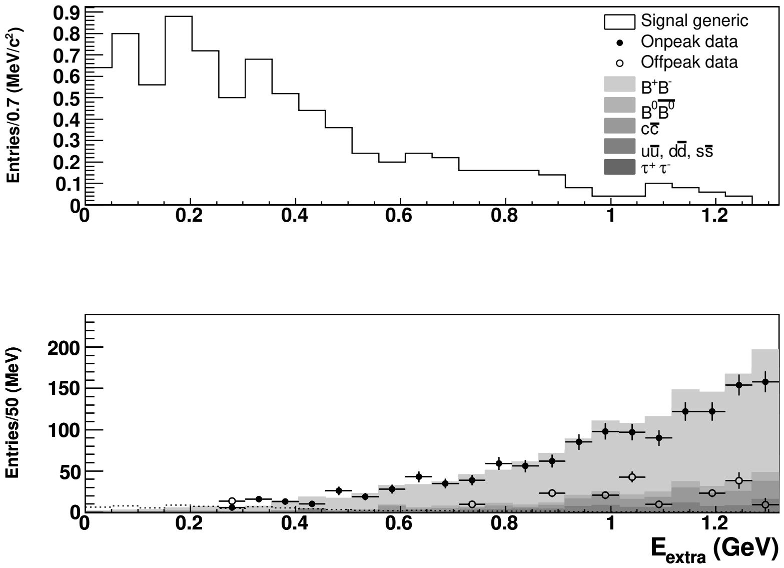

Figure 4–23: $E_{\rm extra}$ distribution for tagged events with a $K^{\pm}$ candidate and $N_{\rm extra} < 3$. The region $E_{\rm extra} < 250$ MeV is kept blind to onpeak data since signal events are important there. As a consequence, we can not directly verify the MC-agreement there. We require $E_{\rm extra} < 0.400$ GeV.

At this point in the analysis most of the background comes from the B^+B^- generic MC sample. These events have a wide range of total neutral energy, and they mostly have a few extra tracks with a wide range of total energy (see section 4.4.1). We could require events to have $N_{\rm extra} = 0$ and place an upper limit on the total neutral energy, but it would be quite hard on $\varepsilon_{\rm sig}$. Instead, in the CM frame, we add the total energy of these extra tracks to the total neutral energy, defining the total extra energy, or $E_{\rm extra}$, and we limit this variable directly. This method improves significantly the background rejection power while yielding higher values of $\varepsilon_{\rm sig}$. The $E_{\rm extra}$ distribution is shown in Figure 4–23, and we observe a good agreement between data and MC samples. However, since the distributions of total energy from tracks and from clusters were both showing significant discrepancies, E_{extra} is potentially a source of large systematic uncertainties and will be studied in greater details in section 4.6.2. We require events to have $E_{\mathrm{extra}} < 0.400$ GeV. After applying that selection, the number of onpeak data events becomes quite low, so in most of the plots, we must stay blind to onpeak data. We must already blind the low-energy part of the E_{extra} distribution, as seen by the dashed line in Figure 4–23. As a consequence, we can not verify directly the MC-data agreement beyond this point, and any further investigation must be done in sideband regions.

Finally, the missing 4-vector, defined as $p^{\mu}_{miss} = p^{\mu}_{e^+beam} + p^{\mu}_{e^-beam} - p^{\mu}_{B_{tag}} - \sum p^{\mu}_{tracks} - \sum p^{\mu}_{clusters}$, is required to point away from the z axis, in order to reject events in which a detectable particle is lost outside of the detector's acceptance. The sums are over the signal side tracks and clusters only. The $\cos\theta_{Pmiss}$ distribution is shown in Figure 4–24 for events with a K^- candidate and $N_{\mathrm{extra}} < 3$, and we reject events that do not satisfy $-0.85 < \cos\theta_{Pmiss} < 0.90$. We notice that the distribution for background events is peaking in the forward and backward directions. The B_{sig} selection criteria are summarized in Table 4–7.

Table 4–7: List of requirements applied on the B_{sig} candidate.

$K^{\pm}$ selected
$\lvert\cos\theta^*_K\rvert < 0.85$
$N_{\mathrm{extra}} < 3$
$E_{\mathrm{extra}} < 0.400$ GeV
$N_{\pi^0} = 0$
$p^B_{\mathrm{K}} > 1.1\,\mathrm{GeV}/c$
$-0.85 < \cos\theta_{Pmiss} < 0.90$

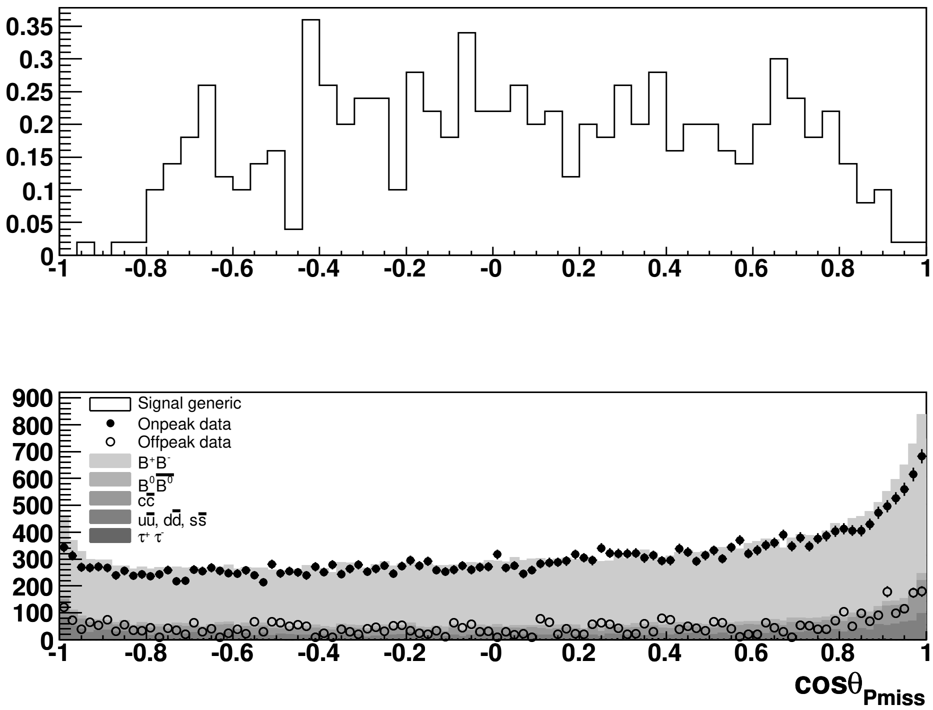

Figure 4–24: $\cos\theta_{Pmiss}$ for tagged events with a $K^{\pm}$ candidate and $N_{\text{extra}} < 3$. We require $-0.85 < \cos\theta_{Pmiss} < 0.90$.

4.4.4 Signal and Total Efficiencies

The signal efficiency ε_{sig} is basically the efficiency at which we can select a $B^- \to K^-\nu\overline{\nu}$ signal event, given a tagged event. ε_{sig} is therefore unaffected by the $(91.5 \pm 5.0 \text{ (syst) })\%$ peaking yield correction factor. Its value is estimated using the generic signal sample and, only to a limited extend, cocktail signal samples. As mentioned in section 4.2.2, cocktail samples are designed to provide a high B_{reco} reconstruction efficiency by restricting its decay to high purity hadronic channels. As a consequence, only a few B_{reco} are mis-reconstructed, lowering significantly the number of extra tracks and of signal side π^0 candidates and clusters. In other words, the N_{extra}, N_{π^0} and E_{extra} distributions of cocktail samples are not typical, hence we can not trust any values of ε_{sig} obtained exclusively from these samples. However, the efficiency at identifying a track as a signal K^- does not depend on the rest of the event, hence it should be the same for cocktail and generic signal samples.

Since the generic signal sample has limited statistics, the strategy is to estimate the efficiency of each signal side requirement with the generic sample, except for the K^- identification criteria, whose efficiency ε_{ID} is estimated from a combination of generic and cocktail samples. Table 4–8 presents the flow of the selection efficiency when applying consecutively the signal side criteria on these three signal samples. The last row shows ε_{ID}, measured after all other requirements have been applied. We observe that the values of ε_{ID} in all three samples agree within statistical error, as expected.

This defines our signal efficiency :

$$\varepsilon_{\mathrm{sig}} = \varepsilon_{NO-ID}^{gen.} \times \varepsilon_{\mathrm{ID}}^{gen.+cock.}$$

$$\varepsilon_{\mathrm{sig}} = (36.1 \pm 2.68 \text{ (stat) }) \,\% \times (87.0 \pm 1.1 \text{ (stat) })\%$$

$$\boxed{\varepsilon_{\mathrm{sig}} = (31.4 \pm 2.3 \text{ (stat) })\%}$$

The number of $B^- \to K^{(*)-}\nu\overline{\nu}$ and $B^- \to \pi^-\nu\overline{\nu}$ MC signal events surviving consecutive requirements is presented in Table 4–9. We observe that $B^- \to K^{*-}\nu\overline{\nu}$ and $B^- \to \pi^-\nu\overline{\nu}$ processes are well suppressed by our selection : their final numbers of events are smaller than the statistical uncertainty on the $B^- \to K^-\nu\overline{\nu}$ sample. Most of the $B^- \to K^{*-}\nu\overline{\nu}$ events fail the requirement on E_{extra}, while most $B^- \to \pi^-\nu\overline{\nu}$ fail the $K^\pm$ selection, hence these two processes are not significant backgrounds.

In this analysis, $\varepsilon_{\mathrm{sig}}$ is completely estimated from MC samples, and such a method has consequences. $B^- \to K^-\nu\overline{\nu}$ signal events are generated according to the dynamics of a phase-space model, which is not believed to reproduce accurately the physics of the decay channel in the SM [3]. This is observed in the distribution of the invariant mass of the $\nu\overline{\nu}$ system, defined as $q^2 = (p_{e^+} + p_{e^-} - p_{B_{tag}} - p_{kaon})^2$ (see top part of Figure 4–25), for all tagged events with a K^- candidate.

Comparison shows that the SM calculation presented in Ref. [3] predicts fewer low-q^2 events than the distribution from the phase-space model, hence, by momentum conservation, fewer high-momentum K^-. We reweight bin-by-bin the signal Monte Carlo events so that both distributions match, and we propagate the effect to the K^- momentum (see bottom of Figure 4–25). This lowers the number of signal events surviving the $p_{\mathrm{K}}^{B} > 1.1\,\mathrm{GeV}/c$ requirement, and as a result, the $\varepsilon_{\mathrm{sig}}$ we previously obtained from the signal MC samples should be scaled by a factor of $(96.6 \pm 1.3$

Table 4–8: Cumulative efficiencies of signal selection criteria for generic and cocktail $B^- \to K^- \nu\overline{\nu}$ events. The last line is the efficiency of the $K^\pm$ identification alone, after all other criteria are applied. The quoted error is statistical only.

Events produced	generic 285 000	cocktail 1 127 000	cocktail 2 123 000
B_{tag}	1.000 ± 0.054	1.000 ± 0.010	1.000 ± 0.015
$K^\pm$ candidate	0.683 ± 0.041	0.744 ± 0.008	0.716 ± 0.012
$\lvert\cos\theta^*_K\rvert < 0.85$	0.655 ± 0.040	0.675 ± 0.007	0.670 ± 0.011
$N_{\text{extra}} < 3$	0.616 ± 0.038	0.651 ± 0.007	0.644 ± 0.011
$E_{\text{extra}} < 0.400$ GeV	0.382 ± 0.028	0.449 ± 0.005	0.436 ± 0.009
$N_{\pi^0} = 0$	0.346 ± 0.026	0.407 ± 0.005	0.394 ± 0.008
$p^B_{\text{K}} > 1.1\,\text{GeV}/c$	0.302 ± 0.024	0.359 ± 0.005	0.341 ± 0.007
$-0.85 < \cos\theta_{Pmiss} < 0.90$	0.302 ± 0.024	0.358 ± 0.005	0.339 ± 0.007
ε_{ID}	0.838 ± 0.079	0.881 ± 0.014	0.844 ± 0.021

Table 4–9: Cumulative effect of signal selection criteria on the number of $B^- \to K^{(*)-}\nu\overline{\nu}$ and $B^- \to \pi^-\nu\overline{\nu}$ generic signal events. Monte Carlo has been scaled to the onpeak data luminosity.

	$B^- \to K^-\nu\overline{\nu}$	$B^- \to K^{*-}\nu\overline{\nu}$	$B^- \to \pi^-\nu\overline{\nu}$
B_{tag}	13.70	47.29	29.22
$K^\pm$ candidate	9.36	10.65	0.58
$\lvert\cos\theta^*_K\rvert < 0.85$	8.98	9.57	0.58
$N_{\text{extra}} < 3$	8.44	8.75	0.58
$E_{\text{extra}} < 0.400$ GeV	5.24	0.83	0.19
$N_{\pi^0} = 0$	4.74	0.66	0.19
$p^B_{\text{K}} > 1.1\,\text{GeV}/c$	4.14	0.25	0.19
$-0.85 < \cos\theta_{Pmiss} < 0.90$	4.14	0.25	0.19
$\varepsilon_{\text{sig}} \pm$ (stat)	$(31.4 \pm 2.3)\%$	$(0.87 \pm 0.39)\%$	$(0.66 \pm 0.66)\%$

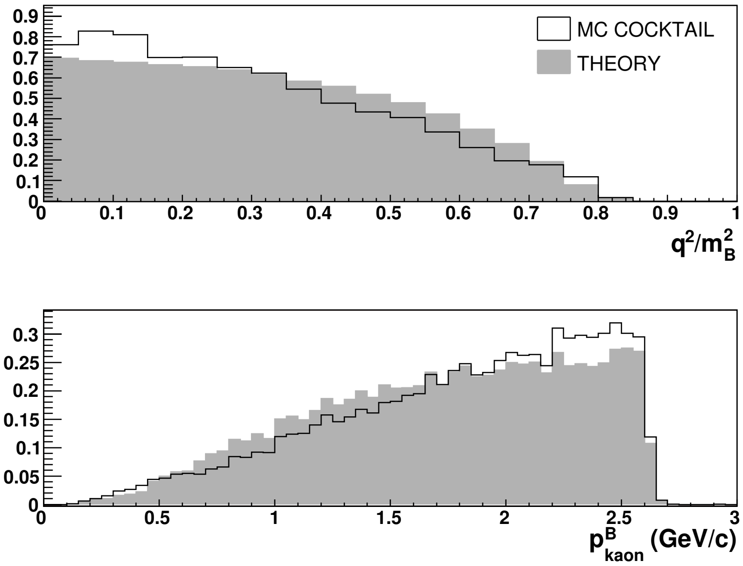

Figure 4–25: MC-theory comparison of the distribution of the dilepton mass q^2 for events with a B_{tag} and a $K^{\pm}$ candidate (top) and of the p_{K}^B distribution for events with a B_{tag} (bottom). The two curves in each plot have equal area, and the dilepton mass is scaled by m_B. The discrepancy in the region $p_{\mathrm{K}}^B > 1.1\,\mathrm{GeV}/c$ induces a correction factor of $(96.6 \pm 1.3$ (syst) $)\%$ on $\varepsilon_{\mathrm{sig}}$.

(syst))% . We finally define the total efficiency of reconstructing a signal event : $\varepsilon_{\mathrm{tot}} = \varepsilon_{\mathrm{tag}} \times \varepsilon_{\mathrm{sig}}$, with the peaking yield correction applied on $\varepsilon_{\mathrm{tag}}$, the phase-space reweighting applied on $\varepsilon_{\mathrm{sig}}$, using the three signal samples to measure $\varepsilon_{\mathrm{ID}}$, and we find that

$$\varepsilon_{\mathrm{tot}} = (\varepsilon_{\mathrm{tag}} \times \text{correction}) \times (\varepsilon_{\mathrm{sig}} \times \text{reweighting})$$

$$\varepsilon_{\mathrm{tot}} = (0.244\ \% \times 91.5\ \%\ ) \times (31.4\% \times 96.6\%\ )$$

$$\boxed{\varepsilon_{\mathrm{tot}} = (0.0678 \pm 0.0043\ \text{(stat)}\ \pm 0.0088\ \text{(syst)}\ )\ \%}$$

4.5 Background Estimate

The "reco" and signal side requirements were chosen to select the largest amount of signal events while suppressing most of the other event types. This section describes how we use both data and generic MC samples to estimate N_{bg}, the total number of background events surviving our selection. We decompose N_{bg} in two pieces, the peaking and the non-peaking components, and study them separately. Tables 4–10 and 4–11 present the number of generic MC and data events selected by each requirement described in section 4.4. We observe that the background is clearly dominated by B^+B^-, which is a mixture of peaking and combinatorial backgrounds, while only a small contribution comes from $B^0\overline{B}^0$, and none from $c\overline{c}$, uds or $\tau^+\tau^-$.

4.5.1 Combinatorial and Continuum Backgrounds

Only a few non-peaking background events survive the B_{sig} selection in the generic MC samples. However, the luminosities of uds and $c\overline{c}$ events produced by the *BABAR* Simulation Group are of the same size as the onpeak data (see Table 4–1), and the absence of such events in our final selection could be in fact a downward fluctuation due to low statistics. In that case, the central value of the continuum background would be slightly bigger.

We use an alternative method to estimate the contribution from combinatorial and continuum backgrounds. It is based on the relationship that exists between the number of events in the region under the peak and the number of events in the region away from the peak, refered to as the $m_{\rm ES}$ *sideband*, in non-peaking events. By definition, the events in the sideband are combinatorial and continuum background, and contain very few signal events (see the top part of Figure 4–5). To avoid accidentally

Table 4–10: Cumulative effect of signal selection criteria on the number of generic MC events, which have been scaled to the onpeak data luminosity. 38.5 $\tau^+\tau^-$ events survive the tagging selection, 0.57 survive the $K^\pm$ selection, but the $|\cos\theta^*_K| < 0.85$ requirement filters out the rest.

	B^+B^-	$B^0\overline{B}^0$	$c\overline{c}$	uds
B_{tag}	8.6388×10^5	2.5003×10^5	2.9364×10^5	2.6204×10^5
$K^\pm$ candidate	97 576	9 152	18 827	14 247
$\lvert\cos\theta^*_K\rvert < 0.85$	90 162	8 434	17 265	13 000
$N_{\mathrm{extra}} < 3$	25 271	1 125	2 962	2 398
$E_{\mathrm{extra}} < 0.400$ GeV	36.77	1.62	3.82	0.64
$N_{\pi^0} = 0$	26.27	0.81	1.27	0.64
$p^B_{\mathrm{K}} > 1.1\,\mathrm{GeV}/c$	12.76	0.20	0.63	0
$-0.85 < \cos\theta_{Pmiss} < 0.90$	12.38	0.20	0	0
$\pm$ (stat)	1.50	0.20	-	-

Table 4–11: Cumulative effect of signal selection criteria on the number of generic MC and data events. Monte Carlo and offpeak data samples have been scaled to the onpeak data luminosity.

	Onpeak	All MC	OffPeak	Continuum
B_{tag}	1.5876×10^6	1.6696×10^6	5.4164×10^5	5.5573×10^5
$K^\pm$ candidate	147 007	139 803	33 263	33 075
$\lvert\cos\theta^*_K\rvert < 0.85$	135 498	128 861	30 592	30 265
$N_{\mathrm{extra}} < 3$	30 888	31 756	4 556	5 360
$E_{\mathrm{extra}} < 0.400$ GeV	(blind)	42.8	9.7	4.4
$N_{\pi^0} = 0$	(blind)	29.1	9.7	1.94
$p^B_{\mathrm{K}} > 1.1\,\mathrm{GeV}/c$	(blind)	13.6	0	0.63
$-0.85 < \cos\theta_{Pmiss} < 0.90$	(blind)	12.6	0	0
$\pm$ (stat)	(blind)	1.70	-	-

unblinding the onpeak data near the peak, we leave a gap between the m_{ES} signal box and the m_{ES} sideband, and define the latter as $5.225 < m_{\mathrm{ES}} < 5.265\,\mathrm{GeV}/c^2$.

We first make the assumption that for non-peaking background events, there is no correlation between the signal side requirements and the value of m_{ES}, so that their overall Argus shape is a constant. In other words, we assume that the shape parameters of the Argus function should be fixed at all steps in our selection. Hence we can use the values of (α, β) obtained with high statistics (already presented in Table 4–5) to model the non-peaking background distribution after all our criteria have been applied. We fix their value, fit the onpeak data in the m_{ES} sideband to find the norm N of the Argus, and then extrapolate the function into the m_{ES} signal box to estimate the amount of combinatorial and continuum events there.

One feature of the Argus function simplifies this proceedure : once the shape parameters are fixed, the ratio between the integral of the function under the peak region and the integral in the sideband region, R^{area}, is a constant. Hence we can multiply the number of events in the sideband of the onpeak data by R^{area} and estimate the number of non-peaking events in the signal box without unblinding. We use different values of α and β from Table 4–5 and obtain an average value of $R^{\mathrm{area}} = 0.29 \pm 0.04$ (syst). With this method, we estimate that with 13 ± 3.6 observed events in the m_{ES} sideband of onpeak data, there should be 3.77 ± 1.05 events in the peak region due to combinatorial and continuum backgrounds.

The first advantage of this method is that it reduces the systematic uncertainty of our result by not relying on MC samples, and the second is a statistical improvement : the non-peaking background is now estimated with 13 events instead of about

Table 4–12: Cumulative effect of signal selection criteria on the number of generic MC and onpeak data events, in the m_{ES} sideband ($5.225 < m_{\mathrm{ES}} < 5.265\,\mathrm{GeV}/c^2$). Monte Carlo samples have been scaled to the onpeak data luminosity. We assume a ratio of 0.29 for R^{area} and we estimate the number of non-peaking events in the m_{ES} signal box from both MC and data sidebands.

Criteria	Number of Events			
	Onpeak data m_{ES} sideband	All MC m_{ES} sideband	Data estimate of non-peaking	MC estimate of non-peaking
B_{tag}	3.9894×10^6	4.0954×10^6	1.1569×10^6	1.1878×10^6
$K^{\pm}$ candidate	2.2566×10^5	1.9910×10^5	65 441	57 738
$\lvert\cos\theta_T\rvert < 0.85$	2.0763×10^5	1.8321×10^5	60 213	53 131
$N_{\mathrm{extra}} < 3$	31 197	31 026	9 047	8 998
E_{extra}	40	30.7	11.60	8.90
$N_{\pi^0} = 0$	30	23.3	8.70	6.76
$p_{\mathrm{K}}^{B} > 1.1\,\mathrm{GeV}/c$	14	8.20	4.06	2.38
$\cos\theta_{Pmiss}$	13	7.69	3.77	2.23

five combinatorial $B\overline{B}$ events. Table 4–12 compares the effect of the B_{sig} selection on the number of events in the m_{ES} sideband for data and $B^{+}B^{-}$ generic MC samples, and how it relates to the number of "non-peaking" events in the signal box using our estimate of R^{area}. We observe from this Table that until the $N_{\mathrm{extra}} < 3$ selection stage, the MC-data samples agree within 1σ, but that the $E_{\mathrm{extra}} < 0.400$ GeV requirement rejects more MC events. This has a direct impact on our estimate of the peaking component, as explained in the next section.

The m_{ES} distribution is shown in Figure 4–26 after all other requirements have been applied. The signal region is blinded, the peaking component in MC sample is still visible and we see a slight under-estimation of MC events in the sideband. The dashed line represents the signal distribution with a branching ratio of 5.2×10^{-4}.

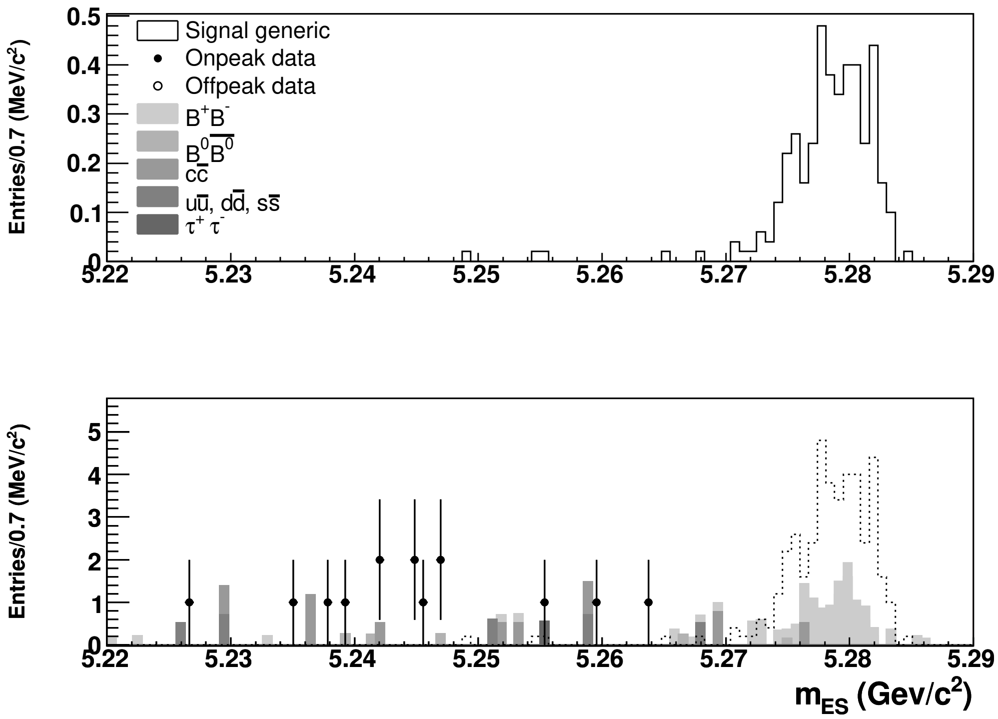

Figure 4–26: $m_{\rm ES}$ distribution after all other selections have been applied. We stay blind to onpeak data in the signal box $5.270 < m_{\rm ES} < 5.288\,{\rm GeV}/c^2$, and count 13 onpeak data events in the sideband $5.225 < m_{\rm ES} < 5.265\,{\rm GeV}/c^2$. The dotted line in the bootom part represents the amplified signal, as explained in section 4.

4.5.2 Peaking Background

The number of background events found after applying the B_{sig} selection on the generic B^+B^- MC sample is a combination of peaking and non-peaking events, and we must isolate the peaking portion, as the non-peaking part is already incorporated in the estimate from last section. Table 4–13 summarizes the background types contained in different samples.

Table 4–13: Different event types contain different event types and are used to estimate specific component of N_{bg}.

Data type	Content	Estimates
Generic B^+B^- MC	Peak + Combinatorial	Peaking Background
Onpeak data (sideband)	Continuum + Combinatorial	Continuum + Combinatorial
Generic uds, $c\overline{c}$ and $B^0\overline{B}^0$ MC	Continuum + Combinatorial	Used for Validation only

We estimate the combinatorial part of the simulated B^+B^- events the same way that estimate the non-peaking part of onpeak data : we multiply the number of events in the m_{ES} sideband by R^{area}. We found 3 ± 1.7 events in m_{ES} sideband of the B^+B^- MC sample, corresponding to 0.16 ± 0.09 combinatorial events in the signal box, after scaling to onpeak luminosity.

This number must then be substracted from the 12.38 ± 1.50 B^+B^- events that survive the B_{sig} selection, in the m_{ES} signal box, and we estimate that 12.22 ± 1.53 (stat) peaking background events should be observed. Since this number is extracted exclusively from peaking B^+B^- samples, the yield correction factor of 91.5 % must be applied, as explained in section 4.3.2. We thus estimate the number of peaking

B^+B^- events to be 11.18 ± 1.40 (stat). As observed in Table 4–12 and mentioned in the previous section, the events in the m_{ES} sideband of the MC samples seem to be more suppressed by the E_{extra} requirement than those of the onpeak data. If the MC samples had results closer to those of data, the Argus extrapolation would results in a higher number of combinatorial events in the B^+B^- m_{ES} signal box and reduce the peaking component.

We note that the estimate of combinatorial background from data is consistent at the 3σ level with the number of MC events directly observed in the signal box, but the result from data has higher statistics and should be more reliable since there are several possible systematic effects that could cause the MC to model the combinatorial background incorrectly. We add the contributions from the peaking, the continuum and the combinatorial backgrounds, and estimate that the total number of background events surviving our selection is

$$\boxed{N_{bg} = 14.95 \pm 1.75 \text{ (stat) } \pm 1.09 \text{ (syst)}}$$

4.6 Error Analysis

This section describes how we treat the statistical and systematic uncertainties on the numbers measured in this analysis, and how they propagate in the numbers used for the upper limit calculation.

4.6.1 Statistical Uncertainty

The statistical error, also called random error, is driven by the assumption that every measurement is a random probing of a population distribution. At many steps in our analysis, we are counting events in bins of histograms, and in such counting experiments, the population should have a Poisson distribution whose mean is estimated by the number of events we observe. A property of the Poisson distribution is that the variance is equal to the mean, and since the random error is the square root of the variance by definition, it means that for N events counted, the statistical uncertainty is $\sqrt{N}$. The way these uncertainties affect functions of N_1, N_2, ... is prescribed by the standard error propagation formula:

$$\sigma^2_{f(N_1,N_2,...)} = (\frac{\partial f}{\partial N_1}\sigma_{N_1})^2 + (\frac{\partial f}{\partial N_2}\sigma_{N_2})^2 + ... \tag{4.3}$$

$\varepsilon_{\rm tag}$ is derived from $B^- \to K^-\nu\overline{\nu}$, $B^- \to K^{*-}\nu\overline{\nu}$ and $B^- \to \pi^-\nu\overline{\nu}$ samples and scaled by the peaking yield correction factor. $\varepsilon_{\rm sig}$ is obtained from both generic and cocktail samples of $B^- \to K^-\nu\overline{\nu}$ events and scaled by a phase-space correction factor. Using the formula 4.3 for $\varepsilon_{\rm tot}$, we factor out the two correction factors from our calculation and find that the statistical error on $\varepsilon_{\rm tot}$ is 0.0047 %.

The estimation of the number of background events N_{bg} involves counting events in the $m_{\rm ES}$ sideband for B^+B^- and onpeak data, as well as in the peaking region for B^+B^-; it also involves $R^{\rm area}$, the peaking yield correction factor and scaling the B^+B^- MC sample to the onpeak data luminosity, but these are factored out of the formula. The uncertainties from the peaking and non-peaking contributions are added in quadrature and we obtain $\sigma_{N_{bg}}$ =1.75.

4.6.2 Systematic Uncertainty

Because this analysis relies on MC samples to measure ε_{tot} and N_{bg}, all selection criteria are sources of systematic uncertainty. However, we focus our attention on the dominant sources that are based on distributions that exhibit a MC-data discrepancy in the selected region. From the overall agreement between generic MC and data samples in all figures, we expect the precision on our measurement to be roughly at the 10 % level. The agreements in Q_{tag} (Fig. 4–3), $\cos\theta_T$ (Fig. 4–4), N_{extra} (Fig: 4–16) and $\cos\theta_{Pmiss}$ (Fig. 4–24) distributions, used as selection criteria, are good enough in the selected regions, so we neglect their contributions to the systematic uncertainty of our measurement. The sources of error relevant for this analysis are :

- Discrepancy in m_{ES} peak shape (Fig. 4–10 and Fig. 4–11)
- Peaking yield correction factor
- Track reconstruction efficiency
- ε_{ID} and $K^{\pm}$ identification
- Discrepancy in $\cos\theta^*_K$ near + 1 (Fig. 4–15)
- Discrepancy in π^0 distribution in the $N_{\pi^0} = 0$ bin (Fig. 4–21)
- Discrepancy in composites of E_{extra} (Figures 4–17, 4–22 and 4–23)
- Discrepancy in p^B_{K} overall shape (Fig. 4–18)
- Phase-space reweighting correction factor
- Choice of Argus shape for R^{area}

Lastly, there are uncertainties on the onpeak data luminosity and on the $B\overline{B}$ cross-section, but when we adjust the MC peaking yield to the data with the scale factor, we implicitly correct for these two effects, hence the uncertainties are already included in the uncertainty on the peaking yield. We calculate the uncertainty on N_{bg}, $\varepsilon_{\rm tag}$ and $\varepsilon_{\rm sig}$, and we combine the latter two into $\varepsilon_{\rm tot}$ afterwards.

The global shape of the peak in the $m_{\rm ES}$ distribution is slightly different in MC and data events, and there is a shift of about 5 MeV/c^2 in MC samples towards lower values. However, the purpose of this distribution is to make sure that the MC-data yields agree. As explained in the section 4.3.2, the $m_{\rm ES}$ signal box is 3σ wide, so these features affect only the tails of the peak that contain a very small portion of the total yield. The overall shape has thus a negligible impact on the value of $\varepsilon_{\rm tag}$, and we assign no systematic uncertainty.

The uncertainty on the peaking yield correction factor is studied by varying the shape of the Argus function (i.e. by trying all sets of (α, β) listed in Table 4–5) and by comparing the correction factors thus obtained. We record a variation of 0.8 % on the 91.5 % correction factor. This method assumes that inside the $m_{\rm ES}$ signal box, the shape of the continuum and combinatoric backgrounds in data is bounded from above and below by these Argus functions, which is not necessarily a valid assumption. Thus, we assign instead a 5 % systematic uncertainty to the correction factor, which represents about half the total observed deviation from unity of the measured factor of 91.5 % . This induces a 0.012 % uncertainty on $\varepsilon_{\rm tag}$ and a 0.56 uncertainty on N_{bg}.

The track reconstruction and the $K^{\pm}$ identification efficiencies have been studied in great details by teams of physists at *BABAR*, and they concluded that systematic uncertainties of 1.2 %/track and 1.1 %/$K^{\pm}$ should be assigned for the track reconstruction and the $K^{\pm}$ identification efficiencies respectively [45] [46]. In our analysis, after the B_{sig} selection, there are on average 1.32 and 1.13 tracks per event in signal and generic MC samples respectively, including the signal $K^{\pm}$, resulting in uncertainties of 0.41 % and 0.33 % on $\varepsilon_{\rm sig}$ due to the tracking efficiency and to $\varepsilon_{\rm ID}$ respectively. For N_{bg}, these numbers become 0.18 and 0.12 respectively. In addition, the algorithm that selects $K^{\pm}$ is more efficient on data than on MC samples by about 1%, probably due to different sigal side track multiplicity. This translates into a systematic uncertainty of 0.38 % on $\varepsilon_{\rm sig}$ and of 0.10 on N_{bg}.

The bump in the $\cos\theta^*_K$ distribution results in an over-estimate of about 3 % of generic B^+B^- MC events. However, these events seem to behave normally in all other distributions, as we do not see distinct discrepancies that could be associated with them, hence we treat them as normal events and assign no uncertainty.

The error from the discrepancy in π^0 multiplicity is evaluated by looking at the distribution of N_{π^0}, and finding the difference in the selection efficiencies for data and MC samples. 20.8 % of data events are accepted by the selection, compared to 18.8 % in MC samples. This difference of 2.0 % results in a 0.65 % uncertainty on $\varepsilon_{\rm sig}$ and in a 0.22 uncertainty on N_{bg}.

The distributions of the total energy from tracks and from clusters both exhibit a discrepancy in the region below 400 MeV. It certainly induces an uncertainty in the $E_{\rm extra}$ distribution, especially in the region $E_{\rm extra} < 0.400$ GeV, and this can be estimated by studying the multiplicity and energy spectrum of clusters and extra tracks. In generic MC samples, events with a B_{tag} have an average of 6.25 extra tracks with a momentum of 306 MeV/c on average, and 12.7 clusters with an energy of 28 MeV. In data, these events contain on average 6.58 extra tracks with an average momentum of 329 MeV/c, and 11.2 clusters with an energy of 40 MeV. We estimate the impact of these discrepancies by "correcting" all MC samples : we add a 329 MeV/c track every three events and we remove three 40 MeV clusters every two events. This results in variations of 3.40 % and 0.70 on $\varepsilon_{\rm sig}$ and N_{bg} respectively, and these numbers dominate both systematic uncertainties.

The impact of the discrepancy in the $p_{\rm K}^{B}$ distribution can be studied by looking at the $p_{\rm K}^{B}$ distribution for events in which the hardest track is not a $K^{\pm}$, and for events with a $K^{\pm}$ but with $0.5 < E_{\rm extra} < 1.5\,{\rm GeV}$ (Figures 4–27 and 4–28). We observe a good MC-data agreement in the $p_{\rm K}^{B} > 1.1\,{\rm GeV}/c$ region in both figures. This confirms that the $p_{\rm K}^{B}$ distribution is probably well modeled after applying the final selection criteria, hence we assign no systematic error.

We estimate the uncertainty related to the reweighting of the phase-space model by comparing the values of $\varepsilon_{\rm sig}$ obtained when reweighting the q^2 spectrum to the 1σ curves in the dynamical model [3]. It results in an uncertainty of 0.41 % on the signal efficiency only.

The only source of systematic uncertainty that affects our estimate of the number of combinatorial and continuum background events comes from measuring $R^{\rm area}$, and its importance is estimated by looking at the variation of $R^{\rm area}$ for different values of (α, β), as explained in section 4.5.1. The Argus shape parameters that we try here are the same that were shown in Table 4–5 in section 4.3.3, except that we do not choose those that were obtained by fitting a sample with a (Gaussian + Argus) function. We find that an uncertainty of 4 % is consistent with all the shapes, and this translates into a 0.52 uncertainty on the non-peaking component of N_{bg}.

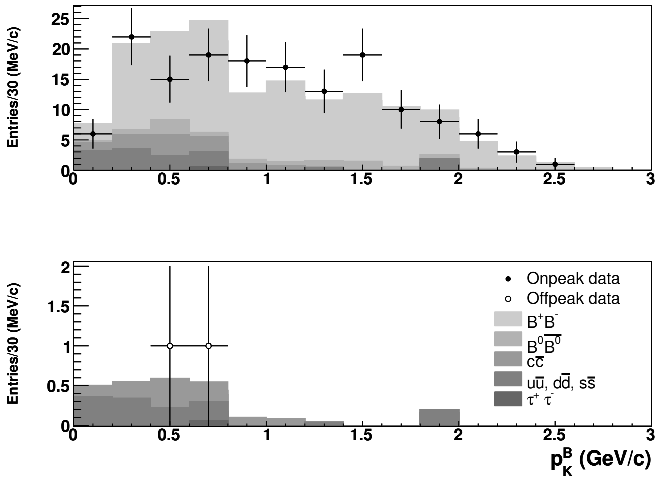

Figure 4–27: p_{K}^{B} distribution for events in which the track with the highest momentum is not a $K^{\pm}$ candidate. Top : Generic Monte Carlo samples are scaled to onpeak data luminosity. The distribution shows a good agreement in the region $p_{\mathrm{K}}^{B} > 1.1\,\mathrm{GeV}/c$. Bottom : Generic $c\overline{c}$, uds and $\tau^{+}\tau^{-}$ Monte Carlo samples are scaled to offpeak data luminosity.

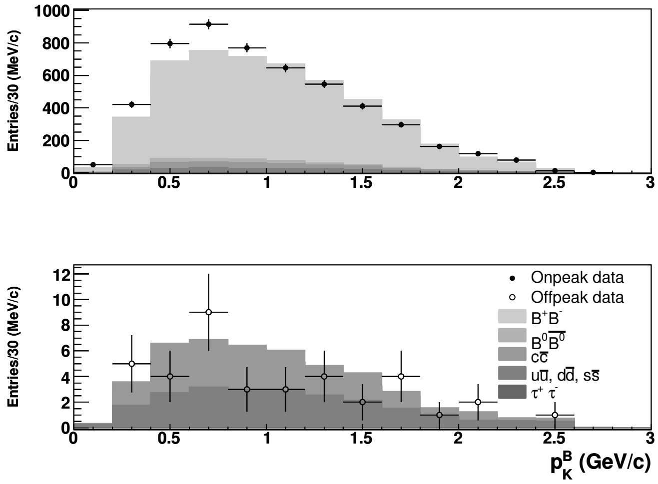

Figure 4–28: p_{K}^{B} distribution in the $0.5 < E_{\mathrm{extra}} < 1.5\,\mathrm{GeV}$ sideband. Top : Generic Monte Carlo samples are scaled to onpeak data luminosity. The distribution shows a good agreement in the region $p_{\mathrm{K}}^{B} > 1.1\,\mathrm{GeV}/c$. Bottom : Generic $c\overline{c}$, uds and $\tau^{+}\tau^{-}$ Monte Carlo samples are scaled to offpeak data luminosity.

The sources of systematic uncertainty for $\varepsilon_{\rm tag}$ and $\varepsilon_{\rm sig}$ are independent, so they are combined as:

$$(\sigma^{syst}_{\varepsilon_{\rm tot}})^2 = (\sigma^{syst}_{\varepsilon_{\rm tag}} \times \varepsilon_{\rm sig})^2 + (\sigma^{syst}_{\varepsilon_{\rm sig}} \times \varepsilon_{\rm tag})^2 \tag{4.4}$$

Tables 4–14 and 4–15 present the complete treatment of statistical and systematic uncertainties, and we obtain that the systematic error on $\varepsilon_{\rm tot}$ and on N_{bg} are 0.0088 % and 1.09 respectively.

Table 4–14: Statistical and systematic uncertainties on ε_{tot}.

Quantity	Source	value	± (stat)	± (syst)
ε_{tag}		0.224 %		
	Statistics		0.006 %	
	Peak Yield Correction			0.012 %
ε_{sig}		30.3 %		
	MC Statistics		2.25 %	
	Tracking Efficiency			0.41 %
	ε_{ID}			0.33 %
	$K^{\pm}$ Selection			0.38 %
	N_{π^0} Discrepancy			0.65 %
	E_{extra}			3.40 %
	Decay Model			0.41 %
	Total Systematic			3.55 %
ε_{tot}		0.0678 %	0.0047 %	0.0088 %

Table 4–15: Statistical and systematic uncertainties on N_{bg}.

Quantity	Source	value	± stat	± syst
Peaking		11.18		
Background	MC Statistics		1.40	
Contribution	Peak Yield Correction			0.56
	Tracking Efficiency			0.18
	ε_{ID}			0.12
	$K^{\pm}$ Selection			0.10
	N_{π^0} Discrepancy			0.22
	E_{extra}			0.70
	Total Systematic			0.95
Combinatorial		3.77		
Background	m_{ES} Sideband Data Statistics		1.05	
Contribution	Argus Shape			0.52
N_{bg}		14.95	1.75	1.09

4.7 Sub-sample Analysis

The previous measurement of $\mathcal{B}(B^- \to K^-\nu\overline{\nu})$ analyzed 80.03 fb^{-1} of onpeak data, a sub-sample about 2.5 times smaller than the one used in this analysis. We study this same sub-sample with the present analysis to verify that we can reproduce the previous results, but also to cross-check the MC-data agreement after all our selection are applied. We do not expect the results to be identical since we are using a distinct MC production that is statistically independent from the previous sample and that is based on a more recent version of `GEANT4`. In addition, although the analysis is similar, the reconstruction code is very different, hence the same data set is likely to produce slightly different results. Using the method described in section 4.5, we estimate that in this 80.03 fb^{-1} sample, there should be 5.53 ± 1.14 (stat) ± 0.41 (syst) background events, more than 80 % of which are peaking backgrounds. We look at the m_{ES} distribution after all other criteria have been applied (Figure 4–29) and observe that only one data event is present in the m_{ES} signal box, an unexpected discrepancy that must be investigated. Figure 4–29 shows a clear over-estimation of peaking B^+B^- MC samples, while the sideband seems correctly modeled by the MC samples. Since the data is correct by definition, we believe that the problem comes from the MC sample, and we examine the different causes that could lead to such an over-estimate.

As explained in section 4.5.2, the under-estimation of B^+B^- events in the m_{ES} sideband of the $208.73\,\text{fb}^{-1}$ sample produces an under-estimation of our estimate of the combinatorial content of the B^+B^- events in the signal box leading to an over-estimation of peaking events. In any case, the effect would be much smaller

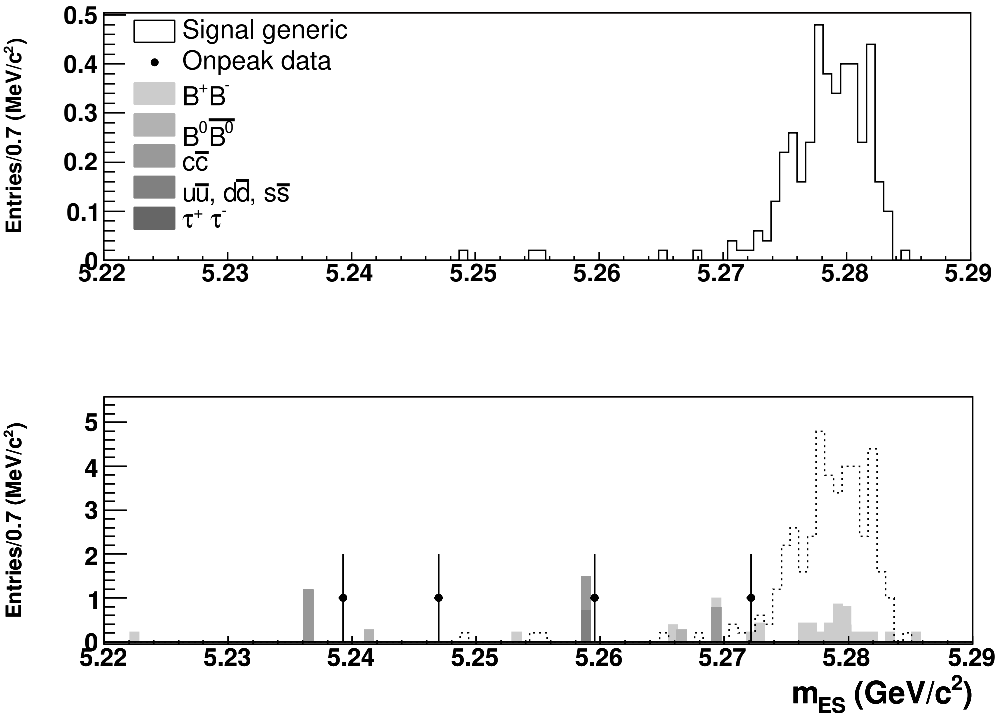

Figure 4–29: m_{ES} distribution after all other selections have been applied. We count 1 onpeak data events in the signal box but expect 5.53 background events. We observe 3 data events in the sideband and expect about the same quantity.

than what we observe, and anyway, this behavior is not observed in the 80.03 fb^{-1} sub-sample. As expected, the cause of the problem must come from the peaking component itself, so we examine our selection criteria one by one.

All the B_{tag} requirements show a good agreement, except for the peaking yield in the m_{ES} distribution, but the method used to correct it has proven to be valid in previous *BABAR* measurements. The $\cos\theta^*_K$, $\cos\theta_{Pmiss}$ and the N_{π^0} distributions also show good agreements, and they have a very small background rejection power on their own, especially after the requirement on E_{extra} has been applied, hence the problem cannot come solely from poor π^0 reconstruction or ($\cos\theta^*_K$, $\cos\theta_{Pmiss}$) modeling. The peaking over-estimation persists even when we remove these three requirements, confirming that they are not guilty. It leaves the requirements on the K^- identification, the p^B_{K} distribution and on the E_{extra} distribution as potential causes.

We first study the effect of loosing up the two criteria ($p^B_{\mathrm{K}} > 0.9\,\mathrm{GeV}/c$ and $E_{\mathrm{extra}} < 0.550$ GeV) in order to determine if the problem persists when additionnal statistics are available, or if it is caused by the actual *value* of our restrictions. As seen in Figure 4–30, the m_{ES} distribution still exhibits an over-estimation of the peaking component after modifying our selection. We conclude that the problem is not simply a statistical fluctuation and that it could be related to the actual shape of the p^B_{K} and E_{extra} distributions.

4.7.1 Examination of E_{extra}

We will now attempt to verify is the discrepancy could be caused by the modelling of the E_{extra} distribution. We recall that this variable, which is plotted in

Figure 4–31, is obtained from combining the energy of all clusters and all extra tracks and is responsible for most of our systematic uncertainty. These two "total energy" distributions are presented in Figures 4–32 and 4–33 for events with a B_{tag}, a K^- candidate and $N_{\mathrm{extra}} < 3$. Since both exhibit a discrepancy in the low-energy region, we study them separately. We start by investigating the cluster contribution and look at the individual cluster energy after applying the requirement our initial E_{extra} (see Figure 4–34). We observe that the low-energy clusters are over-estimated in B^+B^- samples, so we modify the E_{extra} variable and reject the contribution from any individual cluster whose energy is smaller than 50 MeV. With this threshold, the distribution of the total energy from clusters still shows a discrepancy, as seen in Figure 4–35, but the MC-data agreement in the E_{extra} distribution is now very high (see Figure 4–36). We apply this new selection and estimate that about 8.5 background events should be observed in the signal box, but we count only two in data (see Figure 4–37). We conclude that the problem is not caused by the modeling of the low-energy clusters in the energy spectrum, although it may still be related to the neutral energy portion of the E_{extra} variable, as suggested by Figure 4–35.

We then modify our selection by removing the contribution from the extra tracks in the E_{extra} variable, but keeping the 50 MeV threshold on the clusters. We show in Figure 4–38 the m_{ES} distribution after applying all requirements with $N_{\mathrm{extra}} = 1$, and observe an over-estimation of MC events (about 77 expected, compared to 49 observed). When we require $N_{\mathrm{extra}} = 0$, an essential criteria to select signal events with the correct topology, the effect becomes predominant (see Figure 4–39). We conclude that the extra track contribution to the E_{extra} variable cannot

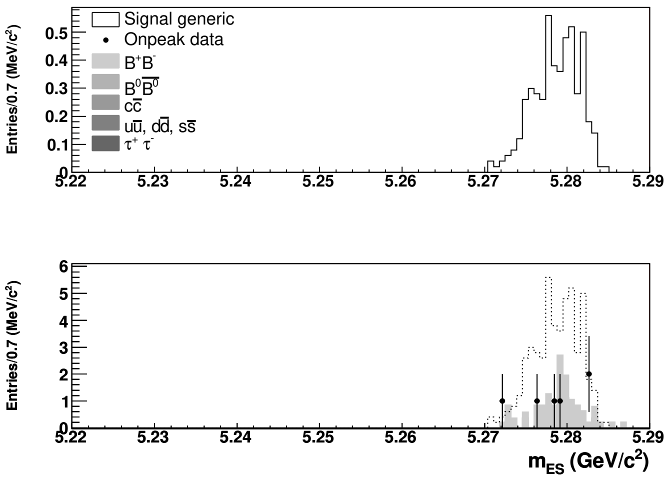

Figure 4–30: m_{ES} distribution after all selections have been applied, with looser restrictions on p_{K}^{B} and E_{extra}. We count 6 onpeak data events in the signal box, but expect about 16 background events.

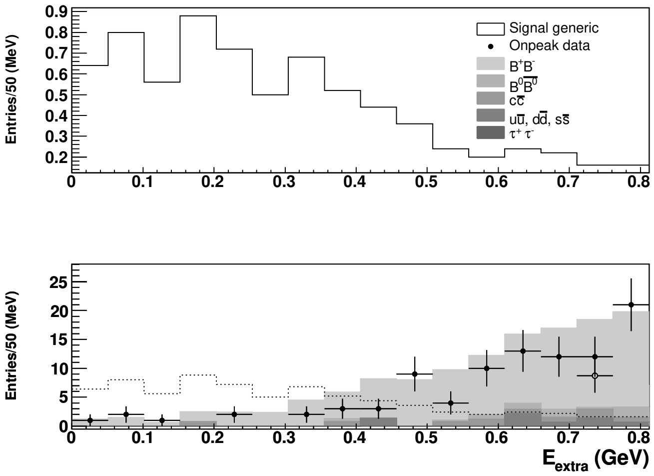

Figure 4–31: E_{extra} distribution for tagged events with a K^- candidate and $N_{\mathrm{extra}} < 3$. We observe a slight over-estimation of MC samples.

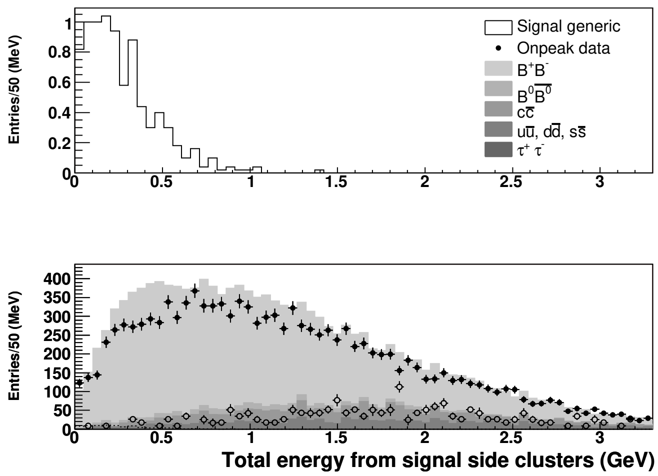

Figure 4–32: Total energy of signal side clusters for tagged events with a K^- candidate and $N_{\mathrm{extra}} < 3$.

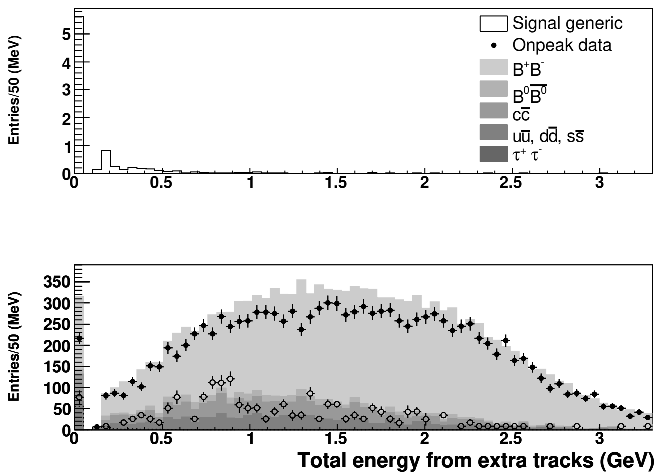

Figure 4–33: Total energy of extra tracks for tagged events with a K^- candidate and $N_{\mathrm{extra}} < 3$.

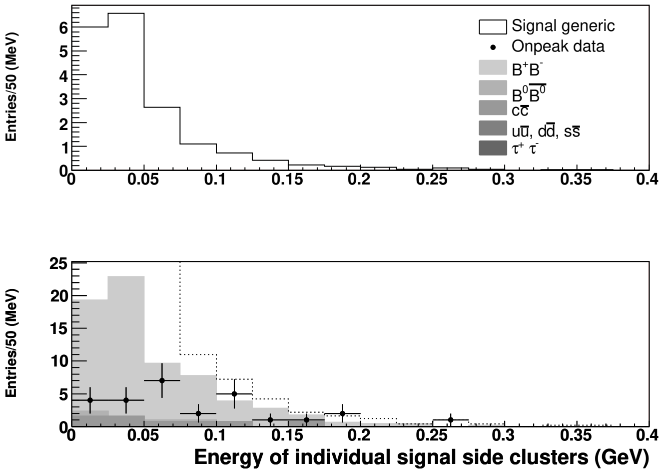

Figure 4–34: Energy distribution of individual clusters for tagged events with a K^- candidate, $N_{\text{extra}} < 3$ and $E_{\text{extra}} < 0.400$ GeV. We observe an over-estimation of clusters with energy below 50 MeV, especially in B^+B^- events.

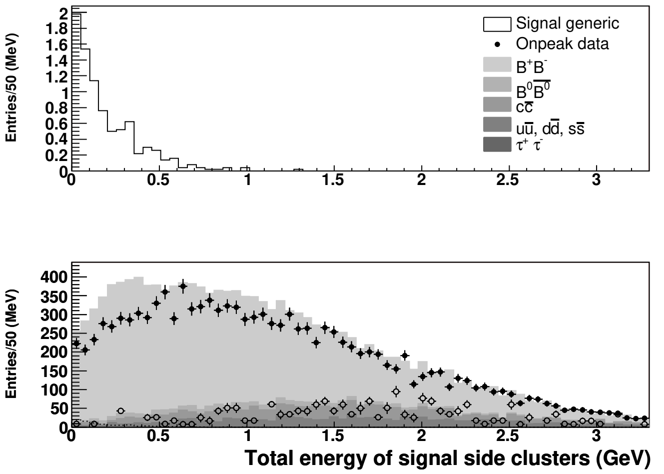

Figure 4–35: Total energy of signal side clusters for tagged events with a K^- candidate and $N_{\text{extra}} < 3$, with a 50 MeV threshold on individual cluster energy. We observe an improved agreement in the low-energy regime.

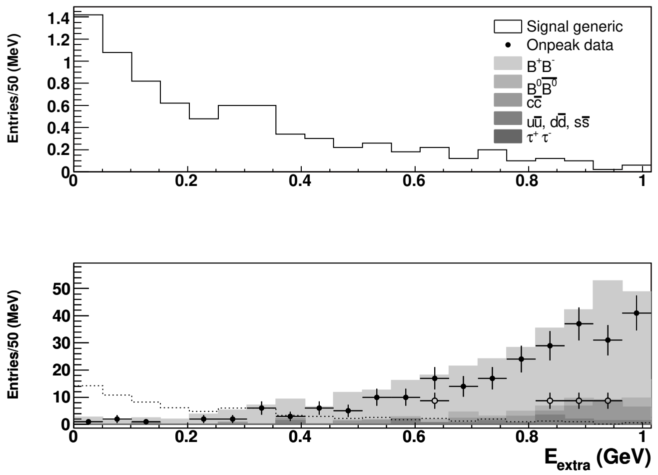

Figure 4–36: $E_{\rm extra}$ distribution for tagged events with a K^- candidate and $N_{\rm extra} < 3$, with a 50 MeV threshold on individual cluster energy. We observe a slight over-estimation of MC samples.

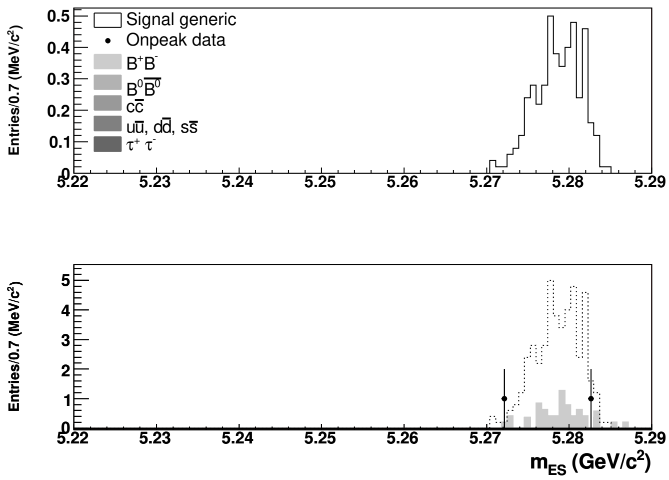

Figure 4–37: $m_{\rm ES}$ distribution after all selections have been applied, with a 50 MeV threshold on the individual cluster energy. We count 2 onpeak data events in the signal box, but expect about 8.5 background events.

be held responsible for the discrepancy since the problem persists with $N_{\mathrm{extra}} = 0$, however it could be caused by an incorrect modeling of the extra track multiplicity in background event. As a matter of fact, Figure 4–33 show a clear excess of MC events in the "zero" bin, suggesting that the events with $N_{\mathrm{extra}} = 0$ are problematic, although is not obvious why at this point.

4.7.2 Examination of the K^- Candidate

We finally turn our attention towards the K^- candidate and its momentum distribution. In order to isolate the problem with a high confidence level, we keep the 50 MeV threshold on the cluster energy, thus reducing the systematic uncertainty. Even before the restriction on E_{extra} is applied, the p_{K}^{B} distribution already shows a discrepancy in the region $p_{\mathrm{K}}^{B} > 1.1\,\mathrm{GeV}/c$ (see Figure 4–40). We study the progressive impact of the E_{extra} restriction by looking at the p_{K}^{B} distribution after requiring $E_{\mathrm{extra}} < 0.600$ GeV, $E_{\mathrm{extra}} < 0.500$ GeV and $E_{\mathrm{extra}} < 0.400$ GeV (Figures 4–41, 4–42 and 4–43). We observe that the region $p_{\mathrm{K}}^{B} > 1.1\,\mathrm{GeV}/c$ gradually looses its data content and exhibits a clear over-estimation of B^+B^- events. That is, the excess of peaking events, especially those with no extra tracks (and low E_{extra}), is predominant in the high momentum region of the p_{K}^{B} distribution, i.e. exactly those with the $B^- \to K^-\nu\overline{\nu}$ topology.

The problem might be related with our general topology selection algorithm, i.e. looping over high-momentum tracks and suppressing the extra energy, or with the K^- identification itself. In order to verify these hypotheses, we reproduce the same analysis but without requiring the high-momentum track to be a K^-. Since there are roughly ten times more $\pi^{\pm}$ than $K^{\pm}$ produced at *BABAR*, we expect that there should

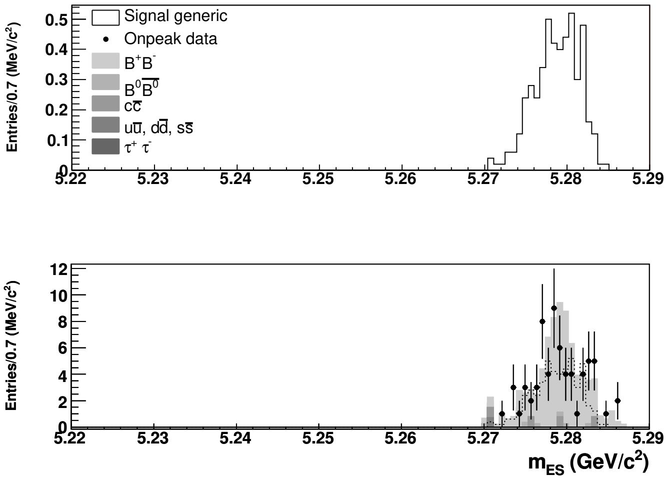

Figure 4–38: m_{ES} distribution for tagged events inside the m_{ES} signal box, with a K^- candidate with $p_{\mathrm{K}}^{B} > 1.1\,\mathrm{GeV}/c$, total neutral energy $< 400\,\mathrm{GeV}$, $N_{\mathrm{extra}} = 1$ and $-0.85 < \cos\theta_{Pmiss} < 0.90$. We count 49 data events and expect about 77 background events.

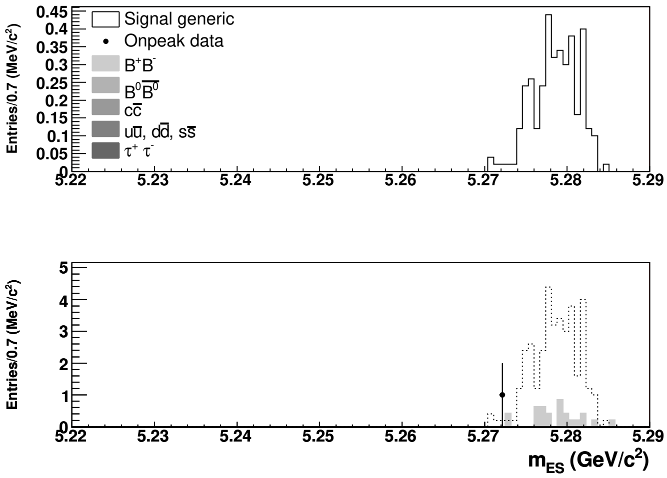

Figure 4–39: m_{ES} distribution for tagged events inside the m_{ES} signal box, with a K^- candidate with $p_{\mathrm{K}}^{B} > 1.1\,\mathrm{GeV}/c$, total neutral energy $< 400\,\mathrm{GeV}$, $N_{\mathrm{extra}} = 0$ and $-0.85 < \cos\theta_{Pmiss} < 0.90$. We count 1 onpeak data events in the signal box and expect about 5 background events.

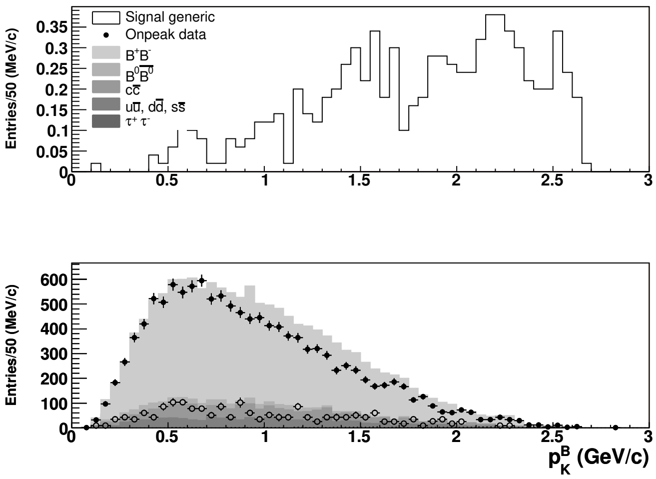

Figure 4–40: p_{K}^{B} distribution for tagged events with a K^- candidate and $N_{\mathrm{extra}} < 3$. We see a discrepancy in the region $p_{\mathrm{K}}^{B} > 1.1\,\mathrm{GeV}/c$.

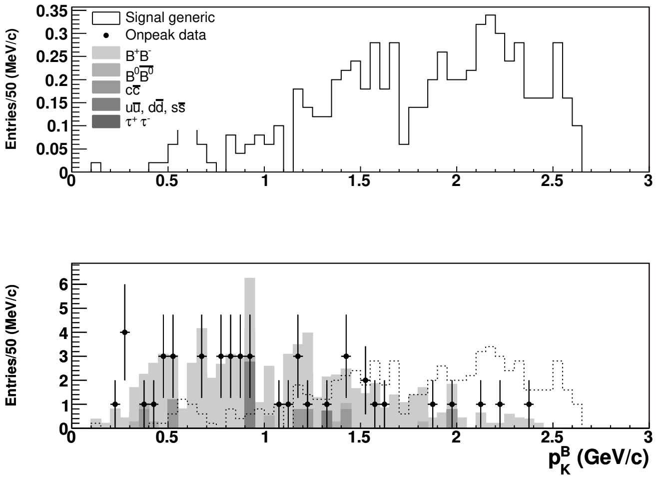

Figure 4–41: p_{K}^{B} distribution for tagged events with a K^- candidate, $N_{\mathrm{extra}} < 3$ and $E_{\mathrm{extra}} < 0.600$ GeV, with a 50 MeV threshold on individual cluster energy.

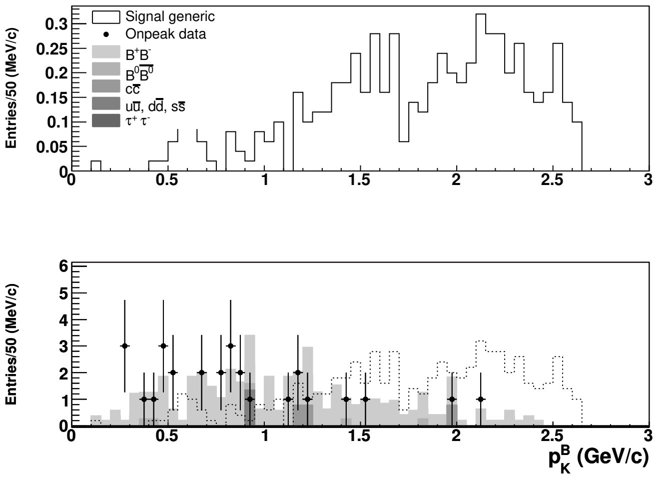

Figure 4–42: p_{K}^{B} distribution for tagged events with a K^{-} candidate, $N_{\mathrm{extra}} < 3$ and $E_{\mathrm{extra}} < 0.500$ GeV, with a 50 MeV threshold on individual cluster energy.

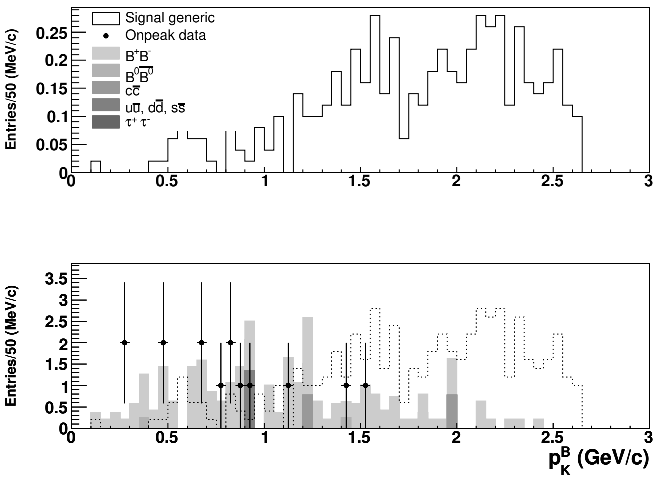

Figure 4–43: p_{K}^{B} distribution for tagged events with a K^{-} candidate, $N_{\mathrm{extra}} < 3$ and $E_{\mathrm{extra}} < 0.400$ GeV, with a 50 MeV threshold on individual cluster energy.

be about ten times more background events surviving the selection. We present in Figures 4–44 and 4–45 the E_{extra} and the p^{B}_{trk} distributions for events with a B_{tag} and $N_{\mathrm{extra}} < 3$, and in Figures 4–46, 4–47 and 4–48 the p^{B}_{trk} distributions after requiring $E_{\mathrm{extra}} < 0.600$ GeV, $E_{\mathrm{extra}} < 0.500$ GeV and $E_{\mathrm{extra}} < 0.400$ GeV. We observe a high degree of agreement in all these distributions, implying that the problem is not related to the general class of events with that topology, but only from the portion of them in which the high-momentum track is a K^{-}. Since the $K^{\pm}$ identification criteria we use have been carefully validated by experts in the *BABAR* collaboration, we conclude that either the MC samples are reconstructing fake high-momentum K^{-}, or the topology of the B_{sig} is not correctly modeled or reconstructed. For example, it could be the case that the extra tracks in MC samples have a lower multiplicity or are simply lost at a greater rate.

4.7.3 Examination of the Monte Carlo "Truth"

To verify whether the problem comes from fake K^{-} candidates, from an incorrect modeling of the multiplicity of the extra tracks or from their recontruction, we look at the decay of the 22 $B^{+}B^{-}$ MC events that are selected using the MC "truth" (or "cheat") information, The decay trees of these events are provided in the Appendix. In all those events, the B_{tag} are correctly reconstructed (i.e. they are peaking events) and the K^{-} candidates selected are real, confirming that our B meson reconstruction and our K^{-} selection algorithm are correct, hence the problem most likely come from N_{extra}. We present in Table 4–17 the decay types, the number of extra tracks observed and generated (N^{obs}_{extra} and N^{gen}_{extra}), the number of signal side clusters generated N^{gen}_{clus} (π^{0} candidates count as two clusters) and the number of particles that are normally

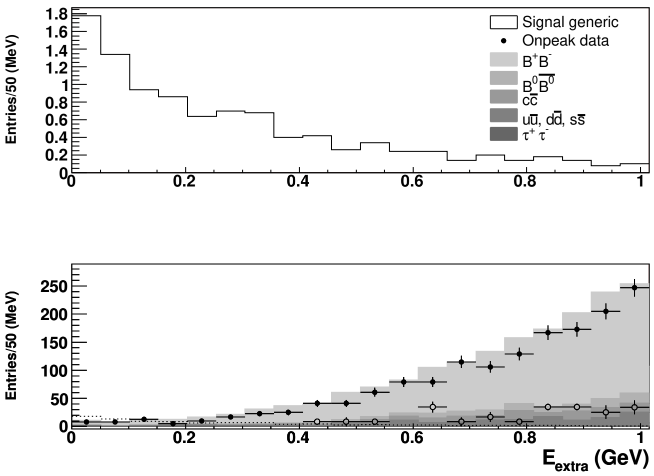

Figure 4–44: E_{extra} distribution for tagged events with a K^- candidate and $N_{\text{extra}} < 3$, with a 50 MeV threshold on individual cluster energy. We observe a slight over-estimation of MC samples.

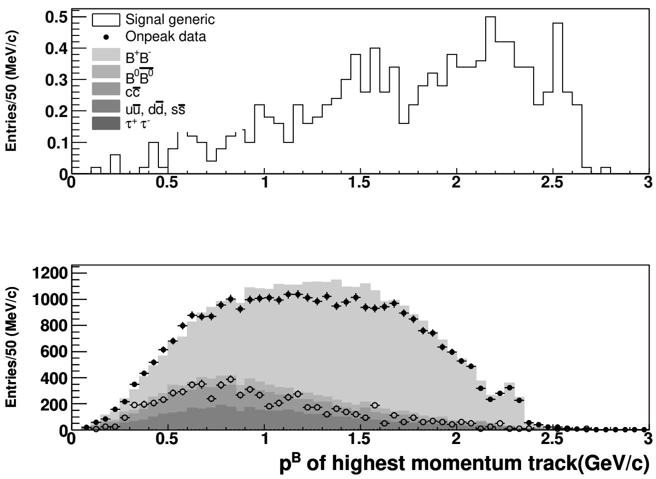

Figure 4–45: p^B distribution of the track with the highest momentum, for tagged events with $N_{\text{extra}} < 3$.

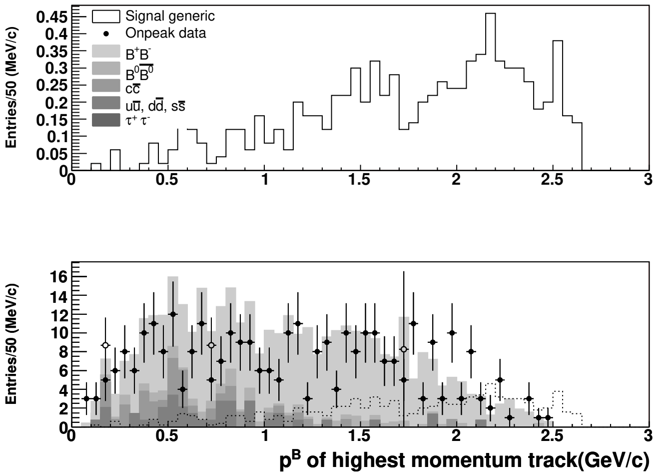

Figure 4–46: p^B distribution of the track with the highest momentum, for tagged events with $N_{\mathrm{extra}} < 3$ and $E_{\mathrm{extra}} < 0.600$ GeV, with a 50 MeV threshold on individual cluster energy.

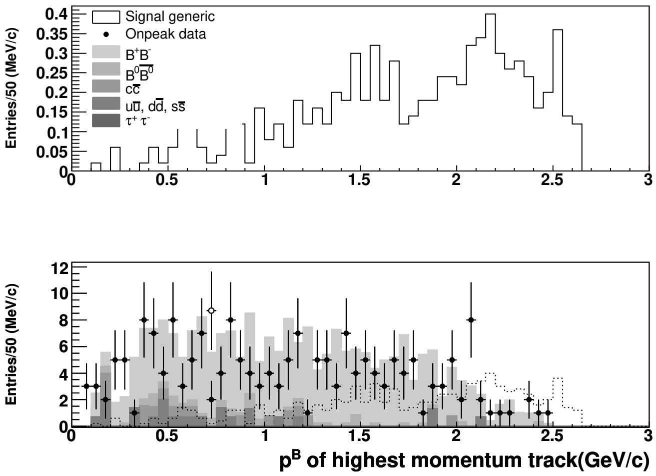

Figure 4–47: p^B distribution of the track with the highest momentum, for tagged events with $N_{\mathrm{extra}} < 3$ and $E_{\mathrm{extra}} < 0.500$ GeV, with a 50 MeV threshold on individual cluster energy.

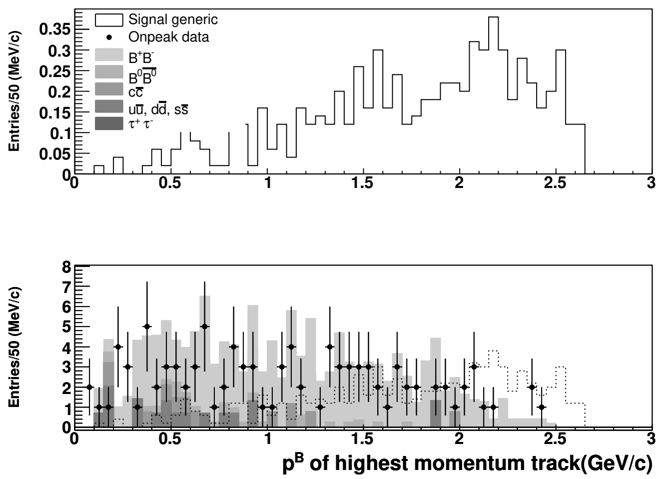

Figure 4–48: p^B distribution of the track with the highest momentum, for tagged events with $N_{\text{extra}} < 3$ and $E_{\text{extra}} < 0.400$ GeV, with a 50 MeV threshold on individual cluster energy.

not detected (ν, $\overline{\nu}$ and K^0_L). We observe 18 events of the type $B^- \rightarrow D^{(*)0}\ell^-\nu_\ell(\gamma)$, three of the type $B^- \rightarrow D^{(*)0}X^-_{c,s}$ where $X^-_{c,s}$ is a hadronic system made of D^-_s, K^0 and $K^\pm$ mesons, and one $B^- \rightarrow \tau^-\overline{\nu}_\tau$. It appears that 20 of these background events have 2 extra tracks generated, usually one from the B^- decay and the other from the D^0 decay, and that most of them are not observed in the detector. Since all the B_{tag} seem correctly reconstructed, we conclude that the extra tracks are probably lost, falling outside the acceptance of the detector or absorbed by inactive material. As a result of this leak, the value of E_{extra} is shifted towards lower values, enhancing the selection efficiency of the peaking background. We notice that all of these events have at least one ν, $\overline{\nu}$ or K^0_L, such that even if a charged particle passes outside the detector's acceptance, the total missing momentum vector can point inside the acceptance. Although the exact source of the over-estimation is not clear, there is definitely a problem with reconstruction of the extra tracks.

We also notice that the K^- candidate comes from the decay of a D^0 in 19 events, 16 of which are of the type $D^0 \rightarrow K^-\ell^+\nu$. The calculation of the braching ratio of these processes involves form factors that are not known with a great precision, so it is possible that the number of these events are over-estimated in MC samples. The same situation exists for the modeling of the $B^- \rightarrow D^{(*)0}\ell^-\nu_\ell(\gamma)$ decays, however it is unlikely that this effect could be large enough to account for the entire observed discrepancy. The $D^0 \rightarrow K^-\ell^+\nu$ decays usually produce low-momentum K^-, while in this analysis, the $B^- \rightarrow \tau^-\overline{\nu}_\tau$ and $B^- \rightarrow D^{*0}K^0K^-$ events produced $p_{\mathrm{K}}^B = 2.42$ and 2.26 GeV/c respectively. If the problem is there, it could be possible to reduce its effect by requiring the K^- candidate to have a higher momentum. However, the investigation that is required in order to confirm or reject these hypotheses is beyond the scope of this research project, hence we do not correct the problem and we fail to recover the previous results with this sub-sample.

4.7.4 Impact of the Discrepancy on the Analysis

The last step is to verify if the over-estimation of peaking background is present in the full $208.73\,\mathrm{fb}^{-1}$ data set. Table 4–16 presents the number of MC and data events selected in the $80.03\ \mathrm{fb}^{-1}$ and in the $208.73\,\mathrm{fb}^{-1}$ data samples. The quantities found in the data sub-sample are also scaled to the full sample luminosity for a more direct comparison. We first observe in this Table that when we remove the $K^{\pm}$ ID requirement, the over-estimation of $B^{+}B^{-}$ events in not present in the full data set, like in the sub-sample. In addition, without the $K^{\pm}$ requirement, the scaled sub-sample agrees with the full sample within statistical error. From these two observations, we conclude that apart from the $K^{\pm}$ identification, the behavior of our full selection operates the same way on the two samples.

We also observe from this Table that in both samples, the number of MC events selected with a $K^{\pm}$ is about a factor of two bigger than what we naively expect. For example, in the $208.73\,\mathrm{fb}^{-1}$ sample, we count 87.30 ± 4.20 events before the $K^{\pm}$ requirement, so we expect about $(87.30 \pm 4.20) \div 10 = 8.73 \pm 0.42$, but we observe 18.96 ± 1.89. This behavior is also present in the $80.03\ \mathrm{fb}^{-1}$ data sub-sample. We conclude that the $K^{\pm}$ identification acts similarly in both data samples, hence the over-estimation of the peaking component should also be present in the full sample. As a consequence, we do not unblind the remainder of the data sample until the problem is fixed.

To summarize our investigation, we first observe that the discrepancy comes from the peaking component of the $B^{+}B^{-}$ MC sample. We examine the selection criteria and find that the problem must be related to either the E_{extra} distribution,

Table 4–16: Comparison between the number of MC and data events selected in the 80.03 fb^{-1} sub-sample and in the 208.73 fb^{-1} sample. We also compare the effect of removing the K^- identification criteria. We recall that in the *BABAR* experiment, there are about ten times more $\pi^\pm$ than $K^\pm$ produced. The errors quoted here are statistical only.

	Events selected in the 80.03 fb^{-1} sample	Events selected in the 80.03 fb^{-1} sample, scaled to the 208.73 fb^{-1} sample	Events selected in the 208.73 fb^{-1} sample
Without the $K^\pm$ ID	MC: 39.27 ± 3.14 Data: 34 ± 5.8	MC: 104.17 ± 8.33 Data: 90.2 ± 15.5	MC: 87.30 ± 4.20 Data: 95 ± 9.8
With the $K^\pm$ ID	MC: 8.32 ± 1.40 Data: 2 ± 1.4	MC: 22.07 ± 3.71 Data: 5.3 ± 3.7	MC: 18.96 ± 1.89 Data: (*blind*)

the p_{K}^{B} distribution, the K^- selection itself, or a combination of them. From our examination of E_{extra}, we find that the discrepancy cannot be due to the excess of low-energy clusters in the B^+B^- sample, but we discover that there is an over-estimation of MC events with no extra tracks. By examining the p_{K}^{B} distribution, we also discover that the events with low E_{extra} are over-estimating the data in the high momentum portion of the distribution. We find that both of these effects disappear if we remove the K^- ID requirement, so the problem concerns only the events in which the track with the highest momentum is a K^-. We finally look at the MC truth information and find out that the reconstructed B_{tag} candidates are peaking backgrounds, that the K^- candidate selected are real K^-, that most extra tracks generated are not reconstructed and that the majority of the B_{sig} decays are or the type $B^- \to D^{(*)0}\ell^-\nu_\ell$. We conclude that, for reasons which are not clear, the B^+B^- MC sample is over-estimating the number of events with a high momentum K^-, with low neutral energy, low extra track multiplicity, and with one or two extra tracks that are lost.

Table 4–17: Decay types, number of extra tracks observed and generated, number of clusters generated and number of ν, $\overline{\nu}$ and K^0_L generated in the selected B^+B^- MC events.

Decay Type	N^{obs}_{extra}	N^{gen}_{extra}	N^{gen}_{clus}	$N_\nu + N_{KL}$
$B^- \to D^{(*)0}\ell^-\nu_\ell$	1	2	3	2
$B^- \to D^{(*)0}\ell^-\nu_\ell$	0	2	1	2
$B^- \to D^{(*)0}\ell^-\nu_\ell$	0	2	0	1
$B^- \to \tau^-\overline{\nu}_\tau$	0	0	0	2
$B^- \to D^{(*)0}\ell^-\nu_\ell\gamma$	0	2	1	2
$B^- \to D^{(*)0}X^-_{c,s}$	0	2	0	3
$B^- \to D^{(*)0}\ell^-\nu_\ell$	1	2	0	2
$B^- \to D^{(*)0}\ell^-\nu_\ell$	1	2	2	2
$B^- \to D^{(*)0}\ell^-\nu_\ell\gamma$	0	2	3	2
$B^- \to D^{(*)0}\ell^-\nu_\ell$	0	2	1	2
$B^- \to D^{(*)0}\ell^-\nu_\ell$	1	2	2	1
$B^- \to D^{(*)0}\ell^-\nu_\ell$	0	2	2	1
$B^- \to D^{(*)0}\ell^-\nu_\ell$	0	2	0	2
$B^- \to D^{(*)0}\ell^-\nu_\ell$	1	2	2	2
$B^- \to D^{(*)0}X^-_{c,s}$	0	0	3	2
$B^- \to D^{(*)0}\ell^-\nu_\ell$	0	2	1	2
$B^- \to D^{(*)0}\ell^-\nu_\ell$	0	2	0	2
$B^- \to D^{(*)0}\ell^-\nu_\ell$	0	2	0	2
$B^- \to D^{(*)0}X^-_{c,s}$	0	2	2	1
$B^- \to D^{(*)0}\ell^-\nu_\ell$	0	2	2	2
$B^- \to D^{(*)0}\ell^-\nu_\ell$	0	2	2	2
$B^- \to D^{(*)0}\ell^-\nu_\ell$	0	2	2	2

CHAPTER 5
Results

In Chapter 4, we have estimated ε_{tot} and N_{bg} using $208.73\,\text{fb}^{-1}$ of onpeak data and various MC samples. In an attempt to reproduce a previous measurement based on 80.03 fb^{-1}, we observed an important over-estimation of peaking $B^{+}B^{-}$ MC event that we believe is present in the full data sample. As a result, we do not trust the quantities obtained from the MC samples, and the measurement of the upper limit of the full sample is not possible at this time. However, the *BABAR* Simulation Production Group generates on a regular basis improved MC samples, so it is likely that the problem we encounter here will be fixed in the next version. In that case, the present analysis could be applied to the updated MC and data samples and would finally measure the upper limit on $\mathcal{B}(B^{-} \to K^{-}\nu\overline{\nu})$.

In this chapter, we describe how we would compute the limit assuming that the MC description had been validated by the sub-sample. We then give recommendations for the future analysis, and we end with a conclusion and a summary of the research.

5.1 The Upper Limit

When the problem with MC-data discrepancy will be corrected, this analysis will set an upper limit (UL) on $\mathcal{B}(B^{-} \to K^{-}\nu\overline{\nu})$ with a confidence level (CL) of 90 % using a frequentist approach that incorporates the statistical and the systematic uncertainties on ε_{tot} and on N_{bg} in the calculation, as well as the number of signal

MC events used [44]. The quantities involved in this measurement are listed in Table 5–1. Since 128.70 fb^{-1} of the data sample remains blinded, we do not know N_{obs}, but we can compute the UL for various values of N_{obs}. In Table 5–2, we organize these results assuming that the population distribution of N_{obs} is a Gaussian centered on N_{bg}. In such a distribution, 70 % of the population lies within 1σ, 25 % in the $1\sigma - 2\sigma$ band, and less than 5 % lies outside the 2σ box. Table 5–3 lists the previous UL obtained by the *BABAR* [1], BELLE [2] and CLEO [47] collaborations, as well as the size of the data sets analyzed.

5.2 Conclusion

As seen in Table 5–1, the sensitivity on the $B^- \to K^-\nu\overline{\nu}$ process is still an order of magnitude above the SM expectation of $3.8^{+0.12}_{-0.06} \times 10^{-6}$. If this analysis was completed with the current estimate of peaking background events, we would not be able to *see* the process at the SM rate, but we could set a UL on its branching ratio. In that case, the UL could still set experimental limits on parameters in various new physics scenarios, as explained in Chapter 2. In order for the signal decay to be observed at a high confidence level, its branching ratio must be greatly enhanced by physics beyond the SM.

If our estimates for the total efficiency and the number of expected background are accurate, we expect the unblinded results to set an UL on the process somewhere between the BELLE and the *BABAR* previous results. It should be mentioned that the previous *BABAR* results is a combination of two independent measurements, which enhances the statistical accuracy of the measurement. If we were to observe a number of data events corresponding to the central value of our background estimate, we

Table 5–1: Numbers used to compute the upper limit on the branching ratio for the process $B^- \to K^- \nu\overline{\nu}$. See beginning of Chapter 4 for the formula of the branching fraction. As explained in the text, we do not measure N_{obs} for the full data set.

$\sigma_{B^+B^-}$	0.525
$\mathcal{L}$	$208.73\,\mathrm{fb}^{-1}$
$N_{B^\pm}$	$(229.953 \pm 1.473) \times 10^6$
$\varepsilon_{\mathrm{tot}}$	$(0.0678 \pm 0.0043$ (stat) ± 0.0088 (syst)) %
N_{bg}	14.95 ± 1.75 (stat) ± 1.09 (syst)
N_{obs}	-

Table 5–2: Upper limits (UL) at 90 % confidence level (CL) on the branching ratio of the process $B^- \to K^- \nu\overline{\nu}$, using the Cousins-Highland method and for various values of N_{obs}. Assuming that the probability distribution of N_{obs} is a Gaussian centered on N_{bg}, 70 % lies within 1σ, 25 % in the 2σ band, and less than 5 % lies outside.

N_{obs}	UL ($\times 10^{-5}$)	σ
$\vdots$	$\vdots$	$\vdots$
10	0.73	3σ
11	1.50	2σ
12	2.27	2σ
13	3.02	1σ
14	3.78	1σ
15	4.54	central
16	5.29	1σ
17	6.07	1σ
18	6.84	2σ
19	7.60	2σ
20	"evidence" for $B^- \to K^- \nu\overline{\nu}$	3σ
$\vdots$	$\vdots$	$\vdots$
24	"discovery" of $B^- \to K^- \nu\overline{\nu}$	5σ

Table 5–3: Previous results for the measurement of $\mathcal{B}(B^- \rightarrow K^- \nu\overline{\nu})$. All upper limits are calculated at a 90% CL. At the moment, the experimental reach is about an order of magnitude above the value predicted by the SM.

Collaboration	$\mathcal{B}$	data set (fb^{-1})
BABAR	$< 5.2 \times 10^{-5}$	82.00
BELLE	$< 3.6 \times 10^{-5}$	253.00
CLEO	$< 6.1 \times 10^{-4}$	9.24
Standard Model	$3.8^{+0.12}_{-0.06} \times 10^{-6}$	-

would set an upper limit of 4.54×10^{-5} on the process. It is likely however that due to statistical fluctuations, the actual N_{obs} will differ from the central value by one or more events, resulting in tighter or looser limits. If we had measured N_{obs} at least 3σ above the central value ($\sim$ 20 events), we would have found "evidence" for the $B^- \rightarrow K^- \nu\overline{\nu}$ process, while at 5σ above ($\sim$ 24 events), we would have attained the "discovery threshold", which lead to a measurement of the branching ratio.

In this analysis we have found that the B^+B^- MC sample appears to overestimate the peaking background in data for reasons that are not clear. Detailed MC-data comparisons and MC truth studies have not identified any clear-cut source of this discrepancy. We recall that the MC samples used in this analysis are statistically independant from the set used by the previous analysis, they have been re-generated, and both MC and data samples have been re-processed since. Moreover, the selection requirements that were used in this analysis are significantly different from those in the previous analysis. Any meaningful comparison should be made on an event-by-event basis, which is not possible due to the different MC samples, consequently our result does not invalidate the previous *BABAR* measurement. The *BABAR* Simulation Production Group is aware of these issues and has worked to improved the situation in the next version of the MC sample, which will soon be ready to analyze. It is thus possible that the discrepancy will not show up that time.

We have recommendations for the next $B^- \to K^-\nu\overline{\nu}$ analysis, which will have a data set at least two times bigger. The systematic uncertainty on E_{extra} can be reduced by applying a 50 MeV threshold on the energy of the individual clusters, but doing so, the full E_{extra} distribution is shifted towards lower energy. The cost is that the requirement on this variable must be re-optimized to a tighter value, reducing ε_{tot}. We also recommend to select K^- candidates with a momentum even higher in order to avoid possible MC-data discrepancy due to uncertainty in the form factor of the $B^+ \to D^{(*)0}\ell\nu$ and $D^0 \to K^-\ell^+\nu$ processes, our main background contribution. We hope that the present work will help the next researcher to overcome the difficulties that will be encountered, and we are looking forward to see the result of the next analysis.

5.3 Summary

We search for the process $B^- \to K^-\nu\overline{\nu}$ in about 230 million $B\overline{B}$ pairs recorded by the *BABAR* detector. We fully reconstruct one of the B^+ meson via specific hadronic channels, and we look in the rest of the event for a high momentum K^-. We optimize our selection requirements in order to maximize the total signal selection efficiency and reject as much background as possible. We obtain an efficiency of $(0.0678 \pm 0.0043\text{ (stat) } \pm 0.0088\text{ (syst) })\ \%$, and we estimate that, with our selection, $14.95 \pm 1.75\text{ (stat) } \pm 1.09\text{ (syst)}$ background events should appear in data. However, we discovered in a sub-sample of 80.03 fb^{-1} of data a discrepancy between the number of events selected in the MC and data samples, and we are not able to attribute this discrepancy to any single source. Since we believe that the same problem is likely to be present in the full sample, we do not attempt to extract a limit on $B^- \to K^-\nu\overline{\nu}$ from the full data set. Instead, we present a number of studies intended to characterize this effect, with the expectation that they will of use for ongoing studies of this decay mode by collaborators of the *BABAR* experiment.

Appendix

This Appendix contains the decay patterns of the 22 B^+B^- events that were selected by our set of requirements. Each pattern must be read from top to bottom, starting from the $\Upsilon(4S)$ ("`Upsilon(4S)`"), which decays in a B_{tag} and a B_{sig}. The B_{tag} decays in one of the allowed channel listed in Table 4–2, and the B_{sig} contains the $K^\pm$ candidate.

```
Upsilon(4S)
|_ B+ --------------B-
   |_ anti-D0 pi+   |_ D*0 anti-nu_mu mu-
      |_ pi0 pi- K+    |_ D0 pi0
                          |_ gamma nu_e e+ K-
Upsilon(4S)
|_ B+ ---------------B-
   |_ anti-D*0 pi+   |_ D*0 anti-nu_e e-
      |_ anti-D0 pi0    |_ D0 gamma
         |_ pi- K+         |_ nu_e e+ K-
Upsilon(4S)
|_ B+ ------------------B-
   |_ anti-D0 nu_mu mu+ |_ D*0 -------------rho-
      |_ pi- K+            |_ D0 pi0        |_ pi0 pi-
                              |_ pi0 pi+ K-
Upsilon(4S)
|_ B+ ------------------------------B-
   |_ anti-D*0 ----------rho+       |_ tau- anti-nu_tau
      |_ anti-D0 gamma   |_ pi0 pi+    |_ nu_tau K-
         |_ gamma pi- K+
Upsilon(4S)
|_ B+ ----------------------B-
   |_ anti-D0 gamma nu_e e+ |_ D*0 -------------rho-
      |_ anti-nu_e e- K+       |_ D0 gamma      |_ pi0 pi-
                                  |_ pi0 pi+ K-
```

```
Upsilon(4S)
|_ B+ -----------------------------------------B-
   |_ anti-D0 -----------D_s+                 |_ rho- ------D0
      |_ anti-nu_e e- K+ |_ tau+ nu_tau          |_ pi0 pi- |_ pi+ K-
                            |_ anti-nu_tau pi+
Upsilon(4S)
|_ B+ --------------------------B-
   |_ anti-D0 ------anti-K*0 K+ |_ D0 anti-nu_mu mu-
      |_ pi0 pi- K+ |_ pi+ K-      |_ nu_e e+ K-
Upsilon(4S)
|_ B+ ------------------------B-
   |_ anti-D*0 nu_e e+        |_ rho- ------D0
      |_ anti-D0 pi0             |_ pi0 pi- |_ pi0 pi+ K-
         |_ anti-nu_mu mu- K+
Upsilon(4S)
|_ B+ -----------------------B-
   |_ anti-D*0 gamma nu_e e+ |_ rho- ------D0
      |_ anti-D0 pi0            |_ pi0 pi- |_ pi0 pi+ K-
         |_ anti-nu_e e- K+
Upsilon(4S)
|_ B+ ------------------------B-
   |_ anti-D*0 nu_mu mu+      |_ a_1- ---------D0
      |_ anti-D0 gamma           |_ rho0 pi-   |_ pi0 pi+ K-
         |_ anti-nu_mu mu- K+       |_ pi- pi+
```

```
Upsilon(4S)
|_ B+ ------------------B-
   |_ anti-D0 nu_mu mu+ |_ rho- ------D0
      |_ pi0 pi- K+        |_ pi0 pi- |_ pi0 pi+ K-
Upsilon(4S)
|_ B+ ----------------B-
   |_ anti-D0 nu_e e+ |_ rho- ------D0
      |_ pi0 pi- K+      |_ pi0 pi- |_ pi0 pi+ K-
Upsilon(4S)
|_ B+ ---------------------B-
   |_ anti-D0 nu_mu mu+    |_ a_1- ---------D0
      |_ anti-nu_mu mu- K+    |_ rho0 pi-   |_ anti-K*0 pi- pi+
                                 |_ pi- pi+    |_ pi+ K-
Upsilon(4S)
|_ B+ ----------------------------B-
   |_ a_1+ ---------anti-D0       |_ D*0 anti-nu_mu mu-
      |_ rho0 pi+   |_ pi0 pi- K+    |_ D0 pi0
         |_ pi- pi+                     |_ nu_e e+ K-
Upsilon(4S)
|_ B+ -------------------------B-
   |_ rho+ ------anti-D0       |_ D*0 --------------K0 K-
      |_ pi0 pi+ |_ pi0 pi- K+    |_ D0 gamma       |_ K_L0
                                     |_ anti-K0 pi0
                                        |_ K_L0
```

```
Upsilon(4S)
|_ B+ ----------------------B-
   |_ anti-D*0 nu_mu mu+    |_ D*0 pi-
      |_ anti-D0 gamma         |_ D0 pi0
         |_ anti-nu_e e- K+       |_ pi0 pi+ K-
Upsilon(4S)
|_ B+ ----------------------------B-
   |_ a_1+ ---------anti-D0       |_ D0 anti-nu_e e-
      |_ rho0 pi+   |_ pi0 pi- K+    |_ nu_mu mu+ K-
         |_ pi- pi+
Upsilon(4S)
|_ B+ ---------------------B-
   |_ anti-D0 nu_mu mu+    |_ D*0 pi-
      |_ anti-nu_mu mu- K+    |_ D0 pi0
                                 |_ pi0 pi+ K-
Upsilon(4S)
|_ B+ ----------------------------------B-
   |_ a_1+ ---------anti-D0             |_ D0 K-
      |_ rho0 pi+   |_ pi0 gamma pi- K+    |_ anti-K0 pi0
         |_ pi- pi+                           |_ K_L0
```

```
Upsilon(4S)
|_ B+ ------------------------B-
   |_ anti-D*0 nu_mu mu+      |_ D*0 -------------rho-
      |_ anti-D0 pi0             |_ D0 pi0        |_ pi0 pi-
         |_ anti-nu_mu mu- K+       |_ pi0 pi+ K-
Upsilon(4S)
|_ B+ -------------------------------B-
   |_ anti-D*0 --------a_1+          |_ D*0 anti-nu_mu mu-
      |_ anti-D0 pi0   |_ rho0 pi+      |_ D0 pi0
         |_ pi0 pi- K+    |_ pi- pi+       |_ nu_e e+ K-
Upsilon(4S)
|_ B+ ----------------------------B-
   |_ rho+ ------anti-D0          |_ D*0 anti-nu_e e-
      |_ pi0 pi+ |_ a_1- K+          |_ D0 pi0
                    |_ rho0 pi-         |_ nu_mu mu+ K-
                       |_ pi- pi+
```

REFERENCES

[1] B. Aubert *et al.*(*BABAR* Collaboration), hep-ex/0408086 (2005).

[2] K. Ikado *et al.*(BELLE Collaboration), hep-ex/0507034 (2005).

[3] G. Buchalla, G. Hiller and G. Isidori, *Phys. Rev. D*, **63**, 014015 (2001).

[4] M. E. Peskin, D. V. Schroeder, *An Introduction to Quantum Field Theory*, Ed. Westview, Boulder (1995).

[5] P. Higgs *Phys. Rev. Lett.* **13**, 508 (1964).

[6] Particle Data Group, D. E. Groom *et al.*, *Eur. Phys. Jour. C* **15** 1 (2004).

[7] *Phenomenology and Lattice QCD*, Proceeding of the Uehling Summer School on Phenomenology and Lattice QCD, Eds. G. Kilcup and S. Sharpe, World Scientist (1995).

[8] M. Neubert, *Phys. Rep.*, **245**, 259 (1994).

[9] S. Narison, *QCD Spectral Sum Rules*, World Scientific (1981).

[10] N. Cabibbo, *Phys. Rev. Lett.*, **10**, 531 (1963).

[11] K. Kobayashi and T. Maskawa, *Prog. Th. Phys.* **49**, 652 (1973).

[12] Super Kamiokande Collaboration, *Phys. Rev. Lett.*, **93**, 101801 (2004).

[13] M. Reuter, H. Weyer, *Phys. Rev. D*, **70**, 124028 (2004).

[14] A. J. Buras, M. Spranger and A. Weilner, *The Impact of Universal Extra Dimensions on the Unitarity Triangle and Rare K and B Decays*, hep-ph/0212143, (2002).

[15] T. Barakat, *Rare* $B^- \to K^{*-}\nu\overline{\nu}$ *Decay with Polarized* K^* *in the Fourth Generation Model*, hep-ph/0106296, (2001).

[16] B. Holdom and M. V. Ramana, *New Flavor Physics in b Decays*, hep-ph 9509272, (1995).

[17] G. Buchalla, G. Burdman, C. T Hill and D. Kominis, *GIM Violation and New Dynamics of the Third Generation*, hep-ph/9510376 (1995).

[18] C. Bird, R. Kowalewski and M. Pospelov, *Mod.Phys.Lett. A*,**21**, 457 (2006)

[19] C. Bobeth, A. Buras, F. Krüger and J. Urban, *QCD Corrections to* $B \to X_{d,s}\nu\overline{\nu}$*,* $B^0 \to \ell^+\ell^-$*,* $K^+ \to \pi^+\nu\overline{\nu}$ *and* $K^0_L \to \mu^+\mu^-$ *in the MSSM*, hep-ph/0112305 (2001).

[20] Z. Xiao and L. Yao, *Rare Decay* $B \to X_s\nu\overline{\nu}$ *in the Two-Higgs-Doublet Model of Type-III*, hep-ph/0212008 (2002).

[21] D. Melikhov, N. Nikitin and S. Simula, *Right-Handed Currents in Rare Exclusive* $B^- \to K^{(*)-}\nu\overline{\nu}$ *Decays*, hep-ph/9803269 (1998).

[22] C. S. Kim, Y. G. Kim and T. Morozumi, *New Physics Effects in* $B^- \to K^{(*)-}\nu\overline{\nu}$ *Decays*, hep-ph/9905528 (1999).

[23] *The BABAR Physics Book, Physics at an Asymmetric B Factory*, Eds. P. F. Harrison, H. R. Quinn, SLAC-R-504 (1998).

[24] J. H. Christenson *et al.*, *Phys. Rev. Lett.* **13**, 138 (1964).

[25] P. Oddone, in *Proceedings of the UCLA Workshop : Linear Collider* $B\overline{B}$ *Factory Conceptual Design*, Ed. D. Stark, World Scientist, 243 (1987).

[26] A. J. Buras, *Flavour Physics : CP Violation and Rare Decays*, hep-ph/0101336 (2001).

[27] G. Buchallas *et al.*, *Rev. Mod. Phys*, **68**, 1125 (1996).

[28] ALEPH Collaboration, *Eur. Phys. J.*, **C19**, 213, (2001).

[29] S. Godfrey and N. Isgur, *Phys. Rev. D*, **32**, 189 (1985).

[30] PEP-II, *An Asymmetric B Factory, Conceptual Design Report*, SLAC-418, LBL-5379 (1993).

[31] B. Aubert *et al.*(BABAR Collaboration), *BABAR Technical Design Report*, SLAC-R-457, (1995).

[32] B. Aubert *et al.*(BABAR Collaboration), *Nucl. Inst. Met. in Phys. Res. A*, **479**, 1-116 (2002).

[33] PEP-II, `http://www2.slac.stanford.edu/vvc/accelerator.html`

[34] H.A.Bethe, *Annalen d.Physik*, **5**, 325 (1930).

[35] `http://www.slac.stanford.edu/BFROOT/www/Organization/PubBoard /OfficialPlots/DRC/DIRC_principle.jpg`

[36] http://www.slac.stanford.edu/BFROOT/www/Organization/PubBoard /OfficialPlots/DRC/NewDirc.gif

[37] B. Aubert *et al.*(*BABAR* Collaboration), hep-ex/0304030 (2003).

[38] S. Agostinelli *et al.*(GEANT4 Collaboration) *Nucl. Inst. and Met. in Phys./ Res. A* **506** 250-303 (2003).

[39] http://www.slac.stanford.edu/BFROOT/www/Computing /Offline/Simulation/web/index.html

[40] http://www.slac.stanford.edu/BFROOT/www/Computing/Operation/skimming /monitor/r16skim.shtml

[41] B. Aubert *et al.*(*BABAR* Collaboration), *Phys. Rev. Lett*, **92**, 071802 (2004).

[42] G. C. Fox and S. Wolfram, *Phys. Rev. Lett.*, **41** 1581 (1978).

[43] H. Albrecht *et al.*(ARGUS Collaboration), *Phys. Rev. Lett. B*, **241**, 278 (1990).

[44] R. Barlow, *Comput. Phys. Commun.*, **149**, 97 (2002).

[45] B. Aubert *et al.*(*BABAR* Collaboration) http://www.slac.stanford.edu/BFROOT/www/Physics/TrackEfficTaskForce /TrackingTaskForce-2004.html

[46] S. Spanier and G. Mancinelli, *Kaon Identification in the BABAR Experiment*, *BABAR* Analysis Document #116 (2001).

[47] CLEO Collaboration, *SEARCH FOR THE RARE DECAY OF A B MESON TO A K MESON AND TWO NEUTRINOS*, http://hdl.handle.net/1813/92 (2004).